JOURNAL OF APPLIED PHYSICS

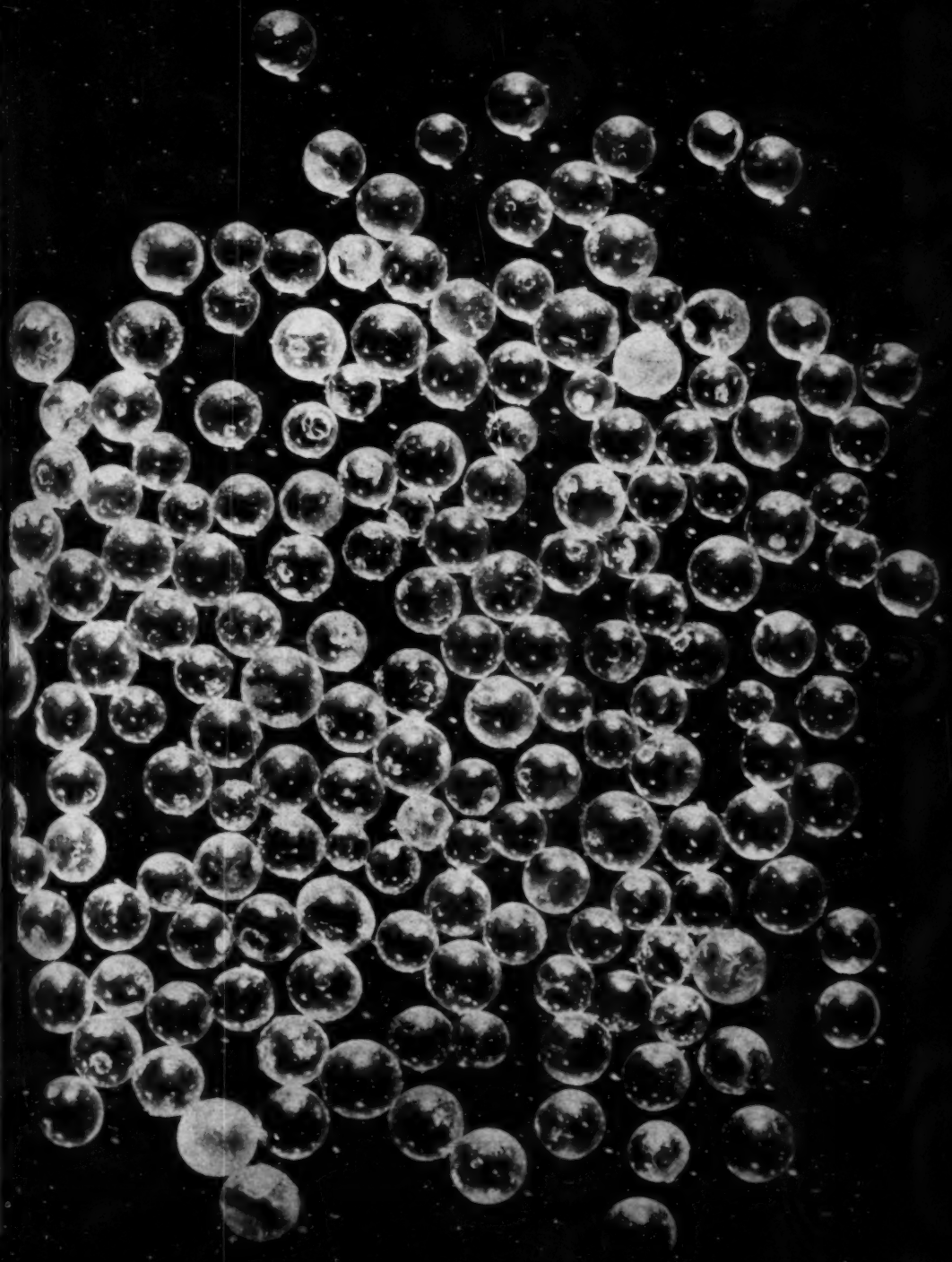

JOURNAL
OF
APPLIED PHYSICS

Vol. 15, No. 6 JUNE, 1944

In This Issue

Page

Measurements of the Adhesion Component in Friction by Means of Radioactive Indicators
B. W. Sakmann, J. T. Burwell, Jr., and J. W. Irvine, Jr. 459

Extension of the Conventional Twist Multiple Formula to New Materials S. L. Gerhard 474

Mechanism of Electrolytic Oxidation of Aluminum
Scott Anderson 477

Mutual and Self-Impedance for Coupled Antennas
Ronold King and Charles W. Harrison, Jr. 481

On the Destructive Action of Cavitation
M. Kornfeld and L. Suvorov 495

X-Ray Study of the Copper-Manganese Binary Alloy System L. D. Ellsworth and F. C. Blake 507

Directional Characteristic of a Half-Wave Doublet Goniometer Robert J. Dwyer 513

In Every Issue

Calendar of Meetings 473
Here and There 515
Recent Applications of Physics xviii
Index to Advertisers xxvi

BOARD OF EDITORS

Elmer Hutchisson,
Editor

Associate Editors
R. B. Barnes
Otto Beeck
W. F. Busse
S. H. Caldwell
Clark Goodman
Selig Hecht
W. J. Lyons
Morris Muskat
Thomas H. Osgood
Paul E Sabine
Frederick Seitz
J. R Townsend

Publication of the American Institute of Physics

ADMINISTRATIVE STAFF

Henry A. Barton,
Director

Madeline M. Mitchell,
Publications Manager

John T. Tate,
Adviser on Publications

GOVERNING BOARD

Paul E. Klopsteg,
Chairman

George B. Pegram,
Secretary

T. D. Cope
R. B. Dow
L. A. DuBridge
Floyd A. Firestone
Harvey Fletcher
R. C. Gibbs
K. S. Gibson
Hermann Mark
A. G. Worthing
John T. Tate
L. W. Taylor
N. W. Taylor
Wallace Waterfall

The Journal of Applied Physics, published monthly at Prince and Lemon Sts., Lancaster, Pa., is devoted to physics in its role as the science basic to other natural sciences and to the arts and industries. Previous to 1937 this publication was known as Physics. The Journal of Applied Physics publishes editorials, news of physicists, and reviews, as well as technical papers of applied physics.

Manuscripts should be submitted to Elmer Hutchisson, Editor, 50th floor, 350 Fifth Avenue, New York 1, New York.

Subscriptions and orders for back numbers should be addressed to Prince and Lemon Streets, Lancaster, Pa. or to the American Institute of Physics, 57 East 55 Street, New York 22, N. Y.

Subscription Price

	U. S. AND CANADA	ELSEWHERE
To members of scientific societies	$5.00	$5.70
To all others	7.00	7.70

Back Number Prices
Complete set: Vol. 1, July, 1931–Vol. 14, 1943—**$87.50**
Yearly back number rate: **$7.70**
Single copies: **$0.70** each.

Changes of address and proofs should be addressed to the Publications Manager.

Advertising rates supplied on request. Orders, advertising copy, and cuts should be sent to the American Institute of Physics.

Entered as second class matter January 22, 1937, at the Post Office at Lancaster, Pennsylvania, under the Act of March 3, 1879.
Accepted for mailing at the special rate of postage provided for in the Act of February 28, 1925, authorized May 2, 1932.

Copyright 1944, by the American Institute of Physics.

Journal
of
Applied Physics

Volume 15, Number 6 June, 1944

Measurements of the Adhesion Component in Friction by Means of Radioactive Indicators

B. W. Sakmann and J. T. Burwell, Jr.,* *Department of Mechanical Engineering*

and

J. W. Irvine, Jr.,** *Department of Physics*
Massachusetts Institute of Technology, Cambridge, Massachusetts

(Received March 6, 1944)

In friction experiments material is exchanged between the sliding surfaces. A study of this transfer of material was made possible by the development of a radioactive tracer method by means of which one could detect quantities of metal as small as 10^{-4} microgram. Spherical or hemispherical specimens were slid over an activated base surface. After the friction experiments, the riders were tested for the presence of radioactive material, and the quantity of metal deposited on the rider was determined as a function of various parameters. A copper-beryllium base surface was used for all measurements reported here. For the materials investigated it was found that the amount of base metal adhering to the rider was proportional to the load and increased with the distance of travel. Under otherwise identical conditions the amount of base metal deposited on the rider depended on surface finish and hardness of the rider. If the rider was harder than the base, the transferred material increased with surface roughness. If, on the other hand, the rider was softer than the base, surface finish was found to be of secondary importance. Measurements made with steel specimens showed that the amount of metal deposited on them was inversely proportional to their Brinell hardness. For riders of different materials, but having the same hardness and surface finish, the amount of transferred metal increased with the solid solubility of the base metal in that of the rider. Lubrication decreased the transfer; the reduction depended on load and, for the same load, on the material of the rider. The influence of lubrication was greater for smaller loads.

INTRODUCTION

AMONG the many attempts to interpret the phenomena of dry friction there are two which are outstanding. The first and oldest theory ascribes the frictional force to the interlocking of irregularities of the sliding surfaces. According to this view, frictional work is required to lift the two bodies over each other's asperities.[1] The second theory maintains that adhesion forces between the atoms of the sliding bodies are responsible for the friction force. Coulomb's law, which states that the friction force is proportional to the normal load and independent of the area of contact, is often mentioned in support of the first hypothesis. Bikerman,[2] for example,

* Now Lieutenant, USNR, stationed in the Office of the Coordinator of Research and Development, Navy Department, Washington, D. C.

** Now Assistant Professor in the Department of Chemistry, Massachusetts Institute of Technology.

[1] C. A. Coulomb, Mém. Acad. Roy. Sci., p. 161 (1785); J. Frenkel, Zeits. f. Physik **37**, 572 (1926); B. Derjaguin, Zeits. f. Physik **88**, 661 (1934).

[2] J. J. Bikerman, Phil. Mag. **32**, 67 (1941).

expresses the opinion that adhesion forces play no part in friction experiments, and that the surface irregularities are entirely responsible for friction effects. Hardy[3] and Tomlinson,[4] on the other hand, claim that adhesion forces are of paramount importance in frictional phenomena. Tomlinson in particular developed a molecular theory of friction expressing the friction force in terms of atomic repulsive and attractive forces. A third group of workers assumes that contact electricity plays a major part in frictional phenomena.[5] More recent investigators have come to the conclusion that frictional effects are too complicated to be explained by any single hypothesis. For instance, Ernst and Merchant[6] interpret their data with the assumption that the friction coefficient is partly due to adhesion and partly due to the finite slope of the surface irregularities. On the other hand, Bowden, Moore, and Tabor[7] conclude that while one factor in dry friction is adhesion of the surfaces, another factor is the ploughing of the asperities of the harder of the two surfaces through the top layer of the softer one.

In view of the controversy over the nature of the friction force, the question as to the ultimate form of the frictional work may afford a better approach to the problem under discussion.[8] All of the following factors contribute to the frictional work.

(1) It is generally assumed that the greater part of the work of the friction force is transformed into thermal energy. Likewise, the part of the frictional work which is stored as elastic energy of the contacting surfaces is dissipated into heat energy.

(2) Another part of the frictional work is stored in the form of cold work of the surfaces. At the end of the friction test some of the atoms of the sliding bodies do not return to equilibrium positions, thus increasing the internal energy. Immediately after the friction test this part of the frictional work does not appear in the form of heat energy. In the course of the slow recrystallization process the cold work is ultimately converted into heat energy. Only under extreme conditions has it been possible to determine the latent heat of cold work.[9] For friction experiments, however, such determinations have not yet been made.

(3) Work is consumed in tearing metal particles out of the bulk material of the sliding bodies, thus increasing the surface energy. This part of the frictional work will not at any time be transformed into heat energy. Some of the torn-out metal particles are deposited on the other surface. This transfer of metal particles from one surface to the other forms the subject of the present paper.

Only under extreme conditions of load is it evident that matter is exchanged. If two clean metal surfaces are rubbed under heavy loads, it is well known that they are welded together. Subsequent separation of the two surfaces makes it apparent that relatively large amounts of one surface adhere to the other. This phenomenon, commonly known as galling, is familiar in the force fits of collars and in journal bearings which are run to seizure. In those cases large metal particles are torn out of the bulk material of one body and transferred to the other surface.

This picture of local welding has been applied in the region of relatively light loads. Bowden and Leben [10] have explained the stick-slip phenomenon in friction by assuming local welding of the surfaces, and more recently Bowden, Moore, and Tabor[7] have demonstrated that even for small normal loads metal is exchanged between the sliding surfaces. They prepared tapered sections of those parts of the surfaces of the friction specimens that were covered by scratches due to the friction experiment. The tapered sections showed that small lumps of metal of various sizes had been transferred from one surface to the other.

---

[3] W. B. Hardy and J. K. Hardy, Phil. Mag. **38**, 32 (1919).
[4] G. A. Tomlinson, Phil. Mag. **7**, 905 (1929).
[5] R. Schnurmann, Proc. Phys. Soc. **52**, 179 (1940); J. App. Phys. **11**, 624 (1940).
[6] H. Ernst and M. E. Merchant, *Proceedings of Conference on Friction and Surface Finish* (Massachusetts Institute of Technology, Cambridge, 1940).
[7] F. P. Bowden, A. J. W. Moore, and D. Tabor, J. App. Phys. **14**, 80 (1943); F. P. Bowden and D. Tabor, Council for Scientific and Industrial Research, Melbourne, 1942.
[8] A. Gemant gives a good summary of the different processes involved in dry friction in J. App. Phys. **14**, 456 (1943).
[9] G. I. Taylor and H. Quinney, Proc. Roy. Soc. **A143**, 307 (1934).
[10] F. P. Bowden and L. Leben, Proc. Roy. Soc. **A169**, 371 (1939).

While the taper-sectioning method makes it possible to demonstrate the exchange of metal, it is not suitable for quantitative measurements. Until recently only microchemical methods, spectroscopic analysis, and the polarograph were available for the detection of small quantities of material. Because of their limited sensitivity, however, these methods are not suitable for quantitative investigations of transfer of material between sliding surfaces under small loads. Only by means of artificial radioactivity is it possible to employ a means of investigation whose sensitivity is 10^4 times as great as that of the older methods. Briefly, the method consists of artificially activating one of the surfaces, performing the friction experiment, and then measuring the activity acquired by the other initially inactive surface. The sensitivity of the method makes it possible to determine quantitatively the dependence of the amount of transferred material on various factors. Moreover, the radioactive method renders it feasible to determine the exchange between identical materials.

On the other hand, the radioactive method is restricted to those elements which can be activated. This restriction is not serious because in many cases alloying elements can be found which make it possible to activate the material. Iron, for instance, cannot be activated to any appreciable extent, but pure iron is only of limited technical interest, and many of the alloying elements of steel can be readily activated. A further limitation of this method is the fact that in a single experiment only the material transferred in one direction can be simply determined; however, it is evident that in all friction processes the exchange of material between the two surfaces takes place in both directions.

In the first experiments the manganese of an alloy steel flat was activated by neutron bombardment. These experiments yielded negative results for two reasons. First, the nuclear reaction did not produce enough intensity of radiation in the activated material. Secondly, because of the high penetrating power of the neutrons the activity is spread uniformly throughout the bulk material of the sample. In friction tests, however, only a comparatively thin surface layer is affected. For this reason it seemed desirable to employ a means of activation which produces a higher concentration of radioactive material near the surface. Activation by deuteron bombardment seemed to be more suitable as deuterons penetrate the target to a very limited depth. At the same time, higher values of specific activity are obtained.

In the next experiments a water-cooled steel block containing 0.6 percent manganese was activated by deuteron bombardment in the cyclotron. For friction tests performed under dry conditions exchange of material could be verified. Under lubricated conditions, however, it was not possible to detect any active material on the initially inert surface; therefore, it seemed desirable to increase further the sensitivity of the method. After some exploratory work on other nuclear reactions it was decided to bombard a copper target with deuterons. The nuclear reactions responsible for the activities of copper are as follows:

$$Cu^{63}+d\rightarrow Zn^{63}+2n,$$
$$Cu^{63}+d\rightarrow Cu^{64}+p.$$

The zinc isotope decays with a half-period of 38 minutes and the copper isotope with a half-period of 12.8 hours under emission of β-rays and γ-rays. Experiments with the copper base showed that the sensitivity of the method was high enough to detect quantities of material which were transferred in friction tests performed under small loads and lubricated conditions. However, pure copper is very soft, and it seemed desirable to use a harder base surface giving as high a yield in radioactivity as copper. Copper-beryllium which seemed to fulfill all these requirements was used as target material for all subsequent experiments which are discussed below.

EXPERIMENTAL METHOD*

The sample to be activated was metallographically polished before exposure to the deuteron beam in the cyclotron of the M.I.T. Radioactivity Center. Its surface roughness was 2.5 to 3.0 micro-inches as determined with an Abbott profilometer. Current and voltage of the deuteron beam varied between 10 and 40

* Radioactivity measurements described in this chapter were made at the Radioactivity Center, M.I.T.

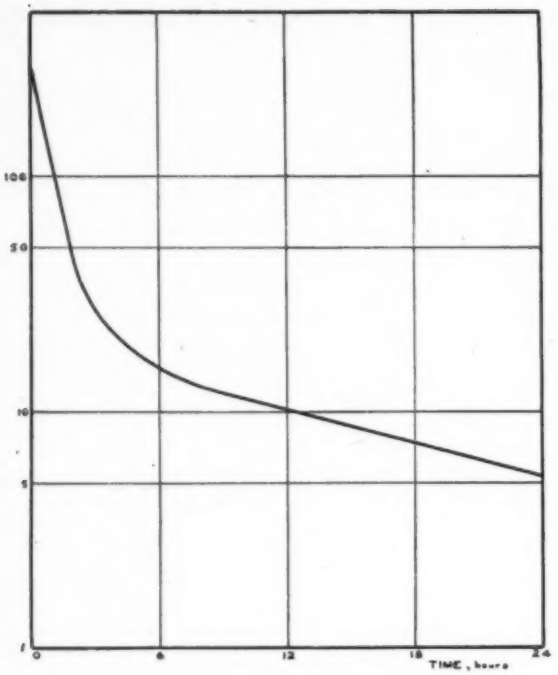

FIG. 1. Activity of copper-beryllium target *versus* time in hours.

microamperes and 10.5 and 14 Mev. Choice of the exposure time depended on the sensitivity required for the particular friction tests, but for all the experiments discussed here it varied between two and seven hours. Most mechanical polishing operations leave loose particles in the surface.[11] For this reason the target was electrolytically polished after the bombardment to remove the "fuzz" thereby ensuring that the transferred matter was bulk material. The target was electropolished in a solution of two volumes of absolute methyl alcohol and one volume of concentrated nitric acid.[12] A current density of 1.0 to 1.5 amp./cm^2 was used. Ten to twenty seconds proved to be sufficient for a satisfactory polish.

After the surface had been electropolished, the copper-beryllium block was fastened to a table and the friction tests were made. The friction samples were held in a compound tool holder of a lathe which was fastened to the table and were slid over the surface of the copper-beryllium block. In the early experiments flat riders were slid over the activated base. The errors of the measurements of those tests were mostly due to the fact that it was difficult to locate the spots at which the transferred material was deposited. With spherical riders, on the other hand, there is no ambiguity as to the location of the deposited material. In all experiments reported here we used hemispherical or spherical friction samples which were held in a fixed position in order to prevent the specimens from rolling over the base surface. Before the friction test the specimens were cleaned with alcohol and ether in order to remove any grease deposits. Use of the tool holder enabled the path of each specimen to be displaced slightly from that of the previous one. It seemed advisable to use a fresh portion of the block for each test because of contamination of the activated surface by material transferred from the rider to the base. Furthermore, use of the tool holder made it possible to define the position of the track of each friction test in terms of the coordinate system which was engraved on the inactive sides of the block. It was necessary to establish the location of each track because the radioactive intensity varied over the surface due to non-uniformity in the irradiating deuteron beam. After the friction tests had been completed, intensity of the radioactivity as a

FIG. 2. Autoradiograph of copper-beryllium target after exposure to deuteron beam. The scratch on the film marks the contour of the target.

[11] J. T. Burwell, J. Kaye, D. W. van Nymegen, and D. A. Morgan, J. App. Mech. **A49** (June, 1941).
[12] G. E. Pellissier, Jr., H. Markus, and R. F. Mehl, Metal Progress **37**, 55 (1940).

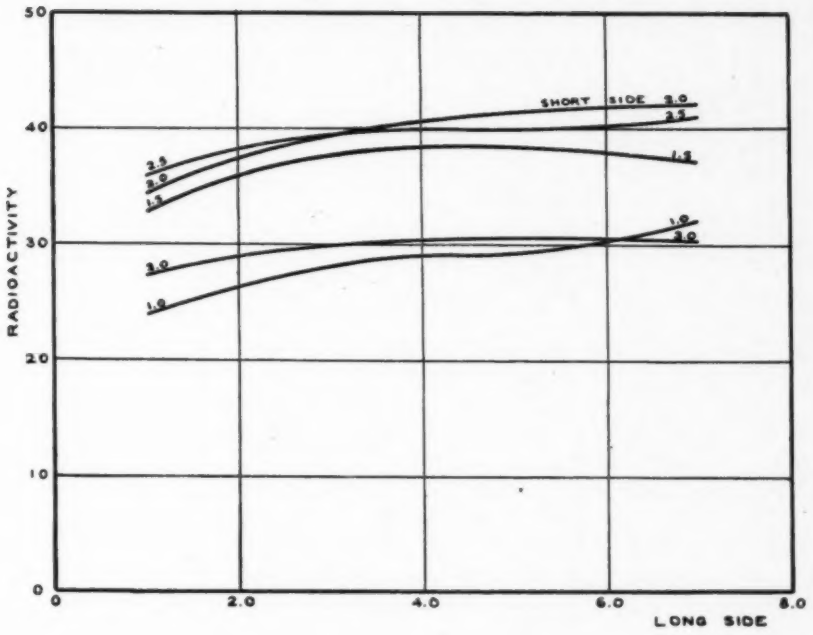

FIG. 3. Variation of activity along length of target for different values of coordinate of short side.

function of position on the surface was determined in terms of the coordinate system.

After the riders had been slid over the base surface, they were tested for the presence of radioactive material with a Geiger-Müller counter and a counting rate meter. In measuring the activity of the copper-beryllium adhering to the friction specimen the surface of the rider nearly touched the counter window. If, as in most of our measurements, several counters were used, a correction factor had to be determined for each counter. This was done by putting the same sample on the different counter windows and recording the readings of the counting rate meters. The correction factor which was thus determined took account of the dissimilar geometry and the different absorption of the counter windows. The intensity of the radiation originating from the transferred copper-beryllium and the time of the measurement were recorded. A decay curve was taken during each run. A filter paper which had been dipped into the polishing solution was used as a decay standard. This decay curve made it possible to take account of the fact that the radioactivity varied while the measurements were made. Figure 1 shows the decay curve of a copper-beryllium block which was exposed to a deuteron beam of 14 Mev and 25 microamperes for a period of two hours. The decay curve shows that the activity had two components with half-lives of 38 minutes and 12.8 hours, respectively.

The heat produced by the impact of the deuteron beam changed the appearance of the copper-beryllium block so that in most cases it was obvious which parts of the surface had been struck by the beam. Sometimes, however, the deuteron beam left no visible marks. In those cases, autoradiographs of the surface were taken which gave a good picture as to where the deuteron beam hit the target. An example is shown in Fig. 2. Exposure of the film beyond the upper boundary of the target originated from radiation of the brass inlets of the cooling water. This method helped in generally positioning the friction runs, but could not be used for quantitative measurements of the intensity distribution of radioactivity over the surface. As pointed out above, such knowledge is essential for a quantitative evaluation of the readings of the counting rate meter. In order to find the intensity distribution, the target was scanned in the following way: The copper-beryllium block was shielded from a counter tube by a set of lead bricks. The target was put on the uppermost brick in which a hole had been drilled; the activated surface of the target faced the counter window. The target was then moved over the hole in the lead brick, and the activity was recorded as a function of the

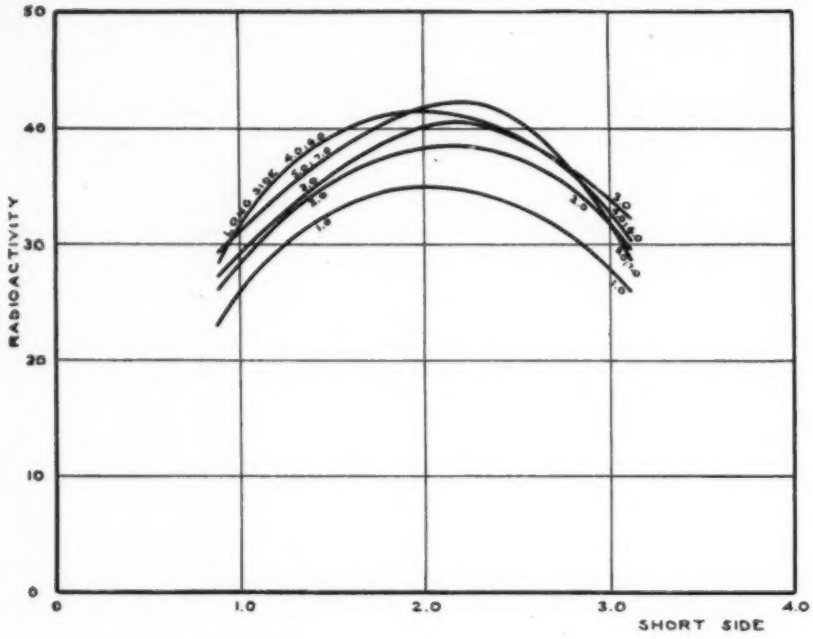

FIG. 4. Variation of activity along width of target for different values of coordinate of long side.

coordinate system engraved on the inactive sides of the block. The intensity distribution measurement had to be made several days after the activation since soon after the bombardment in the cyclotron the activity of the target was beyond the range of the measuring instrument. Figures 3 and 4 show typical intensity distribution curves. In Fig. 3 the activity is plotted *versus* the long side of the target for different values of the coordinates of the short side. Figure 4 shows the variation of activity along the short side of the block. It is evident from Figs. 3 and 4 as well as from the radiogram of Fig. 1 that the activity varies more rapidly along the short side of the block. As the samples were slid parallel to the long side of the block in all friction tests, it is evident from Fig. 3 that only a small correction factor had to be used to account for the variation of activity along each track. However, Fig. 4 suggests that the variation of activity from one track to the next one was by no means negligible. From these distribution curves a correction factor was determined for each friction test. Those measurements for which the distribution correction factor exceeded a value of two were discarded in the final evaluation of the tests.

After the determination of the intensity distribution it was necessary to establish a relationship between the measured activity of the rider and the amount of copper-beryllium deposited on its surface by microchemical analysis. This analysis gave a value of the specific activity of the copper-beryllium near the surface of the target in counts per minute per microgram. After the target had been scanned, the exposed part of the surface of the copper-beryllium block was lightly etched, and a layer of approximately 3 to 10 mg/cm^2 was removed. Activity measurements on an aliquot of the solution furnished a value of the total activity. The dissolved copper was precipitated by 8-hydroxyquinoline, and the specific activity of the surface layer was found by dividing the total activity by the weight of the precipitated copper. The decrease in activity through the etched-off layer is about 5 percent[13] which is within the accuracy of the activity measurements. The boundaries of the etched region were expressed in terms of the coordinate system engraved on the unexposed sides of the target. From the distribution curves of Figs. 3 and 4 a mean value of the relative activity of the etched region was determined. From the coordinates of the track of each friction test a value of the specific activity could be found. The value

[13] E. T. Clarke, Ph.D. Thesis, Massachusetts Institute of Technology, 1944.

of the specific activity at the time of the measurements was determined from the decay curve of Fig. 1.

For a single exposure of the target in the cyclotron one could perform between 30 and 50 friction tests. The reproducibility of the measured values proved to be satisfactory if one compared the measurements performed for the same exposure of the target. The errors which were found for tests of the same exposure are given below with the experimental results. However, a comparison of the measurements performed for different exposures of the target showed that the absolute accuracy leaves much to be desired. The chief reasons for the low absolute accuracy are as follows.

First, in etching the target, the active material is not removed uniformly over the exposed surface. It is, therefore, possible that the specific activity of the microchemical analysis does not correspond to the mean value of the relative activity determined from the distribution curves of Figs. 3 and 4.

Secondly, the specific activity varies over the surface. As pointed out above, we attempted to take account of these variations by scanning the target after the friction tests. This procedure reduces the errors due to local variations of intensity, but does not entirely eliminate them. Both sources of error can be removed by using surfaces which are plated with an activated material. It is planned to use plated materials in future tests.

RESULTS AND DISCUSSION

In all experiments reported here the velocity with which the rider was moved over the surface was kept between 3 and 4 mm/sec. All riders had the shape of spheres or hemispheres of $\frac{3}{16}$-in. radius. A new specimen was taken for each friction test.

It was decided to investigate first a group of materials of very different properties: phosphor bronze, steel, and glass. The riders were slid over the target under identical conditions of load and distance of travel. Table I shows the results of the tests.

It is interesting to note that very different amounts of copper-beryllium were transferred to the riders despite the fact that external conditions of the friction tests were identical. The phosphor bronze specimens took up five times as much material as the steel samples. Furthermore, the fact that even a non-metallic substance like glass takes up a small amount of base material is interesting in view of the controversy over the terminology of the mechanism of adhesion. Some workers have expressed the opinion that local welding takes place over the true area of contact. This picture of local welding is used irrespective of the maximum temperature of the contacting surfaces. If there is reason to believe that the maximum temperature is below the melting point of one of the contacting metals, adhesion is often referred to as cold welding. While one might well speak of cold welding between steel and copper-beryllium, the expression seems to be inappropriate for a pair of materials like glass and copper-beryllium.

TABLE I. Material deposited on riders of various materials.

Material of rider	Deposited material in micrograms
Phosphor bronze	0.043
Steel	.0084
Glass	.0053

Before investigating the influence of the characteristics of the rider material it was decided to determine how the amount of transferred material depended on the external conditions of load and distance of travel.

(a) Load

The load dependence of the transferred material was determined for both phosphor bronze and steel riders; the normal load was varied between 13 g and 200 g. In Fig. 5, which shows the results, each point represents the arithmetic mean value of three measurements. In this particular run the sensitivity, i.e., the smallest amount of material which could be detected, was 4×10^{-5} microgram. The diagram shows that the transferred material increased with the load. Within the accuracy of our measurements the amount was proportional to the applied load. Furthermore, the diagram corroborates the results of Table I that more material is taken up

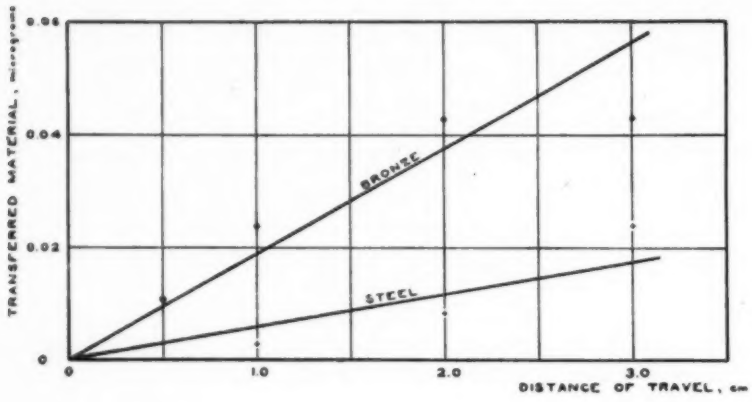

FIG. 6. Amount of transferred material in micrograms *versus* normal load in grams.

by phosphor bronze riders than by steel specimens. This result seemed surprising at the time the measurements were made because the steel specimens were harder than the copper-beryllium base while the phosphor bronze riders were softer.

(b) Distance of Travel

The influence of the distance of travel of the rider over the base surface was next investigated. The same materials were used for these investigations: i.e., steel and phosphor bronze. The distance of travel was varied between 0.5 and 3.0 cm. The results are plotted in Fig. 6 in which each point is the arithmetic mean value of three measurements. The plot shows that the greatest amount of copper-beryllium was deposited on the phosphor bronze samples, a smaller amount on the steel riders. In this respect the measurements corroborate the data of Table I.

These two groups of tests showed clearly that other factors, such as the nature of the material and the hardness of the rider, are important in determining the amount of deposited material. Furthermore, it became apparent that the measured values scatter considerably. In order to improve the accuracy, it was decided to make more measurements per test. In all following runs between five and eight measurements were made for each set of experimental conditions.

(c) Surface Finish

From the performance of journal bearings it is well known that the surface roughness of the shaft is an important factor determining the load capacity.[11] It is, therefore, of interest to know the influence of surface roughness on the amount of transferred material. Steel riders with four different values of surface finish were accordingly prepared. The profilometer readings of the riders varied between 0.6 and 6 micro-inches. Table II and Fig. 7 show the results of these tests. In Fig. 7

TABLE II. Material deposited on steel riders with different surface finishes.

Surface roughness in micro-inches	Deposited material in micrograms
0.6–0.7	0.0025
2.0–2.8	.0085
3.5–4.5	.014
6.0–7.0	.015

the transferred material in micrograms was plotted against the surface roughness in micro-inches. Each point in the plot represents the arithmetic mean value of five to seven measurements. From the plot it is evident that the rough specimens take up more material than the smooth riders. A rough steel sample of surface roughness 6–7 micro-inches takes up six times the amount of material deposited on a smooth specimen of surface rougness 0.6–0.7 micro-inch.

The measurements on load and distance of travel showed that very different amounts of material were deposited on phosphor bronze and steel. It seemed desirable, therefore, to see how the two materials behaved with respect to a change in surface finish. A number of phosphor bronze riders was prepared, whose surface roughness varied between 2.5 and 13 micro-inches. Table III shows the material deposited

TABLE III. Material deposited on phosphor bronze riders with different surface finishes.

Surface roughness in micro-inches	Deposited material in micrograms
2.5–3.0	0.019±0.002
9.0–13.0	0.014±0.002

on phosphor bronze samples as a function of surface roughness.

The errors mentioned in the table are probable errors of the arithmetic mean values of five measurements. The table shows that 26 percent less material is transferred to the rough than to the smooth riders. Because the difference between rough and smooth phosphor bronze specimens is near the error limit of our measurements, a second run was made. This time 36 percent less material was taken up by the rough specimens. Considering the limited accuracy of these measurements the agreement between the two runs can be considered satisfactory.

(d) Surface Finish and Hardness

A comparison of the two sets of measurements of Tables II and III shows clearly that steel and phosphor bronze specimens behave very differently with respect to a change in surface finish. With steel six times as much material is transferred to a rough as to a smooth sample. With phorphor bronze, on the other hand, surface roughness is a relatively unimportant factor; nearly the same amount of material is transferred to the rough as to the smooth riders. In fact, contrary to the behavior of steel samples, rough phosphor bronze specimens seem to take up slightly less material than the smooth ones. It was seen that the different behavior of the two materials might be due either to the difference in material or the difference in hardness. Since the values of the Brinell hardness of the chromium steel samples and the phosphor bronze specimens were 640 and 190, respectively, while the copper-beryllium target had an intermediate hardness of 310 Brinell, it was decided to eliminate the difference in relative hardness by trying annealed steel specimens which were softer than the copper-beryllium target. These steel samples had a hardness of 195 Brinell which was nearly the same as that of the phosphor bronze specimens. Table IV shows the results.

TABLE IV. Material deposited on soft steel riders with different surface finishes.

Surface roughness in micro-inches	Deposited material in micrograms
1–2	0.103±0.006
9–11	.082± .009

The values of the table are arithmetic mean values of five measurements and the errors are probable errors of the mean values. The table shows that about 20 percent less material is transferred to the rough than to the smooth riders. This is about the same relative difference as the one shown in Table III for phosphor bronze specimens.

One may, therefore, conclude that the different behavior of steel and phosphor bronze specimens as shown by Tables II and III is not due to the

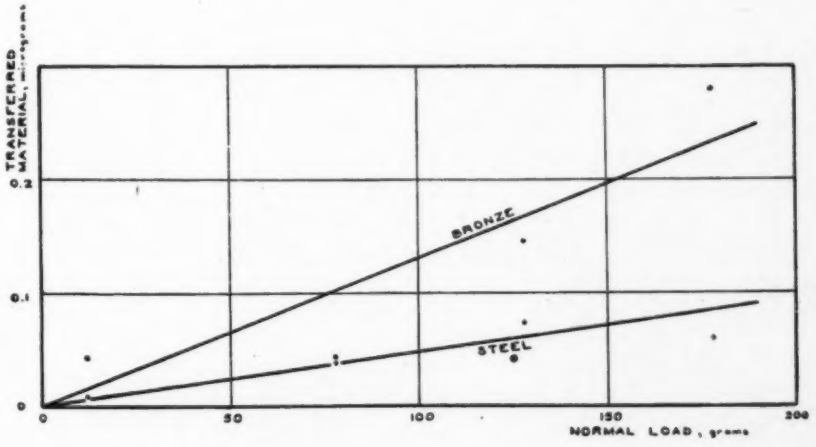

FIG. 5. Amount of transferred material in micrograms *versus* distance of travel in centimeters.

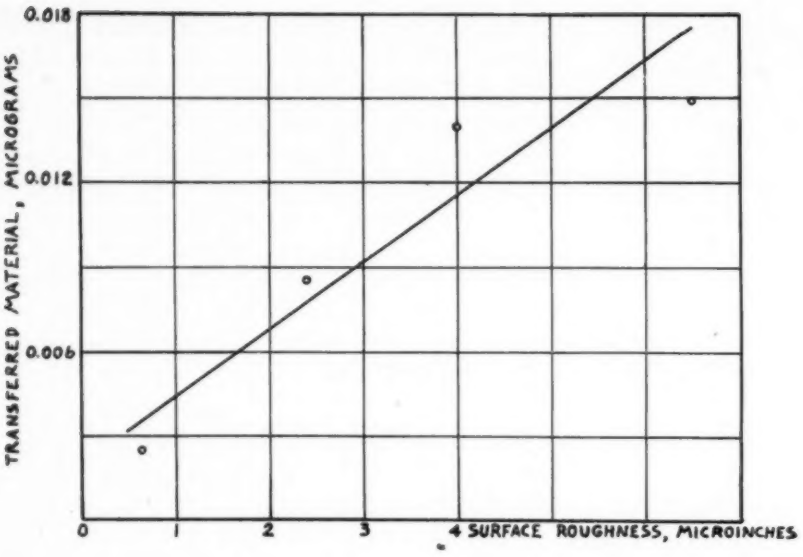

FIG. 7. Amount of transferred material in micrograms *versus* surface roughness in micro-inches for steel riders.

different properties of the rider materials, but rather to the difference in hardness. One may generalize these results by the statement that the amount of deposited material depends on surface roughness of the rider to an appreciable extent only if the material of the rider is harder than that of the base surface. If, on the other hand, the riders are softer than the base, surface finish is of secondary importance. For this latter case the difference between rough and smooth samples is so small as to be near the limit of the present resolving power of the experimental method. However, in all cases so far investigated more material seems to be deposited on the smooth rider.

These findings are in accord with Bowden and Tabor's conclusion[7] that for friction experiments between hard and soft materials the irregularities of the harder material plough through the softer one. It seems plausible that as a result of this ploughing action particles are torn out of the soft material, and that some of these adhere to the hard surface. The fact that more metal is transferred to the smooth than to the rough surface for friction between soft rider and hard base seems to indicate that the true area of contact is greater for the smooth than for the rough specimens.

(e) Hardness

In connection with the investigations on surface roughness it became evident that the relative values of hardness of the riders with respect to the base material are of importance in determining the amount of material transferred. It was decided, therefore, to investigate next the influence of hardness under the same conditions of surface finish. As steel affords the widest range in hardness of all available materials, annealed samples of chromium steel of four different hardness values were prepared; the Brinell hardness of these specimens varied between 190 and 640 kg/mm². Six friction tests were made for each hardness value under identical conditions of load and distance of travel. The surface roughness was approximately the same for all specimens; it varied between 0.7 and 1.5 micro-inch. Table V shows the results of the tests.

TABLE V. Material deposited on steel riders of various hardnesses.

Brinell hardness of steel riders in kg/mm².	Deposited material in micrograms
640	0.026±0.005
530	.040± .007
395	.051± .003
190	.103± .009

The hardnesses of the first three groups of riders exceed that of the base material; the last group of riders of 190 Brinell is softer than the copper-beryllium base of 310 Brinell. In Fig. 8 the amount of deposited material is plotted against the inverse of the Brinell hardness.

Within the accuracy of the tests the measured points can be represented by a straight line. The amount of transferred material is hence inversely proportional to the Brinell hardness.

Now, according to Bowden and Tabor's view, hard riders plough through the soft base material. In the course of this ploughing action a certain amount of bulk material is torn out of the base surface. It was shown above that this picture of ploughing is useful in interpreting the measurements on surface finish. On the basis of this mechanism one might expect to find that the harder riders tore out more material from the base and that, as a consequence, more metal of the base surface adhered to the hard riders. However, a different explanation must be sought for interpreting the data of Table V. Inasmuch as the deformation of the riders during the friction test is plastic rather than elastic, it is to be expected that the true area of contact is inversely proportional to the hardness of the rider. Thus, the data of Fig. 8 might be explained by the assumption that the amount of transferred material is proportional to the true area of contact.

These results for steel riders made it desirable to extend the measurements to other materials having properties different from those of steel with respect to the copper-beryllium base. Although it is difficult to find a material covering a hardness range comparable to that obtainable with steel, these requirements seemed to be best fulfilled by copper-beryllium which covers the widest hardness range of the copper alloys. The hardness of the copper-beryllium samples which were prepared for this run varied between 100 and 300 Brinell. Table VI shows the material deposited on the hardest and the softest riders.

TABLE VI. Material deposited on copper-beryllium riders of various hardnesses.

Brinell hardness of copper-beryllium samples in kg/mm²	Deposited material in micrograms
103	0.031 ± 0.002
315	.026 ± .004

The errors given in Table VI are probable errors of the arithmetic mean value of seven measurements. More material seems to be deposited on the soft riders, although the difference between hard and soft specimens is within the error limit of the measurements. The measurements were repeated with similar, inconclusive results. The negative result of these runs was probably due to the fact that the hardness range was too small. Moreover, all copper-beryllium samples were softer than the base. It is possible that the results would have been different if, as with the steel specimens, the group of riders would have included some specimens harder than the base.

(f) Material

From the tests discussed so far it is evident that the nature of the material of the friction

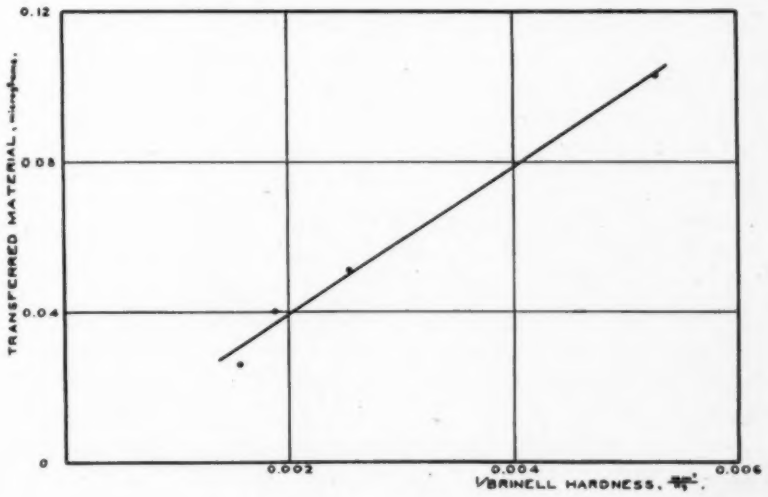

FIG. 8. Amount of transferred material in micrograms *versus* inverse of Brinell hardness in mm²/kg for steel riders.

specimens is one of the important factors determining the mass transferred from base to rider. For that reason it seemed desirable to test a variety of materials irrespective of their difference in hardness. The riders which were prepared for these tests can be divided into two groups. The samples of the first group were cut from solid stock, those of the second group consisted of electroplated steel balls. The interpretation of the results obtained with specimens of the second group was complicated by the fact that the plates were very hard since it was shown above that hardness may be an important factor in determining the amount of material transferred. About a dozen different materials were investigated. Table VII shows the results of these measurements.

TABLE VII. Material deposited on riders of various materials.

Materials	Deposited material in micrograms
A. Cut from solid stock	
Copper-beryllium	0.025
Aluminum	.013
Phosphor bronze	.091
Zinc	.022
Cadmium	.023
Tin	.026
Lead	.036
B. Electroplated materials	
Antimony	0.014
Nickel	.0028
Silver	.0073
Chromium	.00012

It is surprising that soft metals like lead, tin, and cadmium with a Brinell hardness of 3.8, 5.5, and 21 kg/mm², respectively, take up material from the hard copper-beryllium base of 310 Brinell. The table shows further that the quantities of material deposited on those riders cut from solid stock are all of the same order of magnitude, the largest and smallest amounts of copper-beryllium deposited on the riders of the first group differing only by a factor of seven. On the other hand, some of the electroplated specimens picked up amounts of copper beryllium which are smaller by one or two orders of magnitude.

In interpreting the data of Table VII one must keep in mind that not only the material was changed, but other factors as well, such as hardness and, to a lesser extent, surface finish. The values of the Brinell hardness of the riders of the first group ranged from 300 kg/mm² for copper-beryllium to 3.8 kg/mm² for lead; phosphor bronze which showed the greatest amount of deposited material had an intermediate hardness of 190 Brinell. In the tests reported above it has been shown that hardness as well as surface finish are important factors.

The friction tests plastically deform the rider and leave scratches on those parts of the specimen which come in contact with the base surface. The area which is plastically deformed and covered by scratches can be approximately measured under the microscope. In the following we shall call the scratched region the "apparent contact area," since it is certainly not equal to the true area of contact. This apparent contact area can be determined with a fair amount of accuracy for soft materials such as lead, tin, cadmium, and zinc. The measurements are more in the nature of estimates for harder materials such as chromium and nickel plates. The apparent contact area depends on the Brinell hardness of the rider material and—to an even greater extent—on the way the specimen is held when moved over the base surface. It decreases with increasing hardness, being largest for lead and smallest for electroplated chromium. The transferred copper-beryllium is deposited somewhere on this area although it is probably not evenly distributed over it. A mean thickness of the transferred material can be computed from the value of the apparent contact area, the amount of material deposited on the rider, and the density of copper-beryllium. Of the materials cut from solid-stock the following metals showed the thickest layers: copper-beryllium, aluminum, phosphor bronze, and zinc. Copper-beryllium showed the greatest value of average layer thickness, nearly 1000A. The layers are considerably thinner for cadmium, tin, and lead, the thinnest being lead with a thickness of only about 100A. Of the electroplated materials, chromium showed the smallest thickness of deposited material (less than 10A).

From these data it seemed that the transferred layer is thicker for those materials which show a

high value of solid solubility in the material of the base. Of the materials cut from solid stock, copper-beryllium and phosphor bronze showed the highest values of layer thickness and lead had the smallest. The first two materials are completely soluble in copper, while lead is completely insoluble in it. Of the plated materials, chromium riders showed the smallest value of thickness of the transferred deposit. While chromium is insoluble in copper, other effects such as surface films and the hardness of the chromium plate may have contributed to this result. The nickel-plated steel samples, for example, showed a very thin deposit of copper-beryllium although the nickel-copper phase diagram shows that the two constituents are completely soluble. Here again the hardness of the nickel plate may mask the behavior of the material.

It was shown above that for a number of materials the thickness of the deposited layer increases with the solid solubility of the main constituents of the sliding bodies. As the thickness of the transferred layer was determined indirectly, it seems desirable to look for a direct relationship between amount of transferred material and solid solubility of the two constituents. For different materials of the same hardness, the contact area may be assumed the same for a given load and distance of travel, other things being equal. In this case the thickness of the deposit and the amount of transferred material are proportional. If the relationship between thickness of transferred layer and solid solubility of rider and base material is correct, one would expect the quantity of deposited material to increase with the solid solubility of the base material in that of the rider.

In order to ascertain the relationship between solid solubility of the two rubbing surfaces and the amount of mass transfer to the rider, two pairs of specimens were prepared. While the two materials of each pair had the same hardness and surface finish, their solid solubilities in copper were very different.

For the first pair we chose phosphor bronze and annealed chromium steel, with Brinell hardness values of 190 and 195, respectively. The second pair of materials consisted of nickel and low carbon steel having the same Brinell hardness of 220 kg/mm². Copper, the main constituent of phosphor bronze, is completely soluble in the copper-beryllium base. The copper-iron phase diagram, on the other hand, shows only a limited solid solubility of copper in iron. Nickel and copper are completely soluble.

Table VIII shows the amount of copper-beryllium deposited on the riders of the two pairs of materials under identical conditions of load and distance of travel.

TABLE VIII. Material deposited on riders whose solid solubility in the material of the base is very different.

Material of rider	Brinell hardness	Deposited material in micrograms
Annealed chromium steel	195	0.046±0.007
Phosphor bronze	190	.072± .007
Low carbon steel	220	.022± .003
Nickel	220	.047± .007

The errors are probable errors of the arithmetic mean value of eight measurements. For both pairs the difference in deposited material is well outside the error limit of the measurements. The tests show that more matter is transferred if the rider material is soluble in the metal of the base.

(g) Lubrication

It was the aim of the last tests of this series to investigate the influence of a lubricant applied to the rubbing surfaces. Under identical conditions of load and distance of travel, friction tests were made with steel and phosphor bronze balls under dry and lubricated conditions. For the latter tests, the target was copiously covered with pure mineral oil. After the friction test the oil on the specimen was blotted off with filter paper in order to avoid absorption of the β-rays in the oil layer adhering to the surface of the rider. The first test was performed with a normal load of 200 g. For this load the difference in amount of material transferred to the rider under dry and lubricated conditions was small, although well outside the error limit of the measurements. Since it was thought that greater contrast might be obtained with a smaller normal force between the rubbing surfaces, the measurements were repeated with a load of 25 g. Table IX shows the results.

TABLE IX. Material deposited on riders under dry and lubricated conditions.

Material of rider	Deposited material in micrograms Dry	Lubricated
Steel	0.0025±0.0004	0.0006±0.0002
Phosphor bronze	.021 ± .003	.010 ± .002

The errors given in the table are probable errors of the arithmetic mean value of six to eight measurements. The table shows that about four times as much material is transferred to steel under dry as under lubricated conditions, while for phosphor bronze only twice as much is deposited for the dry as for the lubricated case. This different behavior of phosphor bronze and steel may be caused by the characteristics of the material of the rider or it may be due to the difference in hardness. This question can only be decided by further experiments.

CONCLUSIONS

In summarizing we may say that the riders of all materials took up bulk metal from the base. W. B. Hardy's[14] statement that seizure and wear are characteristic of all frictional phenomena is thus corroborated by experiment. Base material was taken up by metals as soft as lead and by substances as dissimilar to the base material as glass. In the case of the soft metals it was evident from visual inspection under the microscope that the amount of rider material smeared over the base surface was considerably greater than the amount of base metal deposited on the rider. Even for the smallest loads matter was transferred under dry as well as lubricated conditions. This fact suggested that the exchange of matter between the sliding surfaces might be of fundamental importance in all frictional phenomena, and it was hoped that systematic investigations of this transfer of matter might lead to a better understanding of friction effects.

It was found that the amount of material transferred under otherwise identical conditions was proportional to the load and increased with the distance traveled.

Moreover, the amount of deposited material increased with the surface roughness of the rider if the latter was harder than the material of the base. If, on the other hand, the riders were softer than the base material, surface finish was of minor importance.

For steel riders it was found that the matter picked up from the copper-beryllium base was inversely proportional to the Brinell hardness of the rider. If the deformation of the rider during the friction test was plastic rather than elastic, the result of these measurements could be explained by the assumption that the amount of deposited material was proportional to the area of contact.

Similar hardness investigations were carried out with copper-beryllium riders, but with less definite results. The inconclusive results of these tests might have been due to the fact that the hardness range of the copper-beryllium samples was considerably smaller than that of the steel riders. Moreover, none of the copper-beryllium specimens was harder than the base, while the hardness of most of the steel riders exceeded that of the copper alloy target.

It was shown that, for identical conditions of hardness and surface finish, the transferred matter increased with the solid solubility of rider material and base metal. Thus, it is interesting to note that the measurements reported here can, to a certain extent, be interpreted in terms of the properties of the bulk material despite the fact that no steps were taken to remove invisible surface films. However, it is difficult to say to what extent one can generalize the limited experimental results thus far obtained. Furthermore, it is to be expected that surface films often mask the relationship between solid solubility and amount of transferred material. Moreover, it is likely that more metal is transferred if these surface films are removed.

Lubrication with pure mineral oil reduced the amount of deposited material. It was shown that the reduction depended on load, and, for the same load, on the nature of the material of the sliding surfaces.

In addition to the tests described above the attempt was made to measure the material picked up by a rider when merely pressed against the base surface without lateral movement. The

[14] W. B. Hardy, Proc. Roy. Inst. Great Britain **23**, 65 (1920).

effect of normal load was studied. In all cases some radioactive material could be detected on the rider, but the result of the tests were inconclusive for the following reasons.

The amount of material deposited on the rider was near the sensitivity of the radioactive method. Furthermore, even with the precautions taken it was impossible to avoid small lateral displacements, a difficulty already pointed out by Claypoole and Cook.[15] Since the effect of the time of contact was not determined, one cannot say what part diffusion may have played.

The errors previously mentioned in the description of the measurements refer to tests performed for the same exposure of the target in the cyclotron. The question arises as to whether these errors originate from inaccuracies of the measurements or whether they are due to real fluctuations of the amount of transferred material. It is not likely that exactly the same amount of material is exchanged for each friction test performed under given conditions. Not all the metal particles torn out of the base stay on the surface of the rider. During the course of the test some may be transferred back to the base, and one may thus expect considerable differences in the net amounts transferred to the riders for a number of friction tests performed under identical conditions. It is, therefore, probable that the errors are partly due to real fluctuations from one test to another. Moreover, the finite mass of the particles torn out of the base surface constitutes a lower limit for the error of the measurements. It is not impossible that the errors mentioned above are a measure of the size of the particles.

The particles of the base metal transferred to the friction specimens adhere quite well to the surface of the rider. The riders of several materials were rinsed in chemically inactive liquids. Even when the riders were shaken violently in the liquid, none of the transferred base metal could be removed. If, on the other hand, the surfaces of the riders were rubbed with soft paper, some of the material could be removed. This, however, is not astonishing in view of the fact that paper can tear metal particles out of the base surface.

[15] W. Claypoole and D. B. Cook, J. Frank. Inst. **233**, 453 (1942).

ACKNOWLEDGMENT

The authors are indebted to Dr. A. F. Kip, Dr. Wendel Peacock, and Mr. Constantin Pancu for assistance in taking the experimental data, and to Professor Wulff and Professor Rightmire for many invaluable discussions. They are also indebted to the Chrysler Corporation for the generous financial assistance which made this work possible.

Calendar of Meetings

June

5– 7 Society of Automotive Engineers, Detroit, Michigan
22–24 American Physical Society, Rochester, New York
22–25 American Association of Physics Teachers, Cincinnati, Ohio
23–24 American Association of Physics Teachers, Rochester, New York
26–30 American Institute of Electrical Engineers, St. Louis, Missouri
26–30 American Society for Testing Materials, New York, New York

July

16–21 American Society of Civil Engineers, Chicago, Illinois
22 American Physical Society, Berkeley, California

August

29–Sept. 1 American Institute of Electrical Engineers, Los Angeles, California

September

11–16 American Association for the Advancement of Science, Cleveland, Ohio
13–15 Society of Automotive Engineers, Milwaukee, Wisconsin

October

5– 6 American Institute of Mining and Metallurgical Engineers, Pittsburgh, Pennsylvania
5– 7 National Electronics Conference, Chicago, Illinois
5– 7 Society of Automotive Engineers, Los Angeles, California
6– 9 Electronic Parts and Equipment Industry Conference, Chicago, Illinois
9–14 American Society of Civil Engineers, Cleveland, Ohio
16–18 American Institute of Mining and Metallurgical Engineers, Cleveland, Ohio
16–20 American Society for Metals, Cleveland, Ohio
16–21 American Welding Society, Cleveland, Ohio
28 American Mathematical Society, New York, New York

November

2– 3 Society of Automotive Engineers, Tulsa, Oklahoma

Extension of the Conventional Twist Multiple Formula to New Materials

S. L. GERHARD
U. S. Rubber Company, Textile Division, Hogansville, Georgia
(Received March 20, 1944)

Mathematical relations between a few geometric yarn properties are used to develop the concept of relative density. With the aid of this idea it is possible to deal with yarns made of different materials but having the same relative density as though they were made of the same material, so far as their geometric properties are concerned. A simple formula is derived to convert twist multiples from one yarn count system to another. The figure obtained for the twist to be put into the new yarn is only an "educated guess," but it is hoped that it will shorten the amount of experimentation necessary for determining the optimum twist in new yarns.

INTRODUCTION

THE purpose of this paper is to show how the formula can be used to copy in a new material a yarn made of a familiar material. This is especially useful now when many new materials are being used in textiles.

The conventional formula

$$T = MC^{\frac{1}{2}}$$

is employed for almost all textiles, but for each material the yarn count C is expressed in different units; consequently the same twist multiple M will produce different twists T, in turns per inch.

DEFINITIONS OF A FEW YARN PROPERTIES

The yarn is assumed to be uniform and homogeneous in diameter, twist, and helix angle throughout its entire length. This is not true for actual yarns, but as the same assumptions were made in deriving the formula originally, they will do for the present purposes.

Diameters, Counts, and Densities

Yarn diameter may be measured by several methods. The numerical values obtained depend somewhat upon the method of measurement employed, and any choice of method is arbitrary. In dealing with the present problem it is assumed that the optical (microscopic) method is used, because the helix angle can be measured best by this method.

Count, yarn number, or size, is measured fundamentally in yards per pound. But for each material one or more multiples of yards are used, such as "hank" (840 yards) for cotton, "cut" (100 yards) for asbestos, "lea" (300 yards) for linen, etc. This property is measured in preference to diameter because the unevenness of most yarns would require a prohibitively large number of observations on diameter to get a representative figure. The count can be used as a valid substitute for diameter in most instances, but it is not sufficient in twist calculations, as will be shown later.

The density of a yarn is rarely ever mentioned in quantitative terms, but it has the usual physical meaning, namely, so many pounds per cubic foot. It varies from one yarn to another, depending upon the construction. It is defined according to the formula

$$v = 192/\pi YD^2, \tag{1}$$

where v = density in pounds per cubic foot, D = diameter in inches, and Y = yards per pound $= uC$, u being the number of yards in the conventional yarn count system. For the sake of generality Y will be used in most instances in place of C.

The relative density r is defined by a simple relation between yarn density v and filament or fiber density f, namely,

$$v = rf, \tag{2}$$

where v and f are in the same units and r is their ratio. This relative density represents the fraction of yarn cross section occupied by material, the balance being air spaces between the filaments. It ranges from about 0.3 to 0.8 in cotton yarns.

In this discussion "filament" is used in a general sense, and its meaning may be extended to include the yarns and plied yarns comprising a cord, as well as fibers and continuous filaments. So far as the geometry of twist is concerned no distinction need be made here between continuous filaments and staple fibers.

Helix Angle

The orientation of an individual filament in the outside layer of a yarn with respect to the yarn axis is known as the helix angle H, or angle of twist, as shown in Fig. 1. Denoting the diameter of the yarn by D (in inches) and the twist in turns per inch by T, we have

$$\tan H = \frac{\pi D}{1/T} = \pi TD. \qquad (3)$$

The diameters of the individual filaments should be taken into account but they are usually small compared to the yarn diameter and can be neglected here.

From experience in yarn manufacture and from considerations of torque and radial pressure produced by twisting, it is fairly evident that the helix angle is the fundamental geometric factor in the relations between twist and yarn properties for a given material, but it is rarely stated explicitly or recognized as such. Other important factors in these relations are the friction between filaments and the staple lengths of fibers, but these factors do not appear in the twist formula.

THE TWIST FORMULA

Derivation

The formula was originally derived as a means for obtaining the same helix angle in yarns of different sizes. The derivation will be repeated as a necessary step in extending its application. From Eq. (3) the condition for equal angles is

$$\tan H' = \tan H, \quad \text{or} \quad D'T' = DT, \qquad (4)$$

where the primed and unprimed letters refer, respectively, to the two yarns. This would be the end of the story if yarn diameters were used, or could be estimated conveniently. As it is impracticable to do this it is necessary to replace diameter by density and size from Eq. (1), giving

$$T'/(v'Y')^{\frac{1}{2}} = T/(vY)^{\frac{1}{2}}. \qquad (5)$$

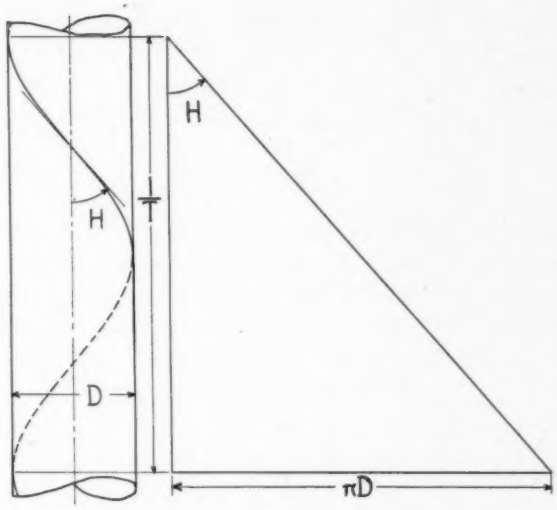

FIG. 1. Helix angle.

Twist Multiple

In Eq. (5) both count and density appear, and we see that count alone is not a sufficient substitute for diameter, as in most other calculations. In order to evade the necessity for measuring density, which requires measuring the diameter, the further assumption was made that the density of the two yarns be equal, and this reduces (5) to the familiar

$$T'/Y'^{\frac{1}{2}} = T/Y^{\frac{1}{2}} \quad \text{or} \quad T = MC^{\frac{1}{2}}. \qquad (6)$$

Formula Purely Relative

The application of the formula is based entirely upon the possession of a model from which to copy the helix angle. This model may be a piece of yarn or it may be a guess at the proper twist multiple, based on past experience and intuition. The formula in any of its forms merely relates one yarn to another. It does not give any information as to what helix angle should be used to produce a yarn with desired physical properties.

EXTENSION OF FORMULA

The problem mentioned in the opening paragraph is that of using available knowledge of familiar yarns to help make yarns out of new materials. It is desirable to have some means for getting at least a rough approximation for the twist that should be inserted in spinning a new

yarn, in order to shorten the trial and error procedure necessary for finding the optimum twist. The extension to different materials is accomplished by replacing v by rf in Eq. (5), giving

$$T'/(r'f'Y')^{\frac{1}{2}} = T/(rfY)^{\frac{1}{2}}. \quad (7)$$

If a yarn of new material, designated by the primed symbols, is copied from a given yarn according to this formula the helix angles in the two yarns will be equal.

Geometric Equality

The above formula is valid whenever the number of filaments in a yarn cross section is large. This will in general be true because the filament diameters of most textiles are of the same order of magnitude and there are usually 20 or more filaments in an ordinary yarn cross section. On this basis we can say that two yarns of different materials are geometrically equal when they have the same diameter, twist, and relative density. Under these conditions the filaments in the two yarns will have approximately the same orientations and spacings relative to each other and to the yarn axis.

Application to New Materials

With this understanding we can use formula (7). The three quantities r, f, and Y must be known for the model and for the new yarn. The filament densities f and f' can be obtained from the densities in Table I, or from the literature. The size of the new yarn C' or Y' is usually specified. The simplest and best choice of a model is on the basis of geometric equality, and one is therefore chosen that is equal to the expected new yarn. By equating D and D' in (4) and r and r' in (7) we obtain

$$Y = Y'f'/f$$

for the size of the old yarn to be used as a model. The twist to be put into the new yarn is that which is found best in the old yarn of this size (Y) for similar purposes. Whether the new yarn will turn out with the expected diameter, twist, and relative density depends upon its spinning characteristics. Also, the optimum helix angles or twist multiples will in general not be the same for the old and new materials, because of differences in filament properties which are not included in the formula. The discussion of these questions is beyond the scope of this paper.

TABLE I. Filament densities.

Material	Density in lb./cu. ft.
Paper	44 to 72
Natural silk	78 to 81
Wool	82 to 83
Acetates	83
Cotton (linen)	94 to 95
Viscose rayon	95
Cupram. rayon	95 to 96
Nitro. rayon	95 to 97
Rubber	56 to 69
Asbestos	156 to 165
Glass	150 to 175

Twist Multiple Conversion Formula

Inasmuch as it is customary to deal with twist multiples instead of actual twists it will be convenient to have a formula for converting from multiples in one system to those in another. The basis for conversion is still between geometrically equal yarns. We obtain from the foregoing equations the conversion formula

$$M' = M(f'u'/fu)^{\frac{1}{2}},$$

where the primed and unprimed symbols refer, respectively, to the two systems. Applied to conversion from cotton to asbestos-cotton yarns this formula predicted 10.5 turns per inch in the asbestos yarn, whereas 12.2 turns per inch were found by actual trial to be most suitable. Although this is not very good agreement it is within the range occasionally encountered in applying the formula to yarns of the same material.

Further analyses of twist problems, taking into account filament diameters and yarn densities, are planned as the subjects of future publications.

The writer gratefully acknowledges helful discussions with Mr. S. H. Sherman and Mr. J. J. Mills during the preparation of this paper, and the permission of the U. S. Rubber Company for publication. The author also takes this opportunity to express his appreciation to Dr. M. Mooney who read the manuscript and offered valuable suggestions.

Mechanism of Electrolytic Oxidation of Aluminum

SCOTT ANDERSON*
Carleton College, Northfield, Minnesota
(Received April 7, 1944)

INTRODUCTION

WHEN aluminum is made the anode in certain electrolytes, a coating forms on its surface as long as the current flows. This coating is predominantly aluminum oxide[1] with the inclusion of adsorbed water and ions from the electrolyte. Except under special conditions of formation, the film has no definite crystalline structure. In some electrolytes, and under certain conditions, the structure of the oxide is that of gamma-alumina. Thick films, for example, those which can be produced in oxalic or sulfuric acid solutions, are penetrated by a multitude of rather evenly spaced pores, perpendicular to the surface of the film. The structure of anodic coatings is discussed in a paper by J. D. Edwards and F. Keller and illustrated by photomicrographs taken with the optical and the electron microscope.[2] Figure 1, a photomicrograph, furnished by G. W. Wilcox of Aluminum Research Laboratories, is suggestive of the porous structure of these coatings. In spite of the porous structure, the films are hard and adhere tenaciously to the aluminum sheet. Moreover, there are many indications that this porous coating is separated from the parent aluminum by an extremely thin, compact barrier layer of aluminum oxide.

This paper proposes to show that the compact barrier layer separating the base of the pores from the aluminum is continuous, unbroken, and is the seat of the growth processes which result in the formation of the oxide coating. The thick, porous film exhibited in Fig. 1 is idle as far as oxide growth is concerned, while the processes leading to increased oxide thickness function entirely within the thin, non-porous layer between the electrolyte at the base of the pores and the metallic aluminum. Specifically, it is proposed that oxide growth occurs by virtue of an outward diffusion of aluminum ions from the metal to the solution and an inward diffusion of oxygen ions supplied at the base of the pores by the electrolyte. The mechanism of the diffusion process is such that the barrier layer always separates the electrolyte from the metal, and the contact between the barrier layer and the metal remains intact. In this way, strongly adherent films are formed. In the proposed mechanism, the aluminum ions that diffuse into the oxide pass on into the electrolyte and do not remain within the film as a part of the aluminum oxide. Consequently, the theory predicts an upper limit to the proportion of oxide formed—a limit which is much lower than that which has been assumed previously on the basis of other theories.

THEORY

In presenting the theory, the anodic coating process under consideration will be that taking place at an anode of high purity aluminum in an electrolyte of dilute sulfuric acid. The mechanism of electrolysis will not be dealt with other than to require that $O^{=}$ ions be made available at the anode by the passage of current through the electrolyte.

If a sheet of aluminum with its natural air-formed oxide film is made the anode in an aqueous solution of sulfuric acid, oxygen will be

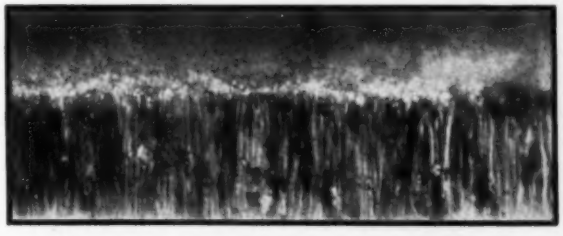

FIG. 1. Cross section of anodic oxide coating on aluminum sheet. Metal-oxide interface is at bottom. Magnification 1000×.

* Formerly of Aluminum Research Laboratories, Aluminum Company of America, New Kensington, Pennsylvania, where the work on this paper was completed.

[1] J. D. Edwards and F. Keller, Trans. Electrochem. Soc. 79, 180 (1940).

[2] J. D. Edwards and F. Keller, Metals Technology, T.P. 1710 (April, 1944).

liberated on its surface by the passage of current and further oxidation will result. The layer of oxide formed in this way establishes a barrier between the solution and the metal, and further passage of current must take place through the oxide film. Continued growth of the film, therefore, is dependent upon the ability of the aluminum and oxygen ions to penetrate the barrier layer. The aluminum ion Al^{3+} has a very small radius of 0.5A and can easily diffuse through the barrier under the influence of the intense electrical field present. This field is of the order of 10^7 volts/cm. The space within the metal lattice vacated by the Al^{3+} ions provides room that can be filled by O^- ions jumping from positions within the adjacent oxide layer. The oxygen ions have a large radius of the order of 1.3A, and can move toward the metal sheet under the influence of the electric field only when sufficient space is provided for them. The oxygen ion positions in the oxide vacated by ions moving into the space left by the migrating Al^{3+} ions are filled by adjacent O^- ions further out in the oxide film. Eventually the unoccupied O^- spaces reach the electrolyte where they are filled by ions from the electrolyte.

It is an observed fact that when aluminum is anodically oxidized, the thickness of the oxide is only moderately greater than that of the aluminum from which it is formed. Hence, when an Al^{3+} ion diffuses into the interstices of the oxide, two of the adjacent metal ions, by some adjustment in position, can create vacancies to be filled by oxygen, thus forming Al_2O_3.

In this way, the oxide layer increases in thickness by a stepwise migration of O^- ions into spaces in the metal lattice that have been previously vacated by Al^{3+} ions diffusing outward through the oxide into the electrolyte. One out of every three Al^{3+} ions on the surface of the metal diffuses through the oxide and leaves the other two to combine with oxygen to form aluminum oxide—Al_2O_3. In this way the oxide thickness increases, with the barrier layer continuously in good contact with the metal, and strongly adherent thereto.

The mobile Al^{3+} ions, which diffuse from the surface of the aluminum sheet, in effect dissolve into the oxide layer and migrate, as a result of the electrical field present. Once within the oxide film, the positive ion finds a sufficient number of like ions already present to neutralize the charge of the O^- ions in the layer. Therefore, it passes on through the layer, diffusing between the ions composing the barrier. When it reaches the electrolyte it forms a soluble sulfate and enters into the solution. Thus one out of every three aluminum ions that leaves the parent metal continues through the oxide film and into the acid electrolyte without ever having been a part of an aluminum oxide molecule. The continued growth of the film is dependent upon this loss of aluminum ions.

The migration of aluminum ions away from the metal-oxide interface creates a transition region between the oxide and the metal. The transition region is essentially the aluminum lattice with numerous vacant lattice sites. Even though the oxide coating is amorphous from the microscopic point of view, there is always a certain amount of short range order. In other words, the aluminum ions in the transition region tend to surround themselves with unlike ions. Consequently, instead of viewing the transition layer as aluminum with vacant lattice sites, it may be considered as aluminum oxide with vacant oxygen sites. These O^- sites can be occupied by ions diffusing from the neighboring oxide. When an O^- jumps into a new position, it may be replaced by another O^- ion in the oxide, leaving its site under the influence of the electrical field. This process repeats itself until at last the empty O^- site occurs at the oxide-electrolyte interface. Here it is filled by an ion from the solution.

In this process it is apparent that within the barrier layer the current is carried in part by the outward diffusion of Al^{3+} ions and the inward shift of O^- ions. Since one out of every three Al^{3+} ions that leave the aluminum sheet diffuses through the oxide film, and since it requires three O^- ions to neutralize the charge on the other two, one-third of the current is carried through the barrier layer by Al^{3+} ions, and the rest is transported by the O^- ions. When the O^- ion jumps from one position to another nearer the metal-oxide interface, it leaves an unbalanced positive charge in the region it vacated. This is commonly referred to as a "positive hole." It is convenient to think of the current carried by the inward movement of the O^- ions as an outward diffusion

of the positive holes. In these terms we would say that one-third of the current in the oxide is transported by positive ions and two-thirds are carried by positive holes, both diffusing from the metal to the electrolyte.

The mechanism so far described produces an oxide layer of uniform thickness. It is known, however, that the solution in which the oxide is being formed will also dissolve the coating after it is formed. The rate of attack of the acid upon the film will depend upon a number of factors such as acid concentration and temperature. When the oxide layer is thin, however, the electrical field strength within it will be very high. As a result, the velocity of the charge carriers will be high, and the oxide growth will be rapid. As the film thickness increases, the field intensity decreases, and the rate of growth of the barrier film diminishes until equilibrium is reached between the rate of acid attack and the rate of growth.

Once the acid attack is initiated at a point, there is established the electrical field distribution of a charged point near a plane. The Al^{3+} ions and positive holes will diffuse toward that point which forms the base of a pore. Thus we have the growth processes taking place in a spherical cap around the base of the pore as a center. Pores are formed with sufficient density that their spheres of action just overlap those of adjacent pores. The diffusing ions move along radius vectors drawn from the base of the pore to the aluminum sheet. This action leads to the dimpled aluminum-oxide interface found by Edwards and Keller.[2]

DISCUSSION OF THEORY

The mechanism of electrolytic oxidation just proposed provides a satisfactory explanation of certain important properties of the anodic oxide films. In the first place, the contact between the oxide coating and the base metal is never severed at any time. This explains the observation that the oxide films are strongly attached to the parent metal. Furthermore, it explains the formation of the porous structure observed in the thicker films.

The theory is also successful in explaining what is otherwise a very puzzling observation. Edwards and Keller[1] investigated the relation between the weight of oxide formed and the weight of metallic aluminum lost. This was done by weighing a sheet of aluminum and oxidizing it electrolytically for a determined period. The coated specimen was then weighed, the oxide coating dissolved off without attacking the metal, and the bare sheet reweighed. From these measurements, the weight of aluminum reacting and lost from the sheet and the weight of oxide formed can be readily calculated. These data can be calculated as an "efficiency ratio" R, which is the ratio of the oxide formed to the weight of aluminum reacting.

If all of the aluminum reacting appeared as oxide, the efficiency ratio would be $(Al_2O_3/2Al) = 1.89$. The data of Edwards and Keller[1] calculated in this way show no values above about 1.46. These values appeared reasonable, however, in view of the fact that some of the formed oxide dissolved in the electrolyte. If, however, the efficiency ratios for different times of oxidation are extrapolated close to zero time, when the amount of dissolved oxide should be very small, the limit seems to fall slightly below the value 1.6.

If the oxidation proceeds in the manner proposed in this paper, two out of every three aluminum ions leaving the sheet form oxide, and the other diffuses into the electrolyte. The efficiency ratio may be written as $(n\,Al+Al_2O_3)/3Al$, where n is the fraction of the diffusing Al^{3+} ions that have not penetrated to the solution. Before the first penetrates the barrier layer, n will equal unity. Therefore, the highest efficiency ratio obtainable is 1.59. This is much lower than the value 1.89 for the ratio Al_2O_3 to 2Al that has been expected on the basis of previous theories. Of course, most of the films dealt with in practice have values of n more nearly equal to zero. When $n=0$, $R=1.26$. Furthermore, thick films are penetrated by pores which were formed by dissolving some 10 to 15 percent or even more of the layer. Consequently, we may expect the practical values of R to be represented by the equation

$$R=(1-S)(n\,Al+Al_2O_3)/3Al, \qquad (1)$$

where S is the fraction of the oxide layer that is dissolved by the acid. R can never be greater than 1.59 in this type of film.

It should be pointed out, however, that the values published by Edwards and Keller are for the weight of oxide uncorrected for adsorbed impurities such as sulfate from the electrolyte. This would tend to raise the apparent value of the efficiency ratio while the solution of oxide by chemical attack of the electrolyte would lower the efficiency ratio. To some extent these effects counterbalance each other; by chemical analysis of the film and the electrolyte, their effect can be appraised. It seems significant, however, that no value of R in excess of 1.59 has yet been observed with electrolytes in which the oxide is slowly soluble.

When employing solutions in which the migrating aluminum ion will not dissolve in the electrolyte, different values of the efficiency ratio would be expected. For example, if the ion is precipitated from the solution as oxide, one might logically expect it to be precipitated on the film and become a part of the coating. In such a case the maximum value of R would be 1.89, because all of the aluminum leaving the sheet would be entering the coating as oxide: two-thirds by an electrochemical process and one-third by chemical precipitation. This is probably the approximate behavior in boric acid solutions. The coating builds up until the electric field falls to such a low value that the Al^{3+} ions diffuse across the barrier layer very slowly and growth practically ceases.

Elsewhere[3] it has been proposed that the luminescence sometimes observed during the electrolytic oxidation of aluminum is a result of leakage electrons being trapped by unbalance positive ion within the barrier layer. It was shown that such a mechanism is more in accord with the observed properties of the luminescence than is the customarily assumed spark discharge.[4] The proposals of that article are in complete agreement with the mechanism of the oxidation outlined above.

[3] Scott Anderson, J. App. Phys. **14**, 601–609 (1943).

SUMMARY

A mechanism of electrolytic oxidation of aluminum in such electrolytes as sulfuric acid or oxalic acid has been presented. In this process, the growth processes take place within a thin compact barrier of aluminum oxide adjacent to the metal. The mode of electrical conduction within the oxide film is such that aluminum ions dissolve from the sheet into the oxide, thus leaving spaces into which oxygen ions may be forced by the electrical field. The theory proposed leads to a consistent explanation of the observed properties of the film, including adherence, porosity, experimental "efficiency ratios," and luminescence.

ACKNOWLEDGMENT

The work reported above was completed while the author was on the staff of Aluminum Research Laboratories, and he is indebted to the Aluminum Company of America for permission to publish these findings. He is especially grateful to J. D. Edwards and F. Keller for many helpful suggestions in the preparation of this manuscript, and to George Wilcox for the use of the photomicrograph of Fig. 1.

[1] H. Fischer and F. Kurtz, Korr. u. Metalls. **18**, 42–49 (1942).

Mutual and Self-Impedance for Coupled Antennas

RONOLD KING AND CHARLES W. HARRISON, JR.
Cruft Laboratory and the Research Laboratory of Physics, Harvard University, Cambridge, Massachusetts

(Received December 21, 1943)

A general theory for the current in coupled antennas is formulated in terms of the vector potential and applied to determine the self-impedance Z_{s1} and the mutual impedance Z_{12} of a center-driven antenna in the presence of a second parallel, identical antenna which may be center-driven or center-loaded in an arbitrary way. Each antenna has a half-length h, a radius a, and the distance between them is b. Curves are shown for Z_{s1} and Z_{12} for $h=\lambda/4$; $\Omega=2\ln(2h/a)=\infty$, 30, 20, 10; $0.05\leqq b/\lambda\leqq 0.4$; and for $h=\lambda/2$; $\Omega=2\ln(2h/a)=30$, 20, 10; $0.05\leqq b/\lambda\leqq 0.5$. It is shown that except for the special case of an indefinitely thin antenna ($\Omega=\infty$) the self-impedance Z_{s1} of an antenna in the presence of a second antenna differs from the self-impedance Z_0 when the antenna is isolated and varies with b/λ. The input impedance Z_{1in} is determined and plotted for the same values of h and Ω, and the same ranges of b/λ for the following special cases: 1. The antennas are both center-driven *in phase* by identical generators. 2. The antennas are both center-driven *in opposite phase* by identical generators; or a driven antenna is parallel to a perfectly conducting plane. 3. Antenna 1 is center-driven; antenna 2 is parasitic and unloaded. 4. Antenna 1 is center-driven, antenna 2 is parasitic and center-tuned to self-resonance ($h=\lambda/2$ only).

EXISTING analyses of the self-impedance and the mutual impedance of a driven antenna in the presence of a second antenna are based on the following assumptions:[1] 1. The distribution of current in every antenna, whether center-driven or parasitic with an arbitrary load at the center, is the same as that in an isolated center-driven antenna of the same length. 2. The distribution of current in an isolated center-driven antenna is sinusoidal. 3. The self-impedance is independent of the presence of a coupled antenna. The first of these assumptions is incorrect unless both antennas are identical with identical generators driving them either in phase or 180° out of phase. The second and third assumptions are correct only for an infinitely thin, center-driven antenna; they are moderately good approximations for thicker antennas of half-length $h=\lambda/4$. Because the distribution of current in an antenna of non-vanishing cross section changes when a second antenna is brought near it, the self-impedance as well as the mutual impedance is a function of the relative orientation and separation of the antennas. Only if it is assumed that the distribution of current in a driven antenna is unchanged when a second antenna is brought near is the self-impedance constant. This is done in the conventional analysis in which a sinusoidal current is postulated, a distribution that is correct only for an antenna of vanishing radius.[2] Note that even in this oversimplified case the *mutual impedance is not independent of the distributions of current* in the coupled antennas, so that it is *never* correct to "assume a *convenient* current flowing in one antenna."

[1] R. King, Proc. I.R.E. **31**, 626–640 (1943).

VECTOR POTENTIAL FORMULATION

An electromagnetically correct formulation of the problem of determining the input impedance of a center-driven antenna in the presence of a second, arbitrarily oriented antenna has been given[3] in terms of the vector potential. It will now be specialized to two parallel antennas and the analysis carried out approximately.

The continuity of the tangential components of the electric field at the surfaces of two antennas, numbered 1 and 2, and oriented parallel to the z axis of a coordinate system, leads directly to the equations:

$$\frac{\partial^2 A_{1z}}{\partial z^2}+\beta^2 A_{1z}=j\frac{\beta^2}{\omega}z_1{}^i I_{1z}, \tag{1}$$

$$\frac{\partial^2 A_{2z}}{\partial z^2}+\beta^2 A_{2z}=j\frac{\beta^2}{\omega}z_2{}^i I_{2z}. \tag{2}$$

Here $\beta=2\pi/\lambda$; z^i is the internal impedance per unit length of the conductors; I_{1z} and I_{2z} are the

[2] R. King and C. W. Harrison, Jr., Proc. I.R.E. **31**, 548 (1943).

[3] R. King and C. W. Harrison, Jr., "The receiving antenna," Proc. I.R.E. (accepted for publication).

currents at points z in antennas 1 and 2; A_{1z} and A_{2z} are the vector potentials at the surfaces of antennas 1 and 2, respectively. The ratio of half-length h to radius a of each antenna is assumed to be large. The vector potential at the surface of each antenna consists of two components: that due to the current in the antenna itself, and that due to the current in the parallel antenna. Thus,

$$A_{1z}=A_{11z}+A_{12z}, \tag{3}$$

$$A_{2z}=A_{22z}+A_{21z}, \tag{4}$$

with

$$A_{11z}=\frac{\Pi}{4\pi}\int_{-h_1}^{h_1} I'_{1z}\frac{\exp(-j\beta r_{11})}{r_{11}}dz_1', \tag{5}$$

$$A_{12z}=\frac{\Pi}{4\pi}\int_{-h_2}^{h_2} I'_{2z}\frac{\exp(-j\beta r_{12})}{r_{12}}dz_2', \tag{6}$$

$$A_{22z}=\frac{\Pi}{4\pi}\int_{-h_2}^{h_2} I'_{2z}\frac{\exp(-j\beta r_{22})}{r_{22}}dz_2', \tag{7}$$

$$A_{21z}=\frac{\Pi}{4\pi}\int_{-h_1}^{h_1} I'_{1z}\frac{\exp(-j\beta r_{21})}{r_{21}}dz_1', \tag{8}$$

with $\Pi=4\pi\times10^{-7}$ henry/m. The following notation is used:

$$r_{11}=[(z_1-z_1')^2+a_1^2]^{\frac{1}{2}}, \tag{9}$$

$$r_{12}=[(z_1-z_2')^2+b^2]^{\frac{1}{2}}, \tag{10}$$

$$r_{22}=[(z_2-z_2')^2+a_2^2]^{\frac{1}{2}}, \tag{11}$$

$$r_{21}=[(z_2-z_1')^2+b^2]^{\frac{1}{2}}. \tag{12}$$

a_1 is the radius, h_1 the half-length of antenna 1; a_2 is the radius, h_2 the half-length of antenna 2; b is the distance between centers of the parallel antennas as shown in Fig. 1.

Solutions of the differential equations[2] are:

$$A_{1z}=\frac{-j}{c}\Big[C_1\cos\beta z_1+\tfrac{1}{2}V_{10}^e\sin\beta|z_1| -z_1^{\,i}\int_0^{z_1} I_1(s)\sin\beta(z_1-s)ds\Big]; \tag{13}$$

$$A_{2z}=\frac{-j}{c}\Big[C_2\cos\beta z_2+\tfrac{1}{2}V_{20}^e\sin\beta|z_2| -z_2^{\,i}\int_0^{z_2} I_2(s)\sin\beta(z_2-s)ds\Big]. \tag{14}$$

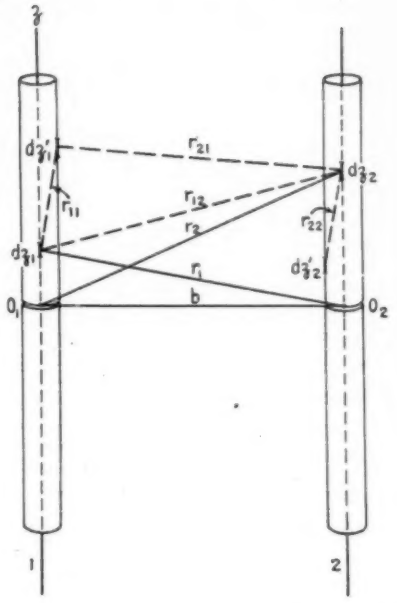

FIG. 1. Sections of two parallel antennas to illustrate the notation. (Primes should be on elements dz_1 and dz_2 on axis instead of at surface to agree with text.)

Here

$$c=1/(\Pi\Delta)^{\frac{1}{2}}\doteq3\times10^8\ \text{m/sec.};\qquad \Delta\equiv8.85\times10^{-12}\ \text{farad/m.} \tag{15}$$

V_{10}^e is the externally maintained driving-potential difference at the terminals of antenna 1; V_{20}^e is the driving-potential difference at the terminals of antenna 2. C_1 and C_2 are constants of integration.

If (3) is inserted at the left in (13) using (5) and (6), and (4) is used at the left in (14) with (7) and (8), two simultaneous integral equations in I_{1z} and I_{2z} are obtained. With

$$R_c\equiv(\Pi/\Delta)^{\frac{1}{2}}=376.7\doteq120\pi\ \text{ohms}, \tag{16}$$

they are

$$\int_{-h_1}^{h_1} I'_{1z}\frac{\exp(-j\beta r_{11})}{r_{11}}dz_1' +\int_{-h_2}^{h_2} I'_{2z}\frac{\exp(-j\beta r_{12})}{r_{12}}dz_2' =\frac{-j4\pi}{R_c}\Big[C_1\cos\beta z_1+\tfrac{1}{2}V_{10}^e\sin\beta|z_1| -z_1^{\,i}\int_0^{z_1} I_1(s)\sin\beta(z_1-s)ds\Big]; \tag{17}$$

$$\int_{-h_2}^{h_2} I_{2z}' \frac{\exp(-j\beta r_{22})}{r_{22}} dz_2' + \int_{-h_1}^{h_1} I_{1z}' \frac{\exp(-j\beta r_{21})}{r_{21}} dz_1'$$
$$= \frac{-j4\pi}{R_c}\left[C_2 \cos\beta z_2 + \tfrac{1}{2} V_{20}^e \sin\beta|z_2| - z_2^i \int_0^{z_2} I_2(s) \sin\beta(z_2 - s) ds \right]. \quad (18)$$

By solving these equations for I_{1z} and I_{2z} subject to the condition that currents vanish at the ends, the distributions of current in two parallel, center-driven antennas of small ratios a/h are determined. The input impedance for antenna 1 is given by

$$Z_{1in} = V_{10}/I_{10}. \quad (19)$$

By writing

$$V_{20} = -I_{20} Z_L \quad (20)$$

Z_{1in} gives the input impedance of a driven antenna in the presence of a parallel, parasitic antenna with impedance Z_L at its center.

SOLUTION FOR THE CURRENTS

The exact solution of (17) and (18) has not been accomplished. An approximate solution is obtained by using the method of successive approximations originally due to Hallén.[2,4] This proceeds from the expression,

$$\int_{-h}^{h} I_z' \frac{e^{-j\beta r}}{r} dz' = I_z \int_{-h}^{h} \frac{dz'}{r} + \int_{-h}^{h} \frac{I_z' e^{-j\beta r} - I_z}{r} dz'$$
$$= I_z[\Omega + \ln(1 - z^2/h^2) + \delta] + \int_{-h}^{+h} \frac{I_z' e^{-j\beta r} - I_z}{r} dz', \quad (21)$$

where

$$\Omega \equiv 2 \ln(2h/a), \quad (22)$$

$$\delta = \ln\left\{ \frac{1}{4}\left[\left(1 + \left(\frac{a}{h-z}\right)^2\right)^{\frac{1}{2}} + 1 \right] \times \left[\left(1 + \left(\frac{a}{h+z}\right)^2\right)^{\frac{1}{2}} + 1 \right] \right\}. \quad (23)$$

(δ is negligible except near the ends, $z = \pm h$, where $\int_{-h}^{h} \frac{dz'}{r}$ is finite approaching $\frac{1}{2}\Omega + \ln 2$ at the ends.) Upon substituting (21) with appropriate subscripts in (17) and solving for I_{1z} one obtains

$$I_{1z} = \frac{-j4\pi}{\Omega_1 R_c}\left\{ C_1 \cos\beta z_1 + \tfrac{1}{2} V_{10}^e \sin\beta|z_1| - z_1^i \int_0^{z_1} I_1(s) \sin\beta(z_1 - s) ds \right\}$$
$$- \frac{1}{\Omega_1}\left\{ I_{1z} \ln(1 - z_1^2/h_1^2) + I_{1z}\delta_1 + \int_{-h_1}^{h_1} \frac{I_{1z}' \exp(-j\beta r_{11}) - I_{1z}}{r_{11}} dz_1' + \int_{-h_2}^{h_2} I_{2z}' \frac{\exp(-j\beta r_{12})}{r_{12}} dz_2' \right\}. \quad (24)$$

The expression for I_{2z} is like (24) with 2 written for 1 and 1 for 2 in the subscripts. Since the current vanishes at the ends $z_1 = \pm h_1$ and $\ln(1 - z_1^2/h_1^2) + \delta_1$ remains finite there (24) reduces to the following at $z = h_1$.

$$0 = \frac{-j4\pi}{\Omega_1 R_c}\left\{ C_1 \cos\beta h_1 + \tfrac{1}{2} V_{10}^e \sin\beta h_1 - z_1^i \int_0^{h_1} I_1(s) \sin\beta(h_1 - s) ds \right\}$$
$$- \frac{1}{\Omega_1}\left\{ \int_{-h_1}^{h_1} I_{1z}' \frac{\exp(-j\beta r_{11h})}{r_{11h}} dz_1' + \int_{-h_2}^{h_2} I_{2z}' \frac{\exp(-j\beta r_{12h})}{r_{12h}} dz_2' \right\}. \quad (25)$$

Here

$$r_{11h} = [(h_1 - z_1')^2 + a_1^2]^{\frac{1}{2}}; \quad r_{12h} = [(h_1 - z_2')^2 + b^2]^{\frac{1}{2}}. \quad (26)$$

Upon subtracting (25) from (26),

[4] E. Hallén, Nova Acta Roy. Soc. Sci. (Upsala) **11**, 1 (1938).

$$I_{1z}=\frac{-j4\pi}{\Omega_1 R_c}\Big\{C_1[\cos\beta z_1-\cos\beta h_1]$$
$$+\tfrac{1}{2}V'_{10}[\sin\beta|z_1|-\sin\beta h_1]$$
$$-z_1{}^i\Big[\int_0^{z_1}I_1(s)\sin\beta(z_1-s)ds$$
$$-\int_0^{h_1}I_1(s)\sin\beta(h_1-s)ds\Big]\Big\}$$
$$-\frac{1}{\Omega_1}\Big\{I_{1z}\ln(1-z_1^2/h_1^2)+I_{1z}\delta_1$$
$$+\int_{-h_1}^{h_1}\frac{I'_{1z}\exp(-j\beta r_{11})-I_{1z}}{r_{11}}dz_1'$$
$$-\int_{-h_1}^{h_1}I'_{1z}\frac{\exp(-j\beta r_{11h})}{r_{11h}}dz_1'\Big\}$$
$$-\frac{1}{\Omega_1}\Big\{\int_{-h_2}^{h_2}I'_{2z}\frac{\exp(-j\beta r_{12})}{r_{12}}dz_2'$$
$$-\int_{-h_1}^{h_2}I'_{2z}\frac{\exp(-j\beta r_{12h})}{r_{12h}}dz_2'\Big\}. \quad (27)$$

The expression for I_{2z} is like (26) with subscripts 1 and 2 interchanged.

The evaluation of (27) may be carried out by the same method of successive approximations previously used[2] following Hallén.[4] It consists in using the leading terms in (27) as a zeroth order approximation of I_{1z} and substituting this value in the remaining terms to obtain the first-order approximation. Successive substitutions yield higher order terms. The following notation is used.

$$F_0(z_1)\equiv\cos\beta z_1,\quad G_0(z_1)\equiv\sin\beta|z_1|\,; \quad (28)$$

$$F_{0z_1}\equiv F_0(z_1)-F_0(h_1),\quad G_{0z_1}\equiv G_0(z_1)-G_0(h_1). \quad (29)$$

$$F_1(z_1)=-\Big\{F_{0z_1}\ln(1-z_1^2/h_1^2)+F_{0z_1}\delta_1$$
$$-\int_{-h_1}^{h_1}\frac{F'_{0z_1}\exp(-j\beta r_{11})-F_{0z_1}}{r_{11}}dz_1'$$
$$-\frac{j4\pi z_1{}^i}{R_c}\int_0^{z_1}F_{0s}\sin\beta(z_1-s)ds\Big\}\,; \quad (30)$$

$$F_1(h_1)=-\Big\{\int_{-h_1}^{h_1}F'_{0z_1}\frac{\exp(-j\beta r_{11h})}{r_{11h}}dz_1'$$
$$-\frac{j4\pi z_1{}^i}{R_c}\int_0^{h_1}F_{0s}\sin(h_1-s)ds\Big\}. \quad (31)$$

$$G_1(z_1)\text{ is like }F_1(z_1)\text{ with }G\text{ written for }F\,; \quad (32)$$

$$G_1(h_1)\text{ is like }F_1(h_1)\text{ with }G\text{ written for }F\,; \quad (33)$$

$$P_1(z_1)=-\int_{-h_2}^{h_2}F'_{0z_2}\frac{\exp(-j\beta r_{12})}{r_{12}}dz_2', \quad (34)$$

$$P_1(h_1)=-\int_{-h_2}^{h_1}F'_{0z_1}\frac{\exp(-j\beta r_{12h})}{r_{12h}}dz_2'\,; \quad (35)$$

$$Q_1(z_1)=-\int_{-h_2}^{h_2}G'_{0z_2}\frac{\exp(-j\beta r_{12})}{r_{12}}dz_2', \quad (36)$$

$$Q_1(h_1)=-\int_{-h_2}^{h_2}G'_{0z_2}\frac{\exp(-j\beta r_{12h})}{r_{12h}}dz_2'. \quad (37)$$

Also let

$$F_{1z_1}\equiv F_1(z_1)-F_1(h_1)\,;$$
$$G_{1z_1}\equiv G_1(z_1)-G_1(h_1)\,; \quad (38)$$
$$P_{1z_1}\equiv P_1(z_1)-P_1(h_1)\,;$$
$$Q_{1z_1}\equiv Q_1(z_1)-Q_1(h_1). \quad (39)$$

Expressions for F_{2z_1}, G_{2z_1}, P_{2z_1}, Q_{2z_1} may be obtained by increasing the subscripts on F, G, P, Q in (30)–(39) by 1. Formulas for use with I_{2z} are the same with subscripts 1 and 2 on z and h interchanged.

Using the above notation in (27) and a similar expression for I_{2z},

$$I_{1z}=\frac{-j4\pi}{\Omega_1 R_c}\Big\{C_1[F_{0z_1}+F_{1z_1}/\Omega_1+F_{2z_1}/\Omega_1{}^2+\cdots]$$
$$+\tfrac{1}{2}V'_{10}[G_{0z_1}+G_{1z_1}/\Omega_1+G_{2z_1}/\Omega_1{}^2+\cdots]$$
$$+C_2[P_{1z_1}/\Omega_1+P_{2z_1}/\Omega_1{}^2+\cdots]$$
$$+\tfrac{1}{2}V'_{20}[Q_{1z_1}/\Omega_1+Q_{2z_1}/\Omega_1{}^2+\cdots]\Big\}\,; \quad (40)$$

$$I_{2z}=\frac{-j4\pi}{\Omega_2 R_c}\Big\{C_2[F_{0z_2}+F_{1z_2}/\Omega_2+F_{2z_2}/\Omega_2{}^2+\cdots]$$
$$+\tfrac{1}{2}V'_{20}[G_{0z_2}+G_{1z_2}/\Omega_2+G_{2z_2}/\Omega_2{}^2+\cdots]$$
$$+C_1[P_{1z_2}/\Omega_2+P_{2z_2}/\Omega_2{}^2+\cdots]$$
$$+\tfrac{1}{2}V'_{10}[Q_{1z_2}/\Omega_2+Q_{2z_2}/\Omega_2{}^2+\cdots]\Big\}. \quad (41)$$

CURRENTS IN IDENTICAL ANTENNAS

The general formulas (40) and (41) can be solved very simply for I_{1z} and I_{2z} in identical antennas in two important special cases. These can then be combined to obtain expressions for the self- and mutual impedances in the general case for identical antennas.

1. Symmetrically Driven Identical Antennas

Let it be assumed that the driving-potential differences at the centers of the two antennas are equal and in phase so that

$$V_{10}^{e} = V_{20}^{e}. \tag{42}$$

Then

$$I_{1z} = I_{2z}; \quad C_1 = C_2. \tag{43}$$

In this case (40) and (41) are the same and equal to

$$I_{2z} = I_{1z} = \frac{-j4\pi}{\Omega R_c}\left\{ C_1\left[F_{0z} + \frac{1}{\Omega}(F_{1z} + P_{1z}) + \frac{1}{\Omega^2}(F_{2z} + P_{2z}) + \cdots \right] + \tfrac{1}{2} V_0^{e}\left[G_{0z} + \frac{1}{\Omega}(G_{1z} + Q_{1z}) + \frac{1}{\Omega^2}(G_{2z} + Q_{2z}) + \cdots \right] \right\}. \tag{44}$$

The constant C_1 can be evaluated by substituting (40) specialized to identical antennas in the integrals of (25). Thus

$$0 = \frac{-j4\pi}{\Omega R_c}\left\{ C_1\left[F_0(h_1) + \frac{1}{\Omega}\{F_1(h_1) + P_1(h_1)\} + \cdots \right] + \tfrac{1}{2} V_{10}^{e}\left[G_0(h_1) + \frac{1}{\Omega}\{G_1(h_1) + Q_1(h_1)\} + \cdots \right] \right\}, \tag{45}$$

or

$$C_1 = -\tfrac{1}{2} V_{10}^{e} \times \left\{ \frac{G_0(h_1) + \frac{1}{\Omega_1}[G_1(h_1) + Q_1(h_1)] + \cdots}{F_0(h_1) + \frac{1}{\Omega_1}[F_1(h_1) + P_1(h_1)] + \cdots} \right\}. \tag{46}$$

Upon substituting (46) in (44) the current is obtained in each of the two identical antennas driven in phase. The subscript s is used to designate the symmetrical case.

$$I_{zs} = \frac{j2\pi V_{0s}^{e}}{\Omega R_c}\left\{ \frac{\left\{ F_{0z} + \frac{1}{\Omega}[F_{1z} + P_{1z}] + \cdots \right\}\left\{ G_0(h) + \frac{1}{\Omega}[G_1(h) + Q_1(h)] + \cdots \right\} - \left\{ G_{0z} + \frac{1}{\Omega}[G_{1z} + Q_{1z}] + \cdots \right\}\left\{ F_0(h) + \frac{1}{\Omega}[F_1(h) + P_1(h)] + \cdots \right\}}{F_0(h) + \frac{1}{\Omega}[F_1(h) + P_1(h)] + \cdots} \right\}. \tag{47}$$

Collecting terms

$$I_{zs} = \frac{j2\pi V_{0s}^{e}}{\Omega R_c}\left\{ \frac{\sin\beta(h - |z|) + \frac{1}{\Omega}\left\{ G_0(h)[F_{1z} + P_{1z}] + F_{0z}[G_1(h) + Q_1(h)] - F_0(h)[G_{1z} + Q_{1z}] - G_{0z}[F_1(h) + P_1(h)] \right\} + \frac{1}{\Omega^2}\{\quad\}}{F_0(h) + \frac{1}{\Omega}[F_1(h) + P_1(h)] + \cdots} \right\}. \tag{48}$$

This is the final expression for the current in each of two identical antennas center-driven in phase by identical generators. The two antennas are parallel and account is taken of the radius of each antenna.

2. Antisymmetrically Driven Identical Antennas

Let it be assumed that the driving potential differences are equal and opposite so that

$$V_{20}^{e} = -V_{10}^{e}. \tag{49}$$

Then

$$I_{2z} = -I_{1z}; \quad C_2 = -C_1. \tag{50}$$

In this case the current in antenna 1 is:

$$-I_{2z} = I_{1z} = \frac{-j4\pi}{\Omega R_c}\left\{ C_1\left[F_{0z} + \frac{1}{\Omega}(F_{1z} - P_{1z}) + \cdots \right] \right.$$

$$+\tfrac{1}{2}V_{10}^{e}\left[G_{0z}+\frac{1}{\Omega}(G_{1z}-Q_{1z})+\frac{1}{\Omega^2}(G_{2z}-Q_{2z_1})\right]. \quad (51)$$

Since (51) differs from (44) only in having the signs of the P's and Q's reversed, the final formula for the current in the antisymmetrical case is obtained from (43) by reversing the signs of the P's and Q's. The subscript a is used to designate the antisymmetrical case.

$$I_{za}=\frac{j2\pi V_{0a}^{e}}{\Omega R_c}\left\{\frac{\sin\beta(h-|z|)+\frac{1}{\Omega}\{G_0(h)[F_{1z}-P_{1z}]+F_{0z}-[G_1(h)-Q_1(h)]-F_0(h)[G_{1z}-Q_{1z}]-G_{0z}[F_1(h)-P_1(h)]\}+\cdots}{F_0(h)+\frac{1}{\Omega}[F_1(h)-P_1(h)]+\cdots}\right\}. \quad (52)$$

3. Arbitrarily Driven Identical Antennas

Let antenna 1 be driven by a generator with driving potential difference

$$V_{10}^{e}=\tfrac{1}{2}(V_{0s}+V_{0a}) \quad (53)$$

while antenna 2 is driven by a generator with e.m.f.

$$V_{20}^{e}=\tfrac{1}{2}(V_{0s}-V_{0a}). \quad (54)$$

Appropriate values of V_{0s} and V_{0a} for arbitrary values of V_{10}^{e} and V_{20}^{e} may be obtained by solving (53) and (54) for V_{0s} and V_{0a}. The currents in the two antennas are obtained by superposition of the symmetrical and asymmetrical currents. Thus

$$I_{1z}=\tfrac{1}{2}(I_{zs}+I_{za}); \quad I_{2z}=\tfrac{1}{2}(I_{zs}-I_{za}). \quad (55)$$

The important case of a parasitic antenna with an arbitrary load Z_L at its center is obtained by writing

$$V_{20}^{e}=-I_{20}Z_L \quad (56)$$

in (54). If the load is zero, I_{2z} is obtained directly from (55) with $V_{0s}=V_{0a}$ in (54). It can be verified using the expressions for P_{1z} and Q_{1z} given in the Appendix that, for large values of b, I_{2z} derived in this way is the same as that previously obtained[3] for a receiving antenna 2 parallel to and in the far zone of a transmitting antenna 1 of the same length and radius. In particular, the leading term is easily obtained in the form

$$I_{2z}=j\frac{E}{\beta}\frac{4\pi}{\Omega R_c}\left(\frac{\cos\beta z_Z-\cos\beta h}{\cos\beta h}\right), \quad (57)$$

with

$$E=\frac{V_{10}^{e}}{\Omega\cos\beta h}(1-\cos\beta h)\frac{e^{-j\beta b}}{b}=-j\frac{R_c}{2\pi}\frac{I_{10}}{\sin\beta h}(1-\cos\beta h)\frac{e^{-j\beta b}}{b}. \quad (58)$$

Here E is the distant electric field due to the transmitting antenna 1. Further discussion of the distribution of current in coupled antennas is reserved for another paper.

INPUT ADMITTANCE

The input admittance of antenna 1 in the general case is defined by

$$Y_{1in}=\frac{I_{10}}{V_{10}^{e}}=\frac{(I_{0s}+I_{0a})}{V_{0s}^{e}+V_{0a}^{e}}=\frac{(V_{0s}^{e}Y_s+V_{0a}^{e}Y_a)}{V_{0s}^{e}+V_{0a}^{e}}. \quad (59)$$

The transfer admittance is

$$Y_t=\frac{I_{20}}{V_{10}^{e}}=\frac{(I_{0s}-I_{0a})}{V_{0s}^{e}+V_{0a}^{e}}=\frac{(V_{0s}^{e}Y_s-V_{0a}^{e}Y_a)}{V_{0s}^{e}+V_{0a}^{e}}. \quad (60)$$

Here

$$Y_s=\frac{1}{Z_s}=\frac{I_{0s}}{V_{0s}^{e}}; \quad Y_a=\frac{1}{Z_a}=\frac{I_{0a}}{V_{0a}^{e}}; \quad (61)$$

with I_{0s} given by (48) with $z=0$, I_{0a} given by (52) with $z=0$.

In the special case defined by

$$V_{0s}^{e}=V_{0a}^{e}, \quad (62)$$

$$(Y_{1in})_{V_s=V_a}\equiv Y_{11}'=\tfrac{1}{2}(Y_s+Y_a)=\frac{Z_a+Z_s}{2Z_sZ_a}, \quad (63)$$

$$(Y_t)_{V_s=-V_a} \equiv Y'_{12} = \tfrac{1}{2}(Y_s - Y_a) = \frac{Z_a - Z_s}{2Z_sZ_a}. \quad (64)$$

Hence

$$Y_s = Y'_{11} + Y'_{12}, \quad (65a)$$

$$Y_a = Y'_{11} - Y'_{12}. \quad (65b)$$

These values can be substituted in (59) and (60) for the general case

$$Y_{\text{lin}} = \left[\frac{Y'_{11}(V^e_{0s} + V^e_{0a}) + Y'_{12}(V^e_{0s} - V^e_{0a})}{V^e_{0s} + V^e_{0a}}\right] = \left[\frac{Y'_{11}V^e_{10} + Y'_{12}V^e_{20}}{V^e_{10}}\right], \quad (66)$$

$$Y_t = \left[\frac{Y'_{11}(V^e_{0s} - V^e_{0a}) + Y'_{12}(V^e_{0s} + V^e_{0a})}{V^e_{0s} + V^e_{0a}}\right] = \left[\frac{Y'_{11}V^e_{20} + Y'_{12}V^e_{10}}{V^e_{10}}\right]. \quad (67)$$

Accordingly,

$$I_{10} = V^e_{10}Y_{\text{lin}} = Y'_{11}V^e_{10} + Y'_{12}V^e_{20}, \quad (68a)$$

$$I_{20} = V^e_{10}Y_t = Y'_{12}V^e_{10} + Y'_{11}V^e_{20}, \quad (68b)$$

or, in matrix form,

$$\left\| \begin{matrix} I_{10} \\ I_{20} \end{matrix} \right\| = \left\| \begin{matrix} Y'_{11} & Y'_{12} \\ Y'_{12} & Y'_{11} \end{matrix} \right\| \left\| \begin{matrix} V^e_{10} \\ V^e_{20} \end{matrix} \right\|. \quad (69)$$

The input currents of both antennas and hence their input impedances are thus determined in the general case of two parallel, identical antennas center-driven or loaded in any way.

If antenna 2 is parasitic and center-loaded with an impedance Z_L, (56) may be used in (68b) solved for the current.

$$I_{20} = V^e_{10}Y'_{12}/(1 + Z_LY'_{11}). \quad (70)$$

Upon substituting this in (68a)

$$I_{10} = V^e_{10}\left(Y'_{11} - \frac{Y'^2_{12}Z_L}{1 + Z_LY'_{11}}\right) = V^e_{10}\left(\frac{Y'_{11} + Z_L(Y'^2_{11} - Y'^2_{12})}{1 + Z_LY'_{11}}\right). \quad (71)$$

The input admittance of antenna 1 in the presence of an arbitrarily loaded parasitic antenna is

$$Y_{\text{lin}} = \frac{I_{10}}{V^e_{10}} = \frac{Y'_{11} + Z_L(Y'^2_{11} - Y'^2_{12})}{1 + Z_LY'_{11}}. \quad (72)$$

INPUT IMPEDANCE

It is customary in antenna analyses to solve (69) and (70) for the driving-potential differences and to define self- and mutual impedances in terms of the resulting simultaneous equations. They are

$$V^e_{10} = I_{10}Z_{s1} + I_{20}Z_{12}, \quad (73a)$$

$$V^e_{20} = I_{10}Z_{21} + I_{20}Z_{s2}, \quad (73b)$$

with

$$Z_{s1} \equiv \frac{Y'_{11}}{Y'^2_{11} - Y'^2_{12}} = \frac{(Z_a + Z_s)/2Z_aZ_s}{[(Z_a + Z_s)^2 - (Z_a - Z_s)^2]/4Z_a^2Z_s^2} = \tfrac{1}{2}(Z_s + Z_a), \quad (74)$$

$$Z_{12} = \frac{-Y'_{12}}{Y'^2_{11} - Y'^2_{12}} = \frac{(Z_s - Z_a)/2Z_aZ_s}{[(Z_a + Z_s)^2 - (Z_a - Z_s)^2]/4Z_a^2Z_s^2} = \tfrac{1}{2}(Z_s - Z_a). \quad (75)$$

By definition the coefficient of I_{10} in (72) is the self-impedance Z_{s1} of antenna 1, the coefficient of I_{20} in (72) the mutual impedance Z_{12} of antenna 1.

If impedances Z_1 and Z_2 are connected in series with the antennas and their generators, it is necessary to replace

$$V^e_{10} \text{ by } V^e_{10} - I_{10}Z_1, \quad (76)$$

$$V^e_{20} \text{ by } V^e_{20} - I_{20}Z_2. \quad (77)$$

Then,

$$V^e_{10} = I_{10}(Z_{s1} + Z_1) + I_{20}Z_{12} = I_{10}Z_{11} + I_{20}Z_{12}, \quad (78a)$$

$$V^e_{20} = I_{10}Z_{12} + I_{20}(Z_{s1} + Z_2) = I_{10}Z_{12} + I_{20}Z_{22}. \quad (78b)$$

These are the conventional equations for two coupled circuits.

If antenna 2 is parasitic,

$$V^e_{20} = 0 \quad (79)$$

so that

$$V^e_{10} = I_{10}Z_{11} + I_{20}Z_{12}, \quad (80a)$$

$$0 = I_{10}Z_{12} + I_{20}Z_{22}. \quad (80b)$$

In this case the impedance seen by the generator is

$$Z_{1g}=Z_{11}-\frac{Z_{12}^2}{Z_{22}}. \tag{81}$$

The input impedance of the antenna is:

$$Z_{1\text{in}}=Z_{1g}-Z_1=Z_{s1}-\frac{Z_{12}^2}{Z_{s1}+Z_{22}}. \tag{82}$$

In the case considered $Z_{s2}=Z_{s1}$. If the parasitic antenna is not loaded

$$Z_{1\text{in}}=Z_{s1}-\frac{Z_{12}^2}{Z_{s1}}=\frac{2Z_sZ_a}{Z_s+Z_a}. \tag{83}$$

INPUT IMPEDANCE OF SYMMETRICALLY DRIVEN ANTENNAS

The input impedance Z_s of antenna 1 in the presence of antenna 2 when this is driven in phase by an identical generator is obtained from (48) with $z=0$. It is defined by:

$$(Z_{1\text{in}})_s\equiv Z_s\equiv\frac{V_{0s}^e}{I_{0s}}. \tag{84}$$

Using the notation (28) and (29) it is

$$Z_s=\frac{-j\Omega R_c}{2\pi}\left\{\frac{\cos\beta h+\frac{1}{\Omega}[(A_1^I+jA_1^{II})+(C_1^I+jC_2^{II})]+\frac{1}{\Omega_2}[\quad]+\cdots}{\sin\beta h+\frac{1}{\Omega}[(B_1^I+jB_1^{II})+(D_1^I+jD_2^{II})]+\frac{1}{\Omega^2}[\quad]+\cdots}\right\}. \tag{85}$$

The real and imaginary parts of the several functions are written explicitly. Thus

$$A_1^I+jA_1^{II}=F_1(h), \tag{86}$$

$$C_1^I+jC_1^{II}=P_1(h), \tag{87}$$

$$B_1^I+jB_1^{II}=F_1(0)+G_1(h), \tag{88}$$

$$D_1^I+jD_1^{II}=P_1(0)+Q_1(h). \tag{89}$$

For $h=\lambda/2$, $\beta h=\pi$

$$B_1^I+jB_1^{II}=G_1(h)+G_1(0), \tag{90}$$

$$D_1^I+jD_1^{II}=Q_1(h)+Q_1(0). \tag{91}$$

General expressions and numerical data for A_1^I, A_1^{II}, B_1^I, and B_1^{II} are given elsewhere.[5-7] Formulas for $P_1(0)$, $P_1(h)$, $Q_1(0)$, and $Q_1(h)$ are derived in the Appendix.

Curves for R_s and X_s in $Z_s=R_s+jX_s$ were computed from (85) neglecting terms in $1/\Omega^2$ and higher powers of $1/\Omega$ and neglecting terms involving the conductivity of the antenna. They are shown in Figs. 2 and 3 for $h=\lambda/4$; $\Omega=10$, 20, 30, ∞; and spacings up to $b=0.4\lambda$; in Figs. 4 and 5 for $h=\lambda/2$; $\Omega=10$, 20, 30; and spacings up to $b=0.5\lambda$. The calculations for R_s and X_s for $b/\lambda=0.05$ may be considerably in error because small differences occur and graphical integration

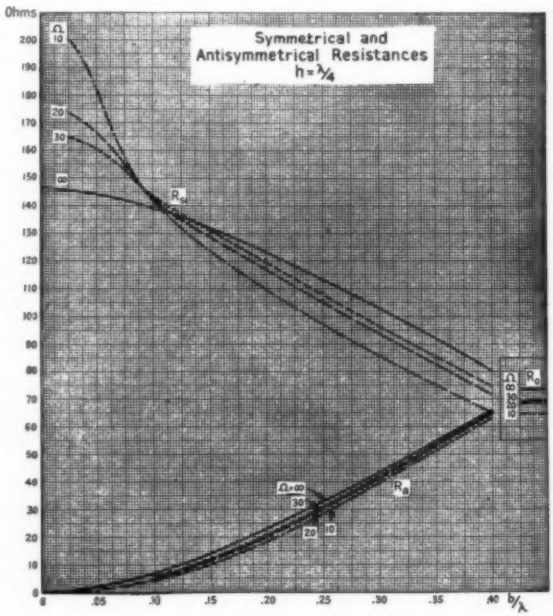

FIG. 2. Input resistance of a center-driven antenna in the presence of an identical antenna center-driven: (a) symmetrically, i.e., in phase, R_s; (b) antisymmetrically, i.e., 180° out of phase, R_a. Antenna half-length $h=\lambda/4$; radius a; $\Omega=2\ln(2h/a)$; spacing b. Self-resistances R_0 for infinite separation are shown at the right.

[5] R. King and F. G. Blake, Jr., Proc. I.R.E. **30**, 335–449 (1942). The limits in the formula for the integral cosine are incorrectly given. The lower limit should be ∞, not 0.

[6] R. King and C. W. Harrison, Jr., J. App. Phys. **15**, 170–185 (1944).

[7] C. W. Harrison, Jr., J. App. Phys. **14**, 537–544 (1943).

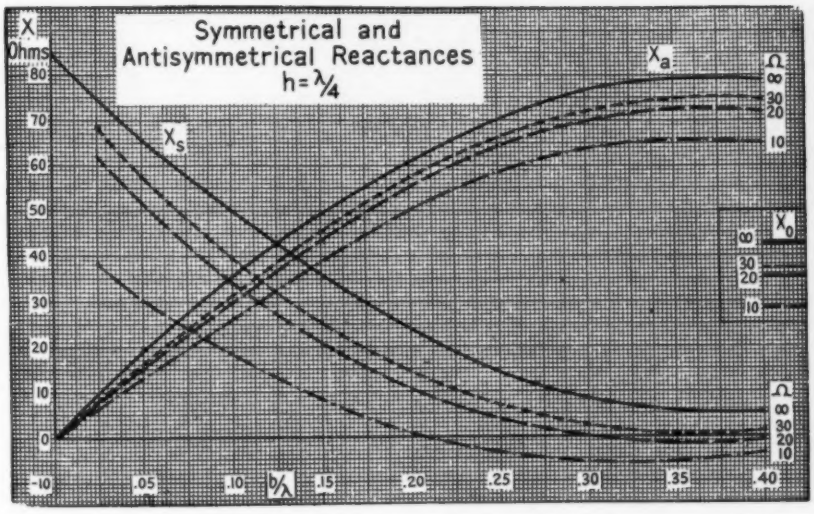

FIG. 3. Input reactances X and X_a corresponding to R_s and R_a of Fig. 2. Self-reactances X_0 for infinite separation are shown at the right.

was used for some terms as explained in the Appendix. The general trend is correctly indicated.

INPUT IMPEDANCE OF ANTISYMMETRICALLY DRIVEN ANTENNAS

The input impedance at the terminals of each of two identical antennas center-driven 180° out of phase by e.m.f.'s of equal magnitude is obtained from (52). By definition

$$(Z_{1\text{in}})_a = Z_a = \frac{V'_{0a}}{I_{0a}}, \tag{92}$$

so that

$$Z_a = \frac{-j\Omega R_c}{2\pi}\left\{\frac{\cos\beta h + \frac{1}{\Omega}[(A_1^I + jA_1^{II}) - (C_1^I + jC_1^{II})] + \frac{1}{\Omega^2}[\quad] + \cdots}{\sin\beta h + \frac{1}{\Omega}[(B_1^I + jB_1^{II}) - (D_1^I + jD_1^{II})] + \frac{1}{\Omega^2}[\quad] + \cdots}\right\}. \tag{93}$$

The same functions appear here as in the symmetrical case. Curves for R_a and X_a in $Z_a = R_a + jX_a$ as computed from (93) neglecting the same terms as in the case of R_s and X_s are also shown in Figs. 2 and 3 with $h = \lambda/4$, and in Figs. 4 and 5 with $h = \lambda/2$.

As a result of the theorem of uniqueness and the theorem of images the input impedance of a center-driven antenna parallel to and at a distance $b/2$ from a perfectly conducting plane is the same as (93). The impedance of an antenna in front of a large but not infinite conducting plane, or even a large metallic parabolic or paraboloidal reflector is probably given approximately by (93) if $b/2$ is the distance from the reflector.

SELF- AND MUTUAL IMPEDANCE

The general formulas (74) and (75) in the simple forms, $Z_{s1} = \frac{1}{2}(Z_s + Z_a)$; $Z_{12} = \frac{1}{2}(Z_s - Z_a)$ permit the computation of self- and mutual impedance of a center-driven antenna of length $2h$ and small radius a in the presence of an identical parallel antenna which may be either center driven or center loaded in an arbitrary way. The symmetrical and antisymmetrical impedances Z_s and Z_a are given by (85) and (93) so that formulas for Z_s and Z_a may be written down directly. Since these are long it is more convenient to evaluate Z_s and Z_a separately and then form Z_{1s} and Z_{12}.

An interesting exception is the mutual impedance of an extremely thin antenna in the range in which only the leading terms are required. Thus in the range where βh is not near $n\pi/2$ with n integral, the leading term is

$$Z_{s1} \doteq Z_s \doteq Z_a \doteq (-j\Omega R_c/2\pi)\cot\beta h. \tag{94}$$

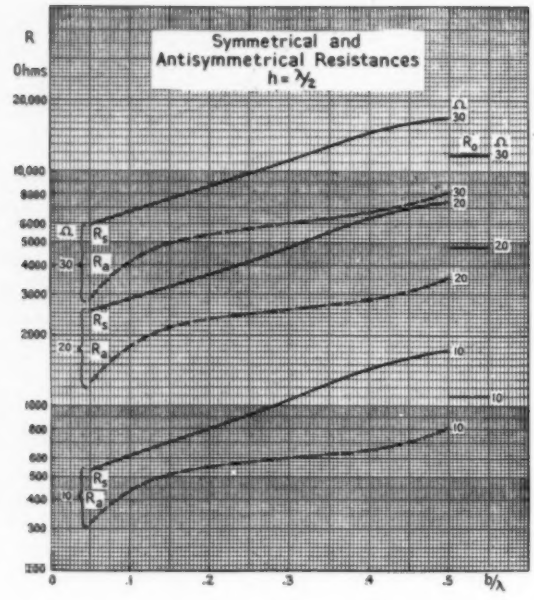

FIG. 4. Like Fig. 2 but with $h=\lambda/2$.

This is the same as the self-impedance Z_0* of a sufficiently thin isolated antenna in the range specified. At $\beta h=\pi/2$ the leading term is

$$Z_{s1}=\frac{-jR_e}{2\pi}(A_1{}^I+jA_1{}^{II}). \tag{95}$$

This is also the same as Z_0.†

The leading terms in the mutual impedance are

$$Z_{12}=\frac{-jR_e}{2\pi}[(C_1{}^I+jC_1{}^{II})\sin\beta h + (D_1{}^I+jD_1{}^{II})\cos\beta h]. \tag{96}$$

If $\beta h=\pi/2$, and using (87) with $P_1(h)$ as given in the Appendix,

$$\begin{aligned}Z_{12}&=\frac{-jR_e}{2\pi}(C_1{}^I+jC_1{}^{II})\\ &=\frac{R_e}{4\pi}[2Ci\beta b-Ci\beta\{[(2h)^2-b^2]^{\frac{1}{2}}+2h\}\\ &\qquad -Ci\beta\{[(2h)^2+b^2]^{\frac{1}{2}}-2h\}]\\ &\quad -\frac{jR_e}{4\pi}[2Si\beta b-Si\beta\{[(2h)^2+b^2]^{\frac{1}{2}}+2h\}\\ &\qquad -Si\{[(2h)^2+b^2]^{\frac{1}{2}}-2h\}].\end{aligned} \tag{97}$$

* See reference 2, Eq. (54).
† See reference 2, Eq. (60).

This agrees with the conventional formula derived under the assumption of sinusoidally distributed currents along both antennas using Poynting vector methods.[8]

Curves for the self- and mutual impedance computed from (74) and (75) for antennas of three practical ratios of h/a corresponding to $\Omega=2\ln(2h/a)=10$, 20, 30 are shown in Fig. 6 for $h=\lambda/4$. Curves for $\Omega=\infty$ are the same as curves commonly given for this length under the assumption that currents in both antennas are sinusoidal.[8,9]

Curves corresponding to those of Fig. 6 are given in Figs. 7 and 8 for $h=\lambda/2$ and with $\Omega=10$, 20, 30. The range of X_{12} near zero is shown in Fig. 9. The case $\Omega=\infty$ has no meaning for this length because the input current vanishes.

It is seen from Figs. 6–8 that the self-impedance of an antenna is independent of the location of a coupled antenna only in a physically unavailable antenna of zero radius and half-

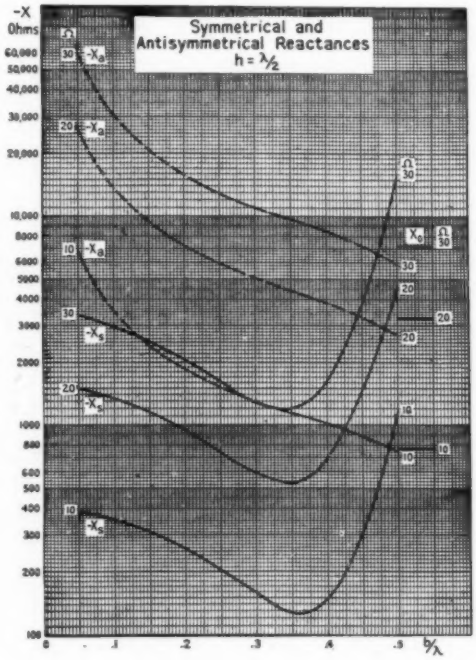

FIG. 5. Like Fig. 3 but with $h=\lambda/2$.

[8] See, for example, G. H. Brown and R. King, Proc. I.R.E. **22**, 471 (1934).
[9] See, for example, F. E. Terman, *Radio Engineers' Handbook* (McGraw-Hill Book Company, Inc., New York, 1943), Fig. 13, p. 780.

length $h=\lambda/4$. In all practical antennas the self-impedance varies with the location of a coupled antenna because the distribution of current in the antenna changes. For antennas of half-length $h=\lambda/4$, the self-impedance Z_{s1} remains nearly constant at the value Z_0 for an isolated antenna except for very close spacings. The mutual impedance of an antenna of half-length $h=\lambda/4$ does not differ greatly from that computed on the assumption of sinusoidally distributed currents in both antennas except with small separation of the antennas. For lengths differing appreciably from $h=\lambda/4$ the assumption of sinusoidally distributed currents is incorrect even for an infinitely thin antenna.

INPUT IMPEDANCE OF ANTENNA WITH UNLOADED PARASITE

The input impedance of a symmetrical, center-driven antenna near a parallel, unloaded parasitic antenna of the same length and radius used as reflector or director is given by (83). Curves for R_{in} and X_{in} are shown in Fig. 10 for $h=\lambda/4$ and $\Omega=10, 20, 30, \infty$ for spacings up to $b=0.4\lambda$; in Fig. 11 for $h=\lambda/2$, $\Omega=10, 20, 30$, for b up to 0.5λ. The curves in Fig. 10 for $h=\lambda/2$, $\Omega=\infty$ are those commonly used.[10] The curves of Fig. 11 for $h=\lambda/2$ are interesting because they show only an extremely small change in the input impedance of the driven antenna for any position of the unloaded parasite. Since the parasite is of such length that it is nearly antiresonant, the current I_{2z} is small and the effect of the parasite both on the input impedance of the driven antenna and on the field pattern is almost negligible. It is well to bear in mind that with $h=\lambda/2$ the leading term in the distribution of current in the driven antenna has the form $I_{1z}\sim\sin\beta|z|$, that in the parasite $I_{2z}\sim\cos\beta|z|+1$. Accordingly I_{1z} is maximum nearly $\lambda/4$ from the center and the ends, minimum near the driving point; whereas I_{2z} is maximum at the center. The maximum current at the center of the parasite is of the same order of magnitude as the minimum current of the driven antenna. From (80b) one has with $Z_{22}=Z_{s1}$

$$\frac{I_{20}}{I_{10}}=-\frac{Z_{12}}{Z_{s1}}. \tag{98}$$

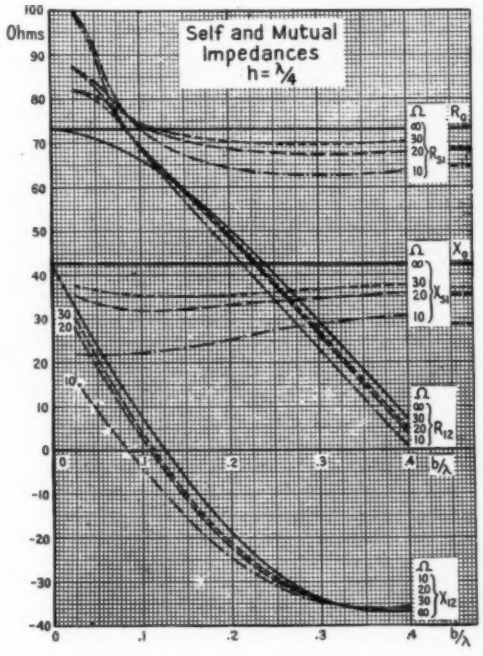

FIG. 6. Self-impedance $Z_{s1}=R_{s1}+jX_{s1}$ and mutual impedance $Z_{12}=R_{12}+jX_{12}$ for parallel identical antennas of half-length $h=\lambda/4$ and spacing b.

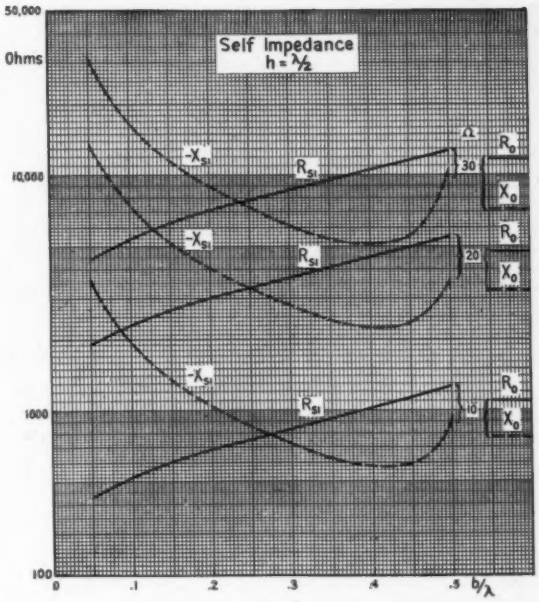

FIG. 7. Self-impedance $Z_{s1}=R_{s1}+jX_{s1}$ as in Fig. 6 but for $h=\lambda/2$.

[10] For example, they are involved in all cases of parasitic antennas in the detailed analyses by G. H. Brown, Proc. I.R.E. 25, 78–145 (1937).

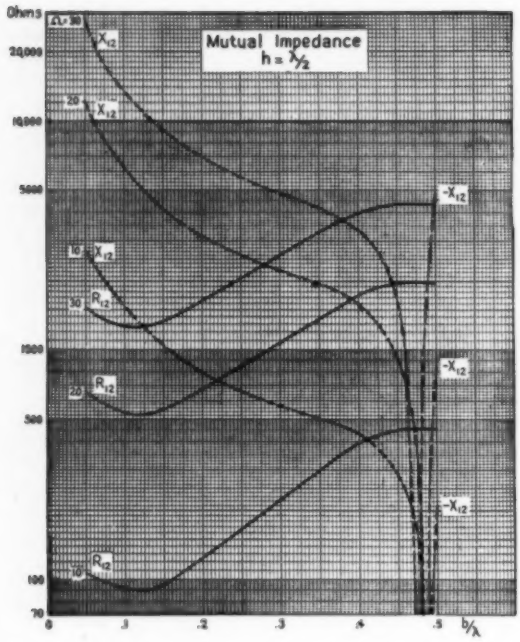

FIG. 8. Mutual impedance $Z_{12}=R_{12}+jX_{12}$ as in Fig. 6 but for $h=\lambda/2$.

Values of Z_{12} and Z_{s1} may be obtained from Figs. 7 and 8.

INPUT IMPEDANCE OF ANTENNA WITH TUNED PARASITE

A parasitic antenna of half-length $h=\lambda/2$ is so far from self-resonance that only a very small current flows. If a tuning reactance consisting of a coil and condenser at low frequencies or a section of transmission line at high frequencies is connected at the center of the parasitic antenna, and the impedance Z_L of this tuning section is adjusted so that

$$X_L=-X_0, \tag{99}$$

where X_0 is the self-reactance of the parasite when isolated and center driven, the current in the parasite will increase to large values. This has already been shown for receiving antennas.[3] Usually the resistance R_L of the tuning reactance is small compared with the self-resistance R_0 of the antenna so that a good analytical approximation is obtained with

$$Z_L \doteq jX_L=-jX_0. \tag{100}$$

Curves for R_{in} and X_{in} of the driven antenna in the presence of a parallel, self-resonant parasitic antenna of the same length $2h=\lambda$ and radius a are shown in Fig. 12 for $\Omega=10$, 20, 30 and for spacings up to $b=0.5\lambda$. Comparison with Fig. 11, which differs only in having $Z_L=0$ instead of $Z_L=-jX_0$, shows the importance of the tuning reactance. It is because the tuned parasite carries large currents distributed with a leading term $I_{2z}\sim\sin\beta|z|$ that it has a significant effect on the field pattern.

INPUT IMPEDANCE OF ANTENNA ERECTED VERTICALLY OVER A PERFECTLY CONDUCTING HALF-SPACE

The entire analysis applies correctly to base-driven and base-loaded antennas of full length h erected vertically over a perfectly conducting half-space if all impedances are divided by 2.

CONCLUSION

A theory for two coupled antennas which are alike in length and radius has been given. All curves have been computed neglecting terms in $1/\Omega^2$ and higher and quantitative accuracy may be expected only when these terms are actually negligible. Brillouin[11] indicates that $1/\Omega^2$ terms

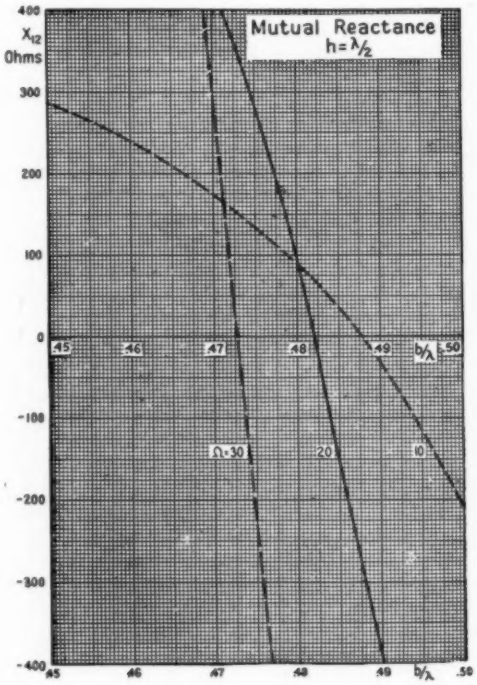

FIG. 9. Range of X_{12} in Fig. 8 near $X_{12}=0$.

[11] L. Brillouin, Quart. App. Math. 1, 201 (1943).

cannot be assumed negligible unless Ω is at least greater than 14. Computations by Bouwkamp[12] for $1/\Omega^2$ terms in Hallén's[4, 5] formula for self-impedance show that these contribute significantly for Ω as small as 10. Glas[13] suggests that for small values of Ω the series in the self-impedance may converge so slowly and oscillate in such a way that the first approximation stopping with terms in $1/\Omega$ may be a better one than if terms in $1/\Omega^2$ are included. In any event it may be concluded that computations for self-impedance and particularly for mutual impedance based on the integration in powers of $1/\Omega$ of the integral equations (17) and (18) are very much better approximations than values based on sinusoidal currents. On the other hand precise quantitative agreement with experiment should not be expected for Ω less than 14 or possibly even larger. It is to be noted that Hallén's formula for self-impedance without terms in $1/\Omega^2$ or higher can be brought into good agreement with the very limited available experimental data for cylinders and with results computed by Schelkunoff[14, 15] if the average values,

$$\Omega_a = 2\left(\ln\frac{2h}{a} - 1\right) \quad \text{of} \quad \int_{-h}^{h}\frac{dz'}{r},$$

in (21) are used instead of the maximum value[16]

$$\Omega = 2\ln\frac{2h}{a}.$$

A similar correction may be necessary in the analysis for mutual impedance since it depends on the self-impedance. This is very easily accomplished by substituting $\Omega_a = \Omega - 2$ for Ω in the several figures.

The present analysis is limited to two parallel antennas of the same length and radius. Extension to more than two antennas is easily formulated, but even the approximate solution of three or more simultaneous integral equations is difficult. The above analysis for two antennas indicates that thin antennas in any number but all of half-length $h = \lambda/4$ may be analyzed roughly for spacings that are not too small by assuming sinusoidal distributions of current in all. For

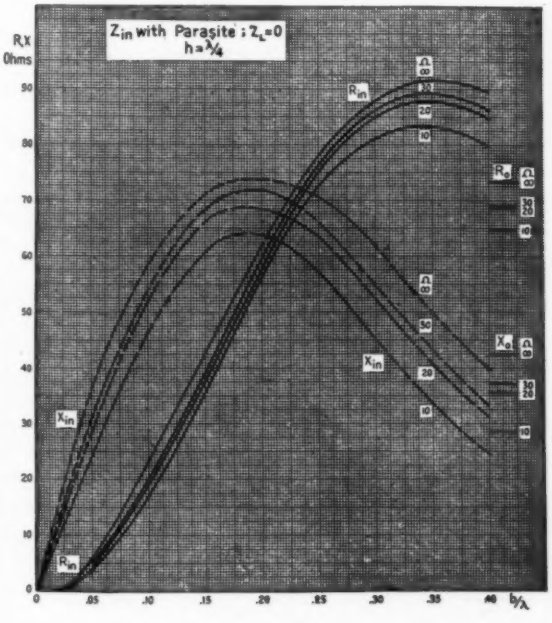

FIG. 10. Input impedance $Z_{in} = R_{in} + jX_{in}$ of a center-driven antenna in the presence of an unloaded parallel parasitic antenna of the same dimensions. $h = \lambda/4$.

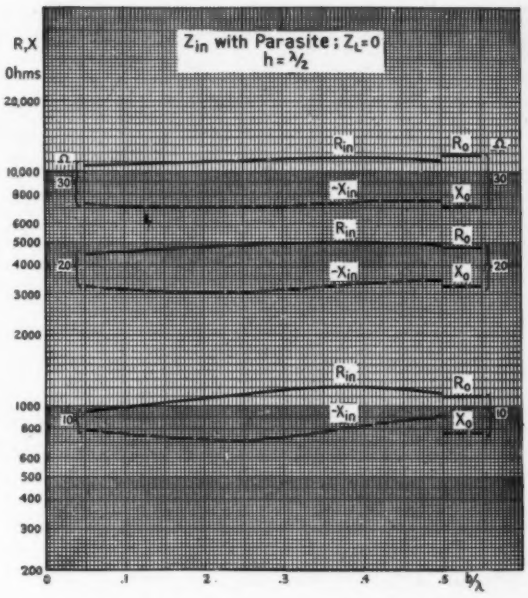

FIG. 11. Like Fig. 10 but with $h = \lambda/2$.

[12] C. J. Bouwkamp, Physica **9**, 609 (1942).
[13] Erik T. Glas, "On radiation problems concerning vertical antennas," dissertation, Royal Administration of Swedish Telegraphs (Stockholm, 1943).

[14] S. A. Schelkunoff, Proc. I.R.E. **29**, 493–520 (1941).
[15] S. A. Schelkunoff, J. App. Phys. **15**, 54–60 (1944).
[16] M. C. Gray, J. App. Phys. **15**, 61–65 (1944).

other lengths and thick antennas the sinusoidal distribution is not adequate. An approximate analysis of two antennas of different lengths is in preparation.

The writers are indebted to Mr. Roger Clapp and to Dr. A. H. Wing, Jr., for independently suggesting a solution using symmetrical and antisymmetrical components. Mr. Clapp worked on the problem while a graduate student at Cruft Laboratory several years ago.

APPENDIX

The computation of self- and mutual impedance depends upon the evaluation of the integrals (34) and (36) with $z_1=0$ and $z_1=h$. They are:

$$P_1(z_1)=-\int_{-h_2}^{h_2}(\cos\beta z_2'-\cos\beta h_2)\times\frac{\exp\{-j\beta[(z_1-z_2')^2+b^2]^{\frac{1}{2}}\}}{[(z_1-z_2')^2+b^2]^{\frac{1}{2}}}dz_2'; \quad (101)$$

$$Q_1(z_1)=-\int_{-h_2}^{h_2}(\sin\beta|z_2'|-\sin\beta h_2)\frac{\exp\{-j\beta[(z_1-z_2')^2+b^2]^{\frac{1}{2}}\}}{[(z_1-z_2')^2+b^2]^{\frac{1}{2}}}dz_2'. \quad (102)$$

There are two integrals in (95) which may be integrated as follows:

$$I_1=\tfrac{1}{2}\int_{-h_2}^{h_2}[\exp(j\beta z_2')+\exp(-j\beta z_2')]\frac{\exp(-j\beta R_1)}{R_1}dz_2'; \quad R_1=[(z_1-z_2')^2+b^2]^{\frac{1}{2}} \quad (103)$$

$$=\frac{\exp(j\beta z_1)}{2}\int_{-h_2}^{h_2}\frac{\exp[-j\beta(R_1-z_2'+z_1)]}{R_1}dz_2'+\frac{\exp(-j\beta z_1)}{2}\int_{-h_2}^{h_2}\frac{\exp[-j\beta(R_1+z_2'-z_1)]}{R_1}dz_2'$$

$$=-\frac{\exp(j\beta z_1)}{2}\int_{u_1}^{u_2}\frac{e^{-ju}}{u}du+\frac{\exp(-j\beta z_1)}{2}\int_{v_1}^{v_2}\frac{e^{-jv}}{v}dv. \quad (104)$$

Here,

$$u_1\equiv j(\chi+\delta); \quad u_2=j(\bar{\chi}+\bar{\delta}); \quad (105a)$$

$$v_1\equiv j(\chi-\delta); \quad v_2=j(\bar{\chi}-\bar{\delta}); \quad (105b)$$

with

$$\chi\equiv\beta\{[(z_1+h_2)^2+b^2]^{\frac{1}{2}}\}; \quad \delta\equiv\beta(z_1+h_2); \quad (105c)$$

$$\bar{\chi}\equiv\beta\{[(z_1-h_2)^2+b^2]^{\frac{1}{2}}\}; \quad \bar{\delta}\equiv\beta(z_1-h_2). \quad (105d)$$

The integrals in (104) are expressible directly in terms of integral sines and cosines.

$$I_1=\frac{\exp(j\beta z_1)}{2}[\mathrm{Ci}(\chi+\delta)-Ci(\bar{\chi}+\bar{\delta})-jSi(\chi+\delta)+jSi(\bar{\chi}+\bar{\delta})-\frac{\exp(-j\beta z_1)}{2}[Ci(\chi-\delta)-Ci(\bar{\chi}-\bar{\delta})-jSi(\chi-\delta)+jSi(\bar{\chi}-\bar{\delta}). \quad (106)$$

The second integral in (101) is:

$$I_2=\int_{-h_2}^{h_2}\frac{\exp(-j\beta R_1)}{R_1}dz_2'=\int_{\bar{\delta}}^{\delta}\frac{\exp[-j(U^2+V^2)^{\frac{1}{2}}]}{(U^2+V^2)^{\frac{1}{2}}}dU. \quad (107)$$

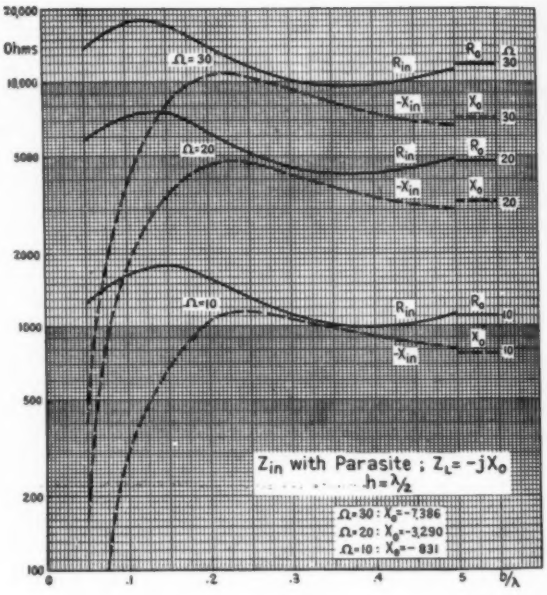

FIG. 12. Like Fig. 11 but with $Z_L=-jX_0$ so that the parasite is self-resonant when isolated.

Rearranging and introducing the symbols,

$$Cuv\,\delta\equiv\int_0^{\delta}\frac{\cos(U^2+V^2)^{\frac{1}{2}}}{(U^2+V^2)^{\frac{1}{2}}}dU, \quad (108)$$

$$Suv\,\delta\equiv\int_0^{\delta}\frac{\sin(U^2+V^2)^{\frac{1}{2}}}{(U^2+V^2)^{\frac{1}{2}}}dU. \quad (109)$$

(Note that $Cuv(-\delta)=-Cuv\,\delta$; $Suv(-\delta)=-Suv\,\delta$.)

$$I_2=Cuv\,\delta-Cuv\,\bar{\delta}-j\,Suv\,\delta+j\,Suv\,\bar{\delta}. \quad (110)$$

Then

$$P_1(z_1)=-(I_1-I_2\cos\beta h_2). \quad (111)$$

The two integrals in (102) may be evaluated in a similar way but care must be taken to take proper account of $|z_2'|$.

$$I_3=\frac{1}{2j}\int_{-h_2}^{h_2}[\exp(j\beta|z_2'|)-\exp(-j\beta|z_2'|)]\frac{\exp(-j\beta R_1)}{R_1}dz_2'; \quad (112)$$

$$I_3=\frac{-j\exp(j\beta z_1)}{2}\int_0^{h_2}\frac{\exp[-j\beta(R_1-z_2'+z_1)]}{R_1}dz_2'+\frac{j\exp(-j\beta z_1)}{2}\int_0^{h_2}\frac{\exp[-j\beta(R_1+z_2'-z_1)]}{R_1}dz_2'-\frac{j\exp(-j\beta z_1)}{2}\int_0^{h_2}\frac{\exp[-j\beta(R_2-z_2'-z_1)]}{R_2}dz_2'+\frac{j\exp(j\beta z_1)}{2}\int_0^{h_2}\frac{\exp[-j\beta(R_2+z_2'+z_1)]}{R_2}dz_2'. \quad (113)$$

Here

$$R_1=[(z_2'-z_1)^2+b^2]^{\frac{1}{2}}; \quad R_2=[(z_2'+z_1)^2+b^2]^{\frac{1}{2}}. \quad (114)$$

Changing variables

$$I_3=\frac{j}{2}\Big[\exp(j\beta z_1)\int_{u_0}^{u_1}\frac{e^{-ju}}{u}du+\exp(-j\beta z_1)\int_{v_0}^{v_1}\frac{e^{-jv}}{v}dv+\exp(-j\beta z_1)\int_{v_0}^{v_2}\frac{e^{-jv}}{v}dv+\exp(j\beta z_1)\int_{u_0}^{u_2}\frac{e^{-ju}}{u}du\Big]. \quad (115)$$

The limits u_1 and u_2 are as defined in (105).

$$u_0=j(\chi_0+\delta_0);\quad v_0=j(\chi_0-\delta_0); \tag{116a}$$

with

$$\chi_0=\beta(z_1^2+b^2)^{\frac{1}{2}};\quad \delta_0=\beta z_1. \tag{116b}$$

In terms of integral sines and cosines (115) has the form

$$\begin{aligned}I_3=&\frac{-j\exp(j\beta z_1)}{2}[2Ci(\chi_0+\delta_0)-2jSi(\chi_0+\delta_0)\\&-Ci(\chi+\delta)+jSi(\chi+\delta)-Ci(\bar{\chi}+\bar{\delta})+jSi(\bar{\chi}+\bar{\delta})]\\&\frac{-j\exp(-j\beta z_1)}{2}[2Ci(\chi_0-\delta_0)-2jSi(\chi_0+\delta_0)\\&-Ci(\chi-\delta)+jSi(\chi-\delta)\\&-Ci(\bar{\chi}-\bar{\delta})+jSi(\bar{\chi}-\bar{\delta})].\end{aligned} \tag{117}$$

The last integral in (102) is the same as I_2. Hence

$$Q_1(z_1)=-(I_3-I_2\sin\beta h_2). \tag{118}$$

In order to specialize to $P_1(h_1)$ and $Q_1(h_1)$ with $h_2=h_1=h$ the following are used in (111) and (118):

$$z_1=h_1=h;\quad h_2=h.$$

$$\chi=\beta\{[(2h)^2+b^2]^{\frac{1}{2}}\};\quad \delta=2\beta h; \tag{119a}$$

$$\bar{\chi}=\beta b;\qquad \bar{\delta}=0; \tag{119b}$$

$$\chi_0=\beta(h^2+b^2)^{\frac{1}{2}};\qquad \delta_0=\beta h. \tag{119c}$$

In order to specialize to $P_1(0)$ and $Q_1(0)$ with $h_2=h_1=h$ the following are used in (111) and (109)

$$z_1=0;\qquad h_2=h; \tag{120a}$$

$$\chi=\beta(h^2+b^2)^{\frac{1}{2}}=\chi;\quad \delta=\beta h=-\bar{\delta}; \tag{120b}$$

$$\chi_0=\beta b;\qquad \delta_0=0. \tag{120c}$$

In calculating the impedance curves the functions *Cuv* 2*H* and *Suv* 2*H* which occur in $P_1(h)$ and $Q_1(h)$ were evaluated graphically. The values previously computed[17] had to be extended somewhat.[18]

Tables for the functions *Cuv* δ and *Suv* δ as defined in (108) and (109) are being computed by the new calculating machine at Harvard University for a range of V extending from 0 to 2π in steps of 0.01 and a range of δ from 0 to 2π in steps of 0.5. The intention is to publish them in this journal as soon as the calculations are completed.

[17] C. W. Harrison, Jr., J. App. Phys. **14**, 306–309 (1943).

[18] In a private communication Dr. Sidney Weinbaum has kindly supplied the following series which may be used for computing *Cuv* δ and *Suv* δ. It converges rapidly for short antennas.

$$\begin{aligned}\int_0^h\frac{\exp[-j\beta(z^2+r^2)^{\frac{1}{2}}]}{(z^2+r^2)^{\frac{1}{2}}}dz=&\tfrac{1}{2}\ln\frac{(h^2+r^2)^{\frac{1}{2}}+h}{(h^2+r^2)^{\frac{1}{2}}-h}J_0(\beta r)\\&+\sum_{p=1}^{\infty}\frac{h}{4(h^2+r^2)^{\frac{1}{2}}}\frac{(-1)^p}{(p!)^2}\left(\frac{\beta r}{2}\right)^{2p}\\&\times\left[\sum_{\mu=1}^{p}\frac{(\mu-1)!}{\mu(\mu+1)\cdots(2\mu-1)}\left(\frac{4h^2+r^2}{r^2}\right)^{\mu}\right]\\&+j\sum_{p=0}^{\infty}(-1)^p\beta h\left[\frac{(2\beta r)^p}{(p+1)(p+2)\cdots(2p+1)}\right]^2\\&\left[1+\sum_{\nu=1}^{p}\frac{(\nu+1)(\nu+2)\cdots 2\nu}{\nu!}\left(\frac{h^2+r^2}{4r^2}\right)^{\nu}\right].\end{aligned}$$

On the Destructive Action of Cavitation

M. Kornfeld and L. Suvorov
The Leningrad Physico-Technical Institute, Leningrad, U.S.S.R.

(Received January 25, 1944)

I. INTRODUCTION

Historical Survey

CAVITATIONAL phenomena were first described by Osborne Reynolds[1] in a paper dated 1894. Reynolds observed these phenomena in water flowing through a tube with a local constriction. In accordance with Bernoulli's law a region of lowered pressure is formed in the narrow part of the tube.

If the rate of the current is sufficiently great, the pressure falls to a value corresponding to the vapor pressure which causes the boiling of the water in the narrow cross section of the tube. The bubbles thus formed may be considered practically "empty," as the water vapor pressure at room temperature is only 0.02 atmos. These empty bubbles, or cavities, as they are usually called, carried along by the current, come into a region of increased pressure, collapse, and vanish. The collapse of a separate bubble which proceeds at a very high rate is accompanied by a kind of a "hydraulic blow" which causes a sound (a click). The clicks of a large number of bubbles unite into one continuous sound which we usually hear when water flows through a tube with a local constriction.

Several years after Reynolds' paper was published, a very strange destruction of the screw propellers of fast steam boats was observed. Such destruction of screws of the ocean liners *Lusitania* and *Mauretania* were described by Silberrad[2] in 1912. Other examples of destruction of screw propellers were given by Ramsay[2,3a] in the same

[1] O. Reynolds, Sci. Pap. **2**, 587 (1894).

[2] D. Silberrad, Engineering, p. 34 (1912).

[3] W. Ramsay, Engineering, p. 687 (1912).

[3a] Thum, *Hydraulische Probleme* (Berlin, 1926), Section 68.

year. These extremely intensive destructions take place only when the ship is in motion. In several cases only a few hours of running are sufficient to make the propeller absolutely unfit for work.

Almost simultaneously with the discovery of the destruction of propeller screws an analogous phenomenon was observed in hydroturbines and other hydrotechnical constructions. The parts of these constructions which move in water or come into direct contact with a water current receive heavy damage, very much like the destruction of propeller screws.

In 1915 a special commission was instituted by the British Admiralty whose aim was to ascertain the cause of the destruction of propellers. According to Parsons and Cook,[4] who published in 1919 a short summary of the work of this commission, the destruction of the screws takes place as a result of the numerous repeated "hydraulic blows" accompanying the collapse of cavities.* Somewhat later Föttinger[5] came to the same conclusion in regard to hydrotechnical constructions.

The first attempt to give a theory of the destructive action of cavities was made by Cook.[4] In 1917 Rayleigh[6] improved and completed this theory. After Rayleigh's work all theoretical development of the problem considered was suspended. Until the present time nothing new has been done in this direction.

The experimental investigations also begin from the work of Parsons and Cook, who attempted, in particular, to discover the destructive action of cavities which arise when water flows through a pipe with a local constriction. These experiments were not successful. Several years later Föttinger[5] and then Schrötter, Haller,[7] Mousson[8] obtained the desired results by using similar though incomparably more effective arrangements in which the cross section of the pipe in the narrow part was a few square centimeters, and the velocity of the water reached 100 m/sec. By placing a specimen of the material under investigation in the path of the movement of cavities, these authors obtained intensive destruction of a series of metals and alloys. The period of time necessary to obtain noticeable destruction varied in these experiments from 10 to 100 hours.

In 1932 Gaines[9] worked out a new way of obtaining cavitational destruction. By making use of the magnetostriction effect, Gaines excited intense longitudinal vibrations in a nickel rod. When the vibrating rod is immersed in water, cavities appear on the end surface of the former and the surface itself is intensively destroyed. These effects are caused by the variable pressures arising in water near the vibrating end of the rod. During that part of the period when the pressure falls to the value corresponding to the vapor pressure, cavities are formed. During the remaining part of the period the pressure increases, while the cavities collapse and disappear. Gaines' method was improved by Hunsaker[10] and used by Kerr,[11] who obtained intensive destruction of various metals and alloys during a time interval of about 1 hour.

It should be pointed out, in conclusion, that the chief object of the experimental investigation of the above-mentioned authors was to find materials which could withstand sufficiently the action of cavitation. From this point of view the investigations of Mousson and Kerr are especially valuable, as they examined several hundreds of technically important materials.

Conception of the Mechanism of the Destructive Action of Cavities

First of all, let us consider the work of Cook and Rayleigh already mentioned.

According to Cook, the destructive action of cavities is caused by the direct blows of the liquid against the surface of the solid body. Without considering the actual conditions under which such blows can exist, Cook calculates the value of the pressures arising during the collision of water with the surface of a solid sphere placed in the center of a collapsing cavity, Fig. 1a. This calculation is, of course, of no practical value. In reality one can speak of the blow of a liquid which takes place when a cavity "sitting" on the surface of a solid body collapses (Fig. 1b). However, in this case the blow takes place only at the moment when the cavity disappears completely, which theoretically corresponds to infinite pressures. Thus for surface cavities Cook's problem is not clear.

Rayleigh attempted to eliminate the difficulties of Cook's theory by showing that very considerable pressures may arise not only as a result of a direct blow of the liquid but also because of a "free" collapse of cavities located at some distance from the surface (Fig. 1c). The following problem is considered by Rayleigh. In an infinite mass of liquid, under a constant pressure a spherical portion is suddenly annihilated. The rate of collapse of the cavity formed and the pressure in its vicinity are to be calculated.

Assuming the liquid to be incompressible, neglecting viscosity, and supposing that there is an absolute vacuum within the cavity, Rayleigh obtains the following results.

The radial velocity of the contraction of the cavity is equal to

$$U_R=\left\{\frac{2}{3}\frac{P}{\rho}\left[\left(\frac{R_0}{R}\right)^3-1\right]\right\}^{\frac{1}{2}}, \qquad (1)$$

where P is the hydrostatic pressure, ρ is the density of the liquid, R_0 is the initial radius of the cavity, and R is the radius of the cavity at the moment under consideration.

The pressure arising in the vicinity of the cavity has a maximum at a distance of $1.57R$ from its center and is

[4] C. A. Parsons and S. S. Cook, Engineering, pp. 107, 501, 515 (1919).

* This point of view had already been expressed by Silberrad, reference 2, but less definitely.

[5] H. Föttinger, *Hydraulische Probleme* (Berlin, 1926), Section 27.

[6] Lord Rayleigh, Phil. Mag. **34**, 94 (1917).

[7] P. de Haller, Schweiz. Bauzeit. **101**, 243 (1933).

[8] J. M. Mousson, Trans. A. S. M. E. **59**, 399 (1937).

[9] N. Gaines, Physics **3**, 209 (1932).

[10] L. Hunsaker, Trans. A. S. M. E. **57**, 423 (1935).

[11] S. L. Kerr, Trans. A. S. M. E. **59**, 373 (1937).

FIG. 1.

equal in this region to

$$P_R \leqq 0.163\left(\frac{R_0}{R}\right)^3 \cdot P. \tag{2}$$

Using Rayleigh's results it is easy to solve Cook's problem. When a liquid and a solid body collide a pressure arises in the plane of collision equal to:*

$$P \leqq U(\rho\beta)^{\frac{1}{2}}, \tag{3}$$

where ρ is the density and β is the modulus of volume compressibility.

Substituting here instead of U its value from formula (1), we will get Cook's formula for the pressure arising during the collision of water with the surface of a solid sphere of a radius:

$$P_R' = \left\{\frac{2}{3}\beta P\left[\left(\frac{R_0}{R}\right)^3 - 1\right]\right\}^{\frac{1}{2}}. \tag{4}$$

In Table I some figures are given calculated with the

TABLE I.

R_0/R	U m/sec.	P_R atmos.	P_R' atmos.
3	57	8	800
5	130	40	1700
10	380	300	5500
20	1000	2500	14500
50	4000	40000	57000
∞	∞	∞	∞

aid of Eqs. (1), (2), and (4) for various R_0/R at $P=2$ atmos.

These figures are definitely exaggerated. In reality liquids are both compressible and viscous; within the cavities there is a certain amount of vapor and gas; then, also, the change of pressure which causes the collapse of cavities takes place not abruptly but at some finite speed. These deviations from the assumptions of the theory can only decrease the rate of collapse of cavities and, consequently, decrease the pressure.

Thus, Rayleigh's theory only shows the possibility of great pressures arising but it fails to give their true values.

This fact prompted Haller[7] to attempt a direct measurement of the pressures arising when cavities collapse. Using the tube with a local constriction in which the destructive action of the cavities was examined, Haller placed therein a piezoquartz indicator instead of the specimen to be destroyed.

The voltage arising on the quartz was recorded with the aid of an oscillograph. The oscillograms obtained by Haller show the presence of impulse pressures of the order of 300 atmos. However, it should be mentioned that the period of the proper vibrations of the indicator, as well as the resolving power of the oscillograph, was of the same order of magnitude as the duration of the pressure impulses (10^{-5} sec.), and consequently the "peaks" of pressure could not be fully resolved. Therefore it seems credible that in reality the true pressures are considerably higher than the value shown.

Such a conclusion is supported by the microstructural investigations of metal specimens destroyed by the action of cavities. Boetcher[12] and later Mousson[8] discovered in the neighborhood of the destroyed surface intercrystalline cracks as well as traces of sliding and twinning. Considering that the elastic limit of the metals investigated is not lower than 20–30 kg/mm² we must conclude that the impulsive pressures on the surface of the specimen equal several thousands of atmospheres.

One can judge the character of the action of such pressures by the outward appearance of the destruction in plastic materials, such as, for instance, lead. Photographs published by Schrötter[13] show the surface of the destroyed specimen to be covered with indentations having protruding edges. The origin of such craterlike indentations may be explained only by the plastic deformation of lead under the action of repeated mechanical blows.

The experimental data set forth above show convincingly that the destructive action of cavities is of a mechanical character. However, some authors suppose that the cavities have a chemical influence upon the surface destroyed. Here only the surface cavities are considered and the chemical action is attributed to the gases contained within them. The chemical activity of gases may be caused either by high temperatures arising within cavities during their contraction or[14] by electric discharges taking place in the "atmosphere" of the cavities at the moment of its formation.

It is necessary to note that no convincing proofs can be given to uphold this viewpoint. On the contrary, experimental data show that the chemical nature of liquid and solid bodies influences the destroying power of cavities to no great extent. Not only metals but even such materials as Bakelite, rubber, glass, quartz, and agate[13,15] are also influenced by the action of cavities and the intensity of destruction is practically unchanged when alcohol is substituted for water.[11]

The Setting of the Problem

From the preceding survey, it follows with certainty that the destructive action of cavities is to a considerable

* Here it is supposed, as is actually the case, that for a solid body $(\rho\beta)^{\frac{1}{2}}$ is greater than for a liquid.

[12] H. N. Boetcher, V.D.I. **80**, 1499 (1936).
[13] H. Schrötter, V.D.I. **76**, 511 (1932); **77**, 365 (1933); **78**, 349 (1934).
[14] J. Frenkel, Acta Physicochimica **12**, 317 (1940).
[15] H. Föttinger, *Hydromechanische Probleme des Schiffsantriebs* (Hamburg, 1932), Section 254.

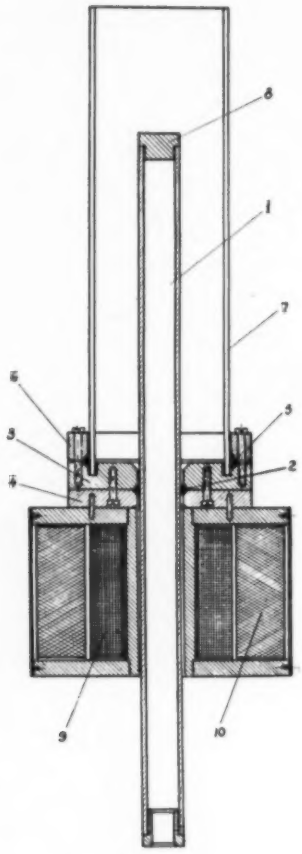

FIG. 2.

extent determined by high pressure impulses arising on the surface of a solid body.

The origin of these pressures is not quite clear.

Cook's theory, as has been seen above, leads to certain contradictions.

Rayleigh's theory does not contain any inner contradictions; it causes, however, serious doubts of qualitative character. The pressures necessary for destruction amount to several thousands of atmospheres. Such pressures, as is shown in Table I, arise at the rate of cavity collapse of the order of thousands of m/sec. It seems hardly probable, however, that such rates may exist in actual conditions, inasmuch as the compressibility and the viscosity of the liquid, as well as vapor and gases contained within cavities, must produce at such high rates of collapse a very strong braking action.

In order to dispel the doubts pointed out, it seems appropriate to turn to experiment. Speaking figuratively, we must attempt to "see" the cavities and to follow the process of their formation and subsequent collapse. Observing simultaneously the destructive action of the latter, we may hope to obtain a sufficiently clear idea of the origin of the impulse pressures we are interested in.

In solving the problem set forth thus, we have considered it most expedient to utilize the Gaines "oscillator." This device, being very convenient in laboratory conditions, permits at the same time the obtaining of intensive destruction.

II. EXPERIMENTAL DEVICE AND PRELIMINARY EXPERIMENTS

Experimental Device

The main part of our device is shown in Fig. 2.

A nickel tube *1*, 300 mm in length and 18 mm in diameter, is fixed on the middle by means of a rubber reinforcement *2* compressed by two Getinax disks *3* and *4*. By means of another rubber reinforcement *5* and a ring *6*, a glass tube *7* which in the course of the experiment is filled by water is pressed against the disk.

A cylindrical specimen *8*, the form and the dimensions of which are shown separately in Fig. 3a, is screwed on to the upper end of the nickel tube. The lower half of the tube is placed in a coil consisting of two windings; the first of these *9* is fed by a constant current and serves for magnetizing; the second *10* is connected with a powerful source of alternating current of sound frequency and is intended for the excitation of longitudinal elastic vibrations in the nickel tube.

The electrical part of the apparatus consists of a generator and two amplifiers. The generator sets up electrical vibrations of the frequency of about 7.5 kHz. Smooth regulation of the frequency close to this value is achieved by a condenser of a variable capacity with a vernier for fine tuning. The vibrations obtained in the generator are passed through a potentiometer on a ten-watt amplifier, after which they are again amplified by a 400-w electron tube in the anode circuit where the excitation coil winding is switched on.

The magnetostriction effect in the alternating magnetic field causes longitudinal vibrations of the nickel tube. The amplitude of these vibrations is measured by means of a microscope with an ocular micrometer.

The maximum amplitude takes place in resonance conditions, when the generator frequency and the frequency of the longitudinal vibrations of the tube are equal. In this case (when the glass vessel is filled by water) the amplitude may reach 0.02 mm.

All the experiments described below were carried out with resonance frequency equalling 7.53 kHz.

Preliminary Observations

Since by means of the potentiometer mentioned above we were able to regulate smoothly the amplitude of vibrations of the tube, even in our first experiments we went somewhat further than Gaines in establishing a certain consecutiveness of the effects observed by him.

In the case of amplitudes of the order of 0.005 mm, there are formed on the end surface of the specimen air bubbles, which later move over the surface at a comparatively slow rate. From time to time, some of these bubbles suddenly acquire a milky white coloring, fall off the specimen, and begin to rush about within the liquid at a very great speed. The trajectories of the motion of these "dancing bubbles," as they were called by Gaines, are zig-zag, resembling the trajectories of the particles suspended in a liquid in the case of the Brownian movement.

After the generator is switched off, there usually remains a bright air bubble instead of the dancing bubble.

In the case of high amplitudes, beginning at about 0.01 mm, on the surface of the specimen there appears a whitish cloud consisting apparently of tiny, rapidly moving bubbles. The "cloud" vanishes altogether when the generator is switched off suddenly, which points to the cavitational nature of the bubbles forming it. The action of the cloud is destructive: In its presence, a well-polished aluminum specimen within 20-30 minutes becomes dull and even somewhat rough.

If the amplitude is increased further, the "cloud" becomes somewhat more distinct, while beginning with an amplitude of about 0.015 mm, there appears in its center a whitish bubble 1–2 mm in diameter. Simultaneously, against the background of a pure high tone produced by the vibrating nickel tube there arises a harsh hissing sound. The "hissing cavity" possesses much greater destructive action than the cloud. After 30–40 seconds, in the center of the aluminium specimen there is formed under the "hissing cavity" a little hole about 1.5 mm in diameter and from 0.5 up to 1 mm in depth.

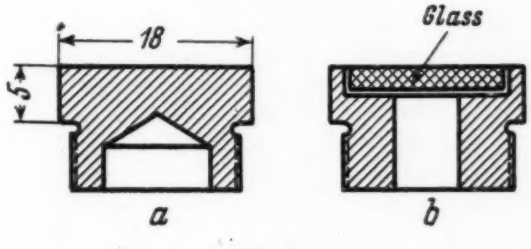

FIG. 3.

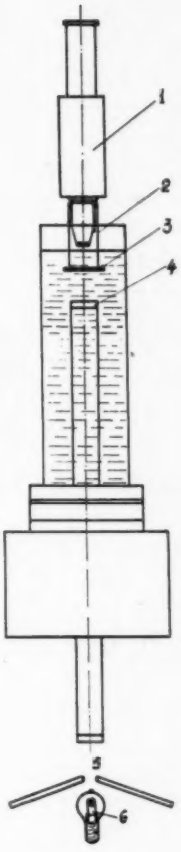

FIG. 4.

Optical Part of the Experimental Arrangement

The naked eye can scarcely distinguish the constantly changing picture that may be detected on the surface of the specimen. With a little imagination one may perhaps make out that this picture is formed by numerous rapidly moving bubbles. However, the visual methods of observation turn out to be wholly unsuitable for judging the size, the shape, and the character of motion of these bubbles and consequently the mechanism of their destructive action.

In order to obtain this information, it seems natural to turn to photographic methods of in-

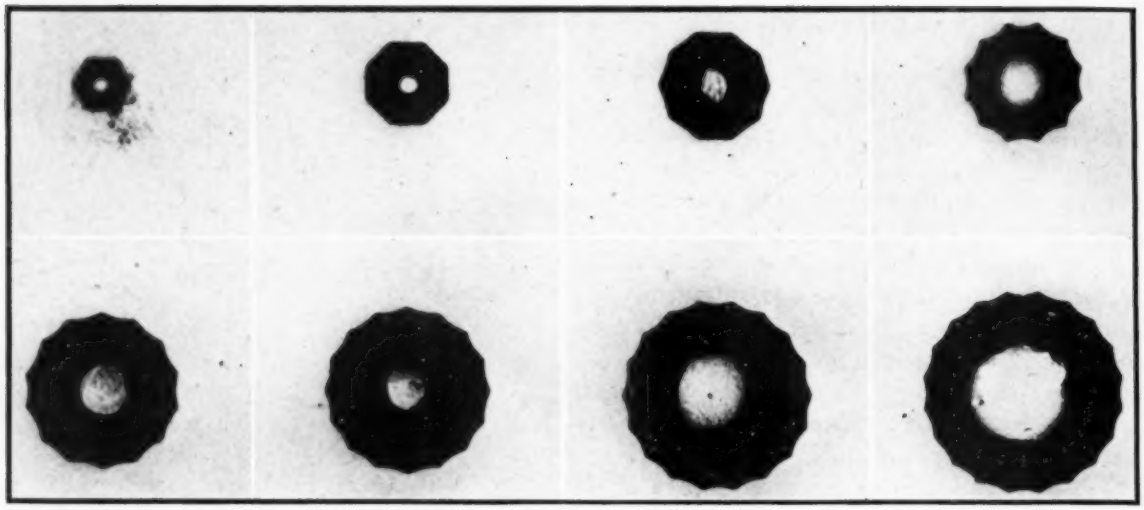

FIG. 5. (×25).

vestigation in which the exposure time is much less than the period of vibrations of the nickel tube. Such short exposures may be achieved by using the light of a spark obtained by the discharge of a condenser. In such a case the duration of a flash of an order of 10^{-6}–10^{-7} is reached without any difficulty, the intensity of light being sufficient for obtaining a photographic image.

Figure 4 shows the scheme of the optical part of the experimental arrangement.

On the objective lens *1* a short glass tube *2* is fixed, at the end of which a plane parallel glass plate *3* is glued on by means of putty. The distance from the plate to the surface of the specimen varies, depending on the focal distance of the objective, from 10 to 30 mm.

A specimen of transparent plastic material *4* is screwed on to the upper end of the nickel tube. In certain cases, a metal specimen with a glass window, the construction of which is shown in Fig. 3b, was utilized.

A spark gap *5* and an electric lamp *6* are located at the lower opening of the tube.

A special attachment was mounted on the microscope tube with a camera which makes it possible to examine the image of the specimen surface on the ground glass, and to take the photograph at a suitable moment. The photograph can be taken either by the light of a lamp with an exposure of 1–2 seconds or by a spark flash, which is obtained by means of a charged 10-kilovolt condenser of 2-microfarad capacity.

III. RESULTS OF EXPERIMENTS AND DISCUSSION

In the following experiments we combined the direct investigation of the image on a ground glass with photographing in the light of a lamp or a spark.

Thus we have succeeded in disclosing a number of new facts of essential significance for the comprehension of the processes taking place at the surface of the specimen.

Radial and Surface Vibration of Air Bubbles

The image of the air bubble on the ground glass looks like a black circle with a light spot

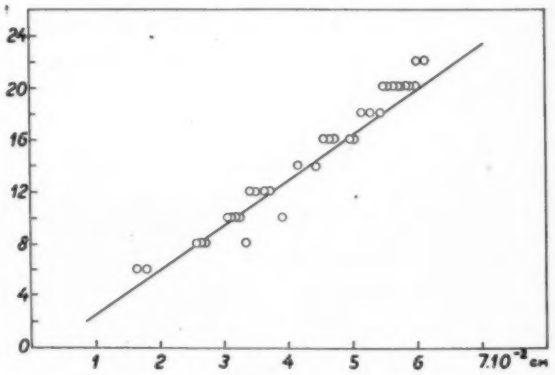

FIG. 6.

in the center. Consequently, the bubble is transparent only for a narrow beam of light which falls normally to its surface. The remaining light is refracted by the surface of the bubble and does not reach the objective of the microscope.

As has been shown in the preceding chapter, in the case of small vibration amplitudes of the tube small air bubbles arise on the surface of the specimen. Observing with the aid of the ground glass the displacement of these bubbles, it is easy to discover the presence of forces acting between them. One can see frequently how two bubbles approach each other with a velocity continuously increasing. If there is a considerable difference in the size of the bubbles, then only the smaller one moves, while the larger one remains practically motionless. In the latter case the smaller bubble sometimes begins to revolve about the larger one in a circular or an elliptical orbit.

It is not always forces of attraction that act between the bubbles. Sometimes one is able to observe how a small bubble carried along by currents of water is repelled by the larger bubble when passing the latter. When two bubbles attracted to each other meet, they unite and form a bubble of larger size; the latter, in its turn, attracts and absorbs smaller bubbles, thus constantly increasing in size.

Upon reaching a certain size, the bubble suddenly changes its shape; its image on the ground glass changes from a circle into a regular polygon with an even number of angles. This picture is retained until the moment when the bubble changes its size by absorbing smaller bubbles. Then the image of a bubble either returns to its original circular shape or it changes into a polygon with a different (but always even) number of angles.

In Fig. 5 some photographs of "polygonal" bubbles are given taken in the light of a lamp with an exposure of 1–2 sec. As may be seen from these photographs, as well as from the curve in Fig. 6, where the data for all the polygonal bubbles photographed by us are given, the number of angles in the polygon increases linearly with increasing radius of the bubble.

The photographs in Fig. 5 give an exact picture as seen by the eye on the ground glass. On the contrary the photographs taken in the flash of a spark differ essentially from the picture observed visually. On these photographs the number of angles of the polygonal bubble is always half that seen by eye. For instance, a bubble which when observed visually has the shape of an octagon will have the shape of a square when photographed by the flash of a spark. We give in Fig. 7 several photographs of polygonal bubbles taken by the flash of a spark. All these bubbles, when examined by eye, had twice as many angles as they have on the photographs.

Now we shall explain the effects investigated. The variable pressures, rising in water as a result of vibrations of the nickel tube, cause forced vibrations of the bubbles. Of all the possible vibrations of the bubble the first ones to arise in any conditions are the radial vibrations (pulsations).

As is known,[16] between two spheres pulsating in liquid there act Bjerknes forces which are attractive forces when the phases coincide and repulsive forces when the phases are opposite.

Using the theory of radial vibrations of bubbles developed by Smith[17] it is easy to calculate the size of a bubble in a state of resonance at a frequency of 7.53 kHz. The radius of a "resonance" bubble in this case is equal to 0.4 mm. It follows

[16] *Handbuch der experimentell Physik* (Leipzig, 1931), Vol. II, Section 107.
[17] F. D. Smith, Phil. Mag. **19**, 1147 (1935).

FIG. 7. (×25).

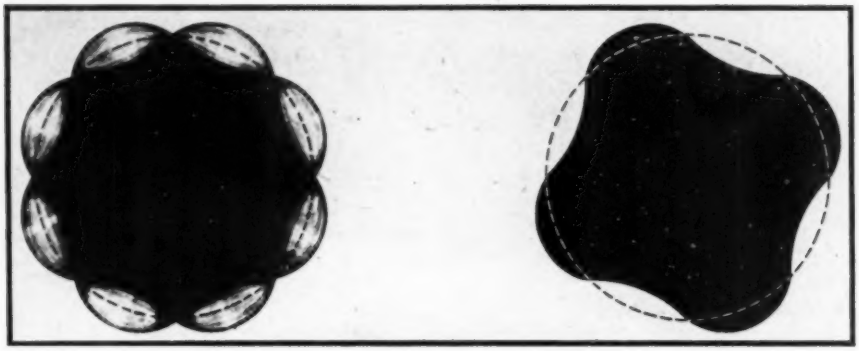

FIG. 8.

from the general theory of vibrations that bubbles of smaller size should vibrate in phase with the exciting force, while the vibrations of larger bubbles must lag behind it 180° in phase. Consequently the vibrations of a pair of bubbles must either coincide in phase or be in different phases depending upon whether the size of these bubbles is on the same or on different sides of the resonance size.

Thus, owing to the action of Bjerknes forces, we have in the first case mutual *attraction* which sometimes causes "planetary" movement and in the second case, *repulsion*.

Besides radial vibrations the bubble can also perform more complicated vibrations connected with a change of its shape. These vibrations (as it was kindly pointed out by Professor J. Frenkel) are similar to surface vibrations of a liquid drop, the theory of which was developed by Rayleigh.[18] A similar theory for the vibration of bubbles was given in our laboratory by J. N. Obraztzov. Since from a mathematical point of view this theory is very close to Rayleigh's theory, we shall restrict ourselves only to its results.

The vibrations performed by a bubble in resonance with an exciting force are characterized by two integers n and m $(m \leqslant n)$. As taken in relation to any axis passing through the center of the bubble, these vibrations may be represented (in a general case) as a superposition of $n+1$ standing surface waves corresponding to various values of the number m $(m=0, 1, 2, \cdots n)$. Each one of these waves forms, respectively, $2m$ and $n-m$ nodal meridians and parallels, which divide the surface of the bubble into spherical rectangles (triangles at the poles). Here, as it is shown in Fig. 8, the neighboring sections vibrate in opposite phases. The proper frequency of vibration of a bubble depends only upon the number n and is given by the expression

$$\nu_n = \frac{1}{2\pi}\left[\frac{\sigma}{\rho r^3}(n+1)(n-1)(n+2)\right]^{\frac{1}{2}}, \qquad (5)$$

r being the radius of the bubble, σ the surface tension, and ρ the density of the liquid.

The contours of the equatorial cross section of the vibrating bubble are projected upon the

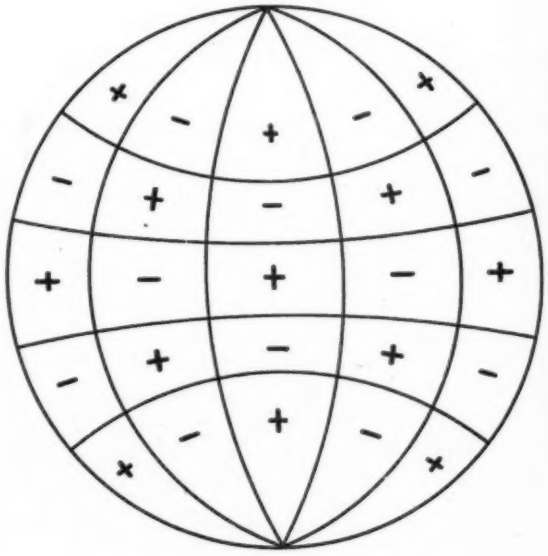

FIG 9.

[18] Lord Rayleigh, Proc. Roy. Soc. **29**, 71 (1879); *Handbuch der Physik*, Vol. VII, Section 369.

ground glass of the camera. The number of nodal points on the equator is equal to the number of nodal meridians which, as it has been shown above, can be only even.

During visual observation, as well as when photographing is performed with sufficiently great expositions (great in comparison with the period of vibrations), the contours of the vibrating sections of the equator are blurred as shown on scheme in Fig. 9 at the left. The number of angles of the polygon thus obtained is equal to the number of nodal points on the equator.

A photograph taken by the flash of a spark lasting about 100 times less than the period of vibrations fixes the momentary position of the vibrating parts of the equator. The figure thus obtained also resembles a polygon. The number of angles of this figure, however, is one-half the number of nodes (see Fig. 9, on the right).

It was shown above that in the *general case* the vibrations of the bubble are a superposition of $n+1$ standing surface waves, each one being characterized by one of the integer values of the number m. However, such vibrations of the bubble which correspond to a smaller number of surface waves are also possible. An elementary analysis of the experimental data of Fig. 6 shows in particular that on the bubbles observed by us only one surface wave, corresponding to $m \cong n/2$, was excited. For such a ratio between the numbers m and n the nodal meridians and parallels are mutually divided into an equal number of parts.

Loss of Stability of Shape of Vibrating Air Bubbles

The preceding section was concerned with comparatively small amplitudes of vibrations of a nickel tube.

By increasing the amplitude up to ~ 0.005 m we are invariably faced by the phenomenon of formation of "dancing bubbles" which was already mentioned previously. Air bubbles with a radius of about 0.5 mm suddenly take on a milky white coloring, break off from the surface of the specimen, and for many minutes energetically rush about the whole vessel. If we hang a strip of thin aluminium foil in the water at a certain distance from the nickel tube we can prove that these bubbles possess a destructive power. In running against the foil they cause inundations in it and sometimes even bore right through it. After a few minutes the foil is torn into shreds.

The effects enumerated are clarified at once by a glance at the photograph of dancing bubbles taken in the flash of a spark, given in Fig. 10.

Judging by the photograph, the bubble changes its shape continuously, disintegrates into parts, then restores its shape, etc.

At every change of shape, every rupture or redintegration, such an unstable bubble experiences a "recoil" which evidently causes its continuous zig-zag motion.

The destructive action of an unstable bubble can be explained by the direct blows of water. The origin of the latter is illustrated in Fig. 11 which shows schematically the consecutive stages in the division of a bubble; the direction of the blows is shown by arrows. The special coloring of the unstable bubble is caused by the roughness of its surface. Being similar to the surface of ground glass it scatters light intensely which makes it look white.

The reasons for the instability of air bubbles are qualitatively entirely comprehensible. On the surface of a vibrating bubble we have besides capillary forces the action of forces of hydrodynamic origin. At sufficiently great amplitudes of vibration the hydrodynamic forces in some points of the surface can compensate and occasionally even surpass the surface tension. In

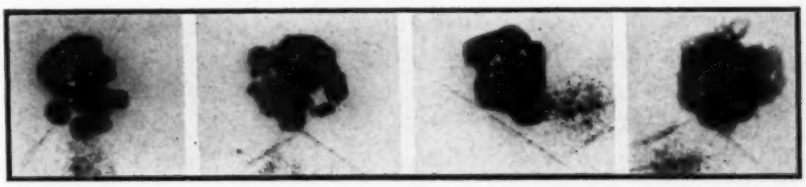

FIG. 10. (×17).

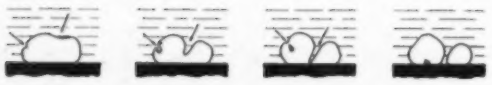

FIG. 11.

this case the spherical form of the bubble which is caused by the action of surface tension becomes unstable and the bubble can change its shape.

Cavities

If the amplitude of the vibrations of the nickel tube exceeds 0.01 mm, a cavitational cloud appears on the surface of the specimen; and if the amplitude is further increased up to ~0.015 mm, a "hissing" cavity is formed in the center of the specimen.

Figure 12 gives a photograph of a cloud obtained with a small magnification in a flash of a spark. Figure 13 shows some photographs of "hissing cavities" taken in the flash of a spark. Figure 14 also shows photographs of "hissing cavities," these latter in distinction from the former taken not from above but from the side.*

Having taken about 500 similar photographs we were able to establish the following:

The size of the cavities (in a given part of the surface of the specimen) changes from one photograph to another not more than 3 to 5 times,** while the total number of cavities remains practically unchanged. Of all the photographs taken by us there is none where the cavities were absent.

The distribution of the photographs according to the size of cavities is the following: On one-third of the photographs the dimensions of the cavities approach the upper limit; on another third the dimensions of the cavities are near the lower limit; and finally on the remaining third they are of intermediate dimensions.

First of all, these facts show that the increase and decrease of cavities proceed synchronously with respect to the change of pressure. During that part of the period when the pressure near the surface of the specimen decreases, cavities increase; during the remaining part of the period the pressure increases and the cavities contract; the size of the cavities on the photograph depends upon the moment of the flash of the spark.

From the photographs in Figs. 13 and 14 we see further that cavities and especially hissing cavities continuously change their shape, disintegrate, etc., in the same way as it was observed in unstable air bubbles. But here in distinction from the air bubbles the dimensions of the cavities change.

The causes of the loss of stability in cavities do not differ in principle from the causes of this phenomenon in air bubbles which we examined above. However, for the formation of large unstable cavities a sufficiently large pressure amplitude is necessary; this exists only in the center of the specimen.

Now let us turn to the question of the destructive action of cavities. The photographs obtained by us show that the cavities contract not over 3–5 times. According to Rayleigh's theory impulse pressures arising during such contractions cannot exceed a few tens of atmospheres, which, of course, is insufficient for destructive action.

Thus, the destructive action of cavities must be ascribed to the direct blow of water against

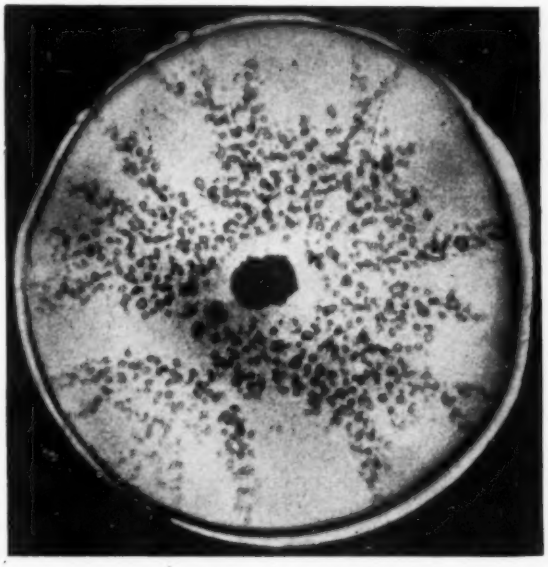

FIG. 12 (×4).

* For the taking of these photographs the cylindrical vessel was replaced by a plane parallel vessel, and the microscope and the spark gap were set along the axis parallel to the plane of the specimen.

** The photographs in Fig. 13 correspond to these two limit cases.

the surface of the specimen (see Fig. 11), in exactly the same way as it was done in the preceding section.

In connection with this we shall investigate briefly the destructive action of repeated blows of water. In the works of Honneger,[19] Cook,[20] Schwarz and Mantel,[21] Mousson,[8] and others, the specimen of the material studied was fixed on the circumference of a rotating disk. The stream of water was directed so as to cause a collision of the specimen and the stream in the course of each revolution when the disk was rotated. The velocity of the water is not of essential significance. However, it must be sufficiently great to allow the stream to recover between two consecutive collisions.

The intensity of the destructive action increases very rapidly with increase of the rate of collisions; when the velocity is of the order of 250 m/sec., a hundred thousand blows, i.e., about five minutes' rotation of the disk, are sufficient for the destruction of the most durable steel.*

By making use of a similar construction, we investigated a specimen of aluminium which was used for studying the destructive force of cavities. The experiments have shown that when the rate of collision was of the order of 50 m/sec., 400,000 blows were necessary for the formation of a small hollow on the surface of the specimen where the stream hits it. The latter in its outward appearance resembles greatly the hollow appearing in the center of the aluminium specimen under the action of hissing cavities after one minute's work of the oscillator, i.e., after about 400,000 vibrations of the nickel tube (see Chapter II). Hence it follows that in the second case also the rate of collision of water and the surface of the specimen equals several tens of meters per second. Similar rates, as may be easily shown by means of direct, though very rough estimations, may really arise in the case of deformations of unstable cavities.

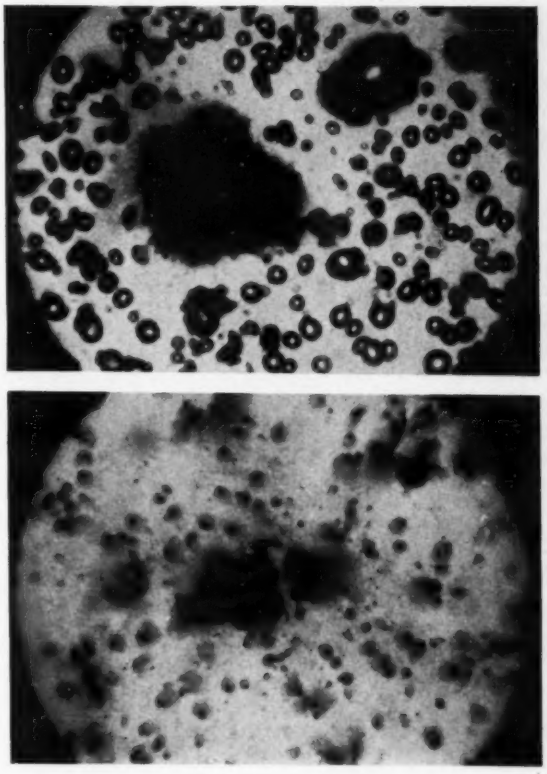

FIG. 13 (×14).

Concluding Remarks

Cook's and Rayleigh's theoretical investigations are based on the conception of cavities retaining spherical or semi-spherical shape in the course of the entire period of their existence.

As we have seen, this conception is by no means always justified by the experiments, inasmuch as cavities very easily lose their stability of shape.

The main ideas of Cook and Rayleigh, however, remain valid in this case also. Indeed, we may with respect to any kind of cavity speak of the pressures conditioned both by the direct blow of the liquid (Cook) and by purely hydrodynamic processes (Rayleigh).

Hydrodynamic pressures cannot be greater for the unstable cavities than for the spherical ones, in connection with which in estimating the upper limit of these pressures Table I may be used. Inasmuch as cavities are not contracted more than 3–5 times, the pressures investigated must be definitely less than several tens of atmospheres. However, it is by no means ex-

[19] E. Honneger, B.B.C. Hft. **4**, 95 (1927).
[20] S. S. Cook, Proc. Roy. Soc. London **A119**, 481 (1928).
[21] V. Schwarz and Mantel, V.D.I. **80**, 363 (1936).
* The pressure arising when the specimen collides with the current is determined by formula (3). They reach up to several thousands atmospheres when the rate is 250 m/sec.

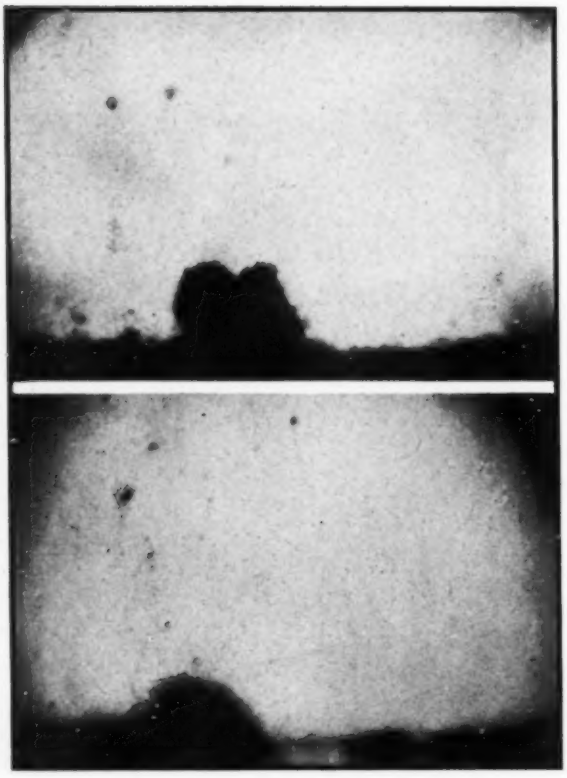

FIG. 14 (×12.5).

cluded that in the course of very short intervals of time (which have not been accidentally recorded by our photographs), cavities undergo greater contractions which cause pressures of the order of several thousands of atmospheres. This supposition, however, seems hardly probable; all the more so since it leads to the difficulties of Rayleigh's theory, already noted above. Thus, the destructive action of cavities may hardly be ascribed to hydrodynamic pressures. On the contrary, the pressure conditioned by direct blows of the liquid easily explains the destructive action. Indeed, the contradictions of Cook's theory do not hold for unstable cavities, inasmuch as in this case the blows of the liquid take place at rather small contractions. The pressures conditioned by these blows may reach up to several thousand atmospheres, i.e., they are quite sufficient for destroying the most durable materials.

The phenomenon of the loss of stability is undoubtedly characteristic of cavities of any origin, and particularly of those cavities that are responsible for the destruction of ship propellers. We may suppose, therefore, that in the latter case also the main part is played by the *unstable surface cavities*.

Such a supposition, of course, calls for definite experimental confirmation. Nevertheless, certain practical conclusions may already be drawn from it.

1. In investigating "the cavitational durability" of materials there is no need of either the expensive hydrotechnical constructions of the type used by Schrötter, or the complicated magnetostriction oscillators. Inasmuch as cavitational destruction is ultimately conditioned by the direct blows of water, we may, in investigating the materials, make use of Honneger's rotating disk.

2. *Vibrations of the screw and its blades* must by no means be allowed, since they may lead to the formation of surface cavities of very strong destructive action.

3. In carrying on model experiments, the purpose of which is to discover the optimal (from the point of view of cavitational destruction) geometrical shape of the propeller and the body of the ship, only *the pressure on the very surface of the propeller* need be taken into consideration. We must strive to keep the pressure at any point of the surface from falling off to the vapor pressure, or in any case keep it as constant as possible in the course of a full revolution of the propeller.

An X-Ray Study of the Copper-Manganese Binary Alloy System

L. D. Ellsworth* and F. C. Blake
Department of Physics, The Ohio State University, Columbus, Ohio
(Received December 20, 1943)

The powder method of x-ray analysis has been applied to a series of slowly cooled copper-manganese alloys to ascertain whether anomalous physical effects of these alloys, detected by the Metallurgical Division of the United States Bureau of Mines, may be ascribed to the presence of superstructures. The x-ray analysis does not indicate superstructures, but it presents results quite different from those one would expect from examination of the accepted equilibrium diagram of the copper-manganese binary alloy system. Slowly cooled and annealed samples both give identical results; namely, that copper enters into a continuous series of solid solutions with manganese, crystallizing in a face-centered cubic lattice with a gradually increasing parameter as the manganese content is increased from zero to sixty percent. Above sixty percent manganese, and up to ninety percent manganese, the lattice is face-centered tetragonal. Between ninety and one hundred percent manganese, two phases are present, one phase being the solid solution phase corresponding to an alloy with ninety percent manganese, the other phase being that of alpha-manganese.

INTRODUCTION

THE x-ray study reported in this article was made to determine whether superstructures are present in the copper-manganese binary alloy system. It was made in cooperation with the Metallurgical Division of the United States Bureau of Mines in a particular effort to ascertain whether anomalous physical effects measured in certain copper-manganese alloys by the Bureau of Mines[1] could be attributed to the formation of ordered structures in the alloys.

METHODS OF DETECTING SUPERSTRUCTURES

Superstructures are detected by virtue of the anomalous physical effects existing in ordered lattices as compared to the normal conditions present in disordered structures. These distinguishing effects combined with definite x-ray results give positive evidence of superlattices and yield valuable numerical data and information for constructing and checking theories of superstructure formation.

Ordered lattices are generally found to have an electrical resistance much less than that of a disordered lattice of the same composition. The specific heat-temperature curve for an alloy which is ordered below the critical temperature exhibits an anomalous specific heat because of a heat capacity in addition to what is predicted on the basis of the Dulong-Petit law for ordinary thermal motion; the curve rises to a sharp maximum at the critical temperature and then drops to approximately the normal value.

In many cases, the creation of an ordered lattice results in an increase in the magnetic susceptibility of the alloy. Some alloys are increased in hardness and tensile strength by the onset of order.

Since the ultimate atomic structure of matter is detected only by means of x-rays, and more recently by electron waves, then the existence of superstructures in alloy systems can be definitely confirmed by x-ray or electron diffraction methods alone. If one considers the typical case of a copper-gold alloy containing twenty-five atomic percent gold, one finds that the disordered structure is a face-centered cubic structure in which the copper and gold atoms are distributed at random on the lattice sites. A powder x-ray photograph of this lattice shows only the face-centered cubic lines. When the lattice becomes ordered, however, the gold atoms are found at the cube corners and the copper atoms at the cube faces. If the x-rays are scattered more strongly by one of the elements, then the structure appears, as far as the x-ray effect is concerned, to consist of two interpenetrating simple

* Now at the Radiation Laboratory, Massachusetts Institute of Technology, Cambridge, Massachusetts.
[1] Progress Reports, No. 33, *Manganese and Its Alloys*, Metallurgical Division of U. S. Bureau of Mines.

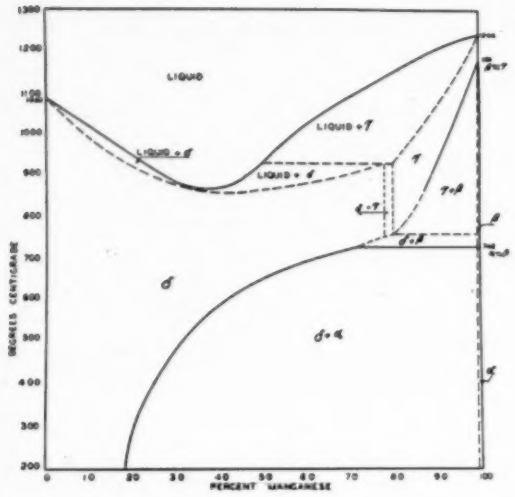

FIG. 1. Equilibrium diagram of copper-manganese alloys (taken from Hansen).

cubic lattices. This exhibits itself on the x-ray picture of the ordered alloy by the presence of the simple cubic lines, that is, lines in addition to the face-centered cubic lines. The extra lines are called superlattice lines for they indicate the presence of superlattices.

Superlattice lines are easy to detect in ordered copper-gold alloys, since the reflecting power of copper is much different from that of gold (the intensity of reflection of x-rays from an atom is generally proportional to the square of the atomic number). In the case of copper-manganese alloys, however, in which the atomic numbers of the components are almost the same, one must resort to the use of the anomalous scattering of x-rays near the critical absorption limit in order to detect superlattice lines. Iron $K\alpha$ radiation has a wave-length just above the critical absorption wave-length of manganese so that the scattering power of manganese for iron radiation is three units less than normal, whereas the scattering power of copper is normal. For this reason, iron $K\alpha$ radiation is capable of distinguishing between the copper and manganese atoms, and hence of producing superlattice lines on the x-ray film, if an ordered structure is present.

THE COPPER-MANGANESE ALLOY SYSTEM

The copper-manganese alloy system has been thoroughly investigated, but there is still a lack of complete agreement about the equilibrium diagram of the alloys. The accepted diagram, as taken from Hansen,[2] is shown in Fig. 1. Manganese has three allotropic forms; the low temperature form is alpha-manganese which has a cubic lattice with 58 atoms and a cell size of 8.901A. Beta-manganese is stable at intermediate temperatures; it has a body-centered cubic lattice with 20 atoms to the unit cell and a unit cell size of 6.305A. The high temperature modification of manganese is the gamma-form with a face-centered tetragonal lattice, having four atoms to the unit cell and a value of a equal to 3.767A and the axial ratio c/a equal to 0.934. Persson[3] found gamma-manganese to form a continuous series of solid solutions with copper, in that the face-centered cubic lattice of copper gradually stretched as manganese was added up to 80 percent manganese; above this point the lattice became face-centered tetragonal and the axial ratio decreased to the value of 0.934 as more manganese was added. Persson's results are shown graphically in Figs. 2 and 3. Ishiwara[4] does not agree with some of the phase boundaries of the accepted diagram as shown in Fig. 4, taken from the *Metals Handbook*. In addition, Ishiwara found it impossible to determine the lower limit of the gamma-phase boundary because of the extreme sluggishness of copper-manganese in attaining equilibrium conditions.

APPARATUS AND EQUIPMENT

The x-ray powder photographs were taken with a Debye camera, 2.856 cm in radius. The x-ray beam was defined by two pinholes in the camera collimating system, the outer one being 0.040 inch in diameter. The camera was cylindrical in shape so the lines could be measured to a Bragg reflecting angle of approximately eighty degrees. The camera was mounted on a base during exposure, which contained a synchronous motor drive to rotate the sample, if necessary. The x-rays were produced by a demountable tube, filament type, with a water-cooled target,

[2] M. Hansen, *Der Aufbau der Zweistofflegierungen* (Julius Springer, Berlin, 1936).
[3] E. Persson, Zeits. f. physik. Chemie **B9**, 25 (1930).
[4] T. Ishiwara, Tohoku Imp. Univ. Sci. Reports **19**, 499 (1930).

designed by Dr. P. M. Harris of the Department of Chemistry, The Ohio State University.

MATERIALS AND METHOD OF X-RAY ANALYSIS

The alloy samples were prepared by the Metallurgical Division of the United States Bureau of Mines. Pure copper and very pure electrolytic manganese were melted in a 3-kva induction furnace and cast into ingots. The ingots were reduced about 80 percent in area by swaging and then were heat treated. The swaged rods were $\frac{1}{4}$ inch in diameter; and of the total length of each rod, about $\frac{1}{2}$-inch length was cut off and sent to this laboratory for x-ray analysis.

The samples were heat treated in a silica tube in a helium atmosphere. Initially the alloys were heated to a point just below the solidus line for at least two hours. Then they were allowed to cool overnight in the furnace, the minimum time of cooling being sixteen hours. Therefore these copper-manganese alloys, of extremely high purity, are slowly cooled, and should be in the equilibrium state at room temperature. Since they were slowly cooled, any superstructures that may be present in the alloy system should be present in these samples.

Because of the possibility that the slowly cooled samples did not represent the equilibrium state at room temperature, several specimens were powdered and annealed at 460°C for periods ranging from 7 days to 12 days. These were examined by x-rays and the results were compared with the unannealed samples.

The purity of the samples is shown in Table I, which gives the results of the chemical analysis as determined by the Bureau of Mines.

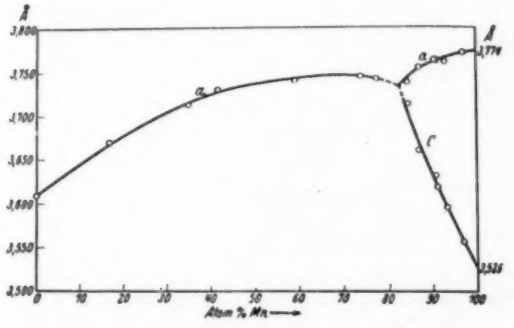

FIG. 2. Variation of lattice parameter of copper-manganese alloys at high temperatures (taken from Persson).

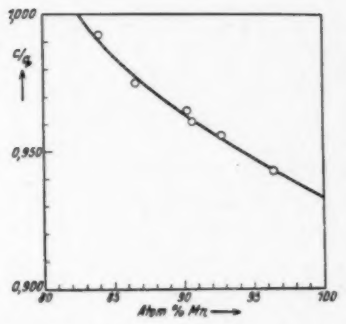

FIG. 3. Variation of axial ratio c/a of copper-manganese alloys at high temperatures (taken from Persson).

TABLE I. Chemical analysis of copper-manganese alloys. (These percentages represent percent by weight.)

Indicated composition	Chemical analysis Percent manganese	Percent copper
40Mn–60Cu	39.74	60.25
45Mn–55Cu	46.44	53.55
50Mn–50Cu	48.73	49.83
55Mn–45Cu	53.82	44.55
60Mn–40Cu	60.08	39.90
65Mn–35Cu	64.78	35.21
70Mn–30Cu	70.53	29.44
75Mn–25Cu	75.49	24.48
80Mn–20Cu	80.56	19.43
82Mn–18Cu	82.40	17.58
85Mn–15Cu	85.36	14.62
88Mn–12Cu	87.92	12.06
90Mn–10Cu	89.95	10.03
92Mn– 8Cu	91.89	8.09
93Mn– 7Cu	92.85	7.13
95Mn– 5Cu	94.83	5.15

The compositions not listed here were not checked by chemical analysis.

In the x-ray investigation, the Debye-Sherrer powder method was used. The swaged rods were filed to give a very fine powder, and any file particles that possibly were present in the powder were removed by a permanent magnet. The filings were passed through a 325-mesh sieve and the 325-mesh powder was used to make up the x-ray specimen. The usual procedure of annealing the powder after filing to reduce the width of the x-ray lines was not followed because any such annealing process would introduce impurities into the alloy specimens.

The specimens that were annealed in the powdered form to check the presence of the equilibrium state were used directly in the x-ray analysis. These samples included the following compositions and periods of annealing at 460°C:

Mn66–Cu34, annealed for 7 days (in this case, at 600°C).
Mn79–Cu21, annealed for 12 days.
Mn89–Cu11, annealed for 7 days.

In preparing the sample for mounting in the x-ray cassette, a small glass capillary tube, approximately 0.5 mm in outside diameter and ½ inch long, was moistened slightly with mucilage and then dipped into the 325-mesh powder to give a very thin, uniform layer of powder over the cylindrical glass surface. The uncoated end of the glass tube was inserted into a small chuck which was then mounted at the center of the camera.

In the first two series of runs, Fe $K\alpha$ radiation was used, the radiation from an iron target being filtered through a layer of $MnCO_3$, which had been mixed with Duco cement diluted with acetone, mounted as a paste on a piece of paper, and allowed to dry. To check the results obtained with iron radiation, a third run was made with unfiltered chromium x-rays.

The usual time of exposure for the filtered Fe $K\alpha$ radiation was four hours, when the tube was operated at 30 kvp and 10 ma. For unfiltered chromium x-rays, the exposure time was two hours.

CALCULATIONS AND RESULTS OF X-RAY ANALYSIS

The x-ray films were measured on a Société Genevoise comparator; the experimental error involved in measurement was approximately one-tenth of one percent. By making corrections

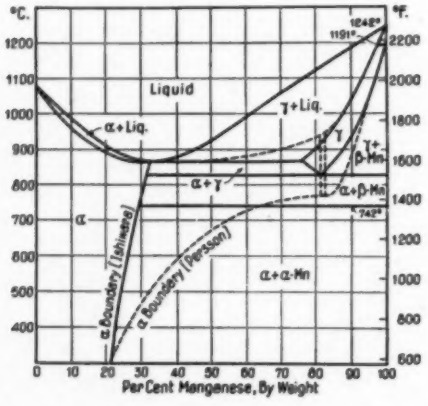

FIG. 4. Equilibrium diagram of copper-manganese alloys (taken from *Metals Handbook*).

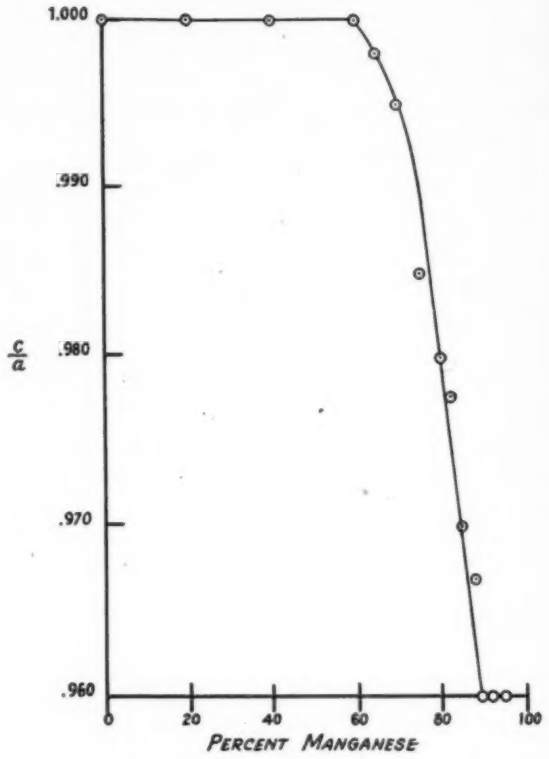

FIG. 5. Axial ratio *vs.* composition.

for errors due to absorption of the x-rays in the sample, errors due to eccentricity of the sample about the center of the camera, and errors due to film shrinkage, the numerical results of the cell size, as obtained from the various reflecting planes in a given alloy, were found to agree within the experimental error of measurement. This correction was made to the separations of the corresponding lines on a given x-ray film by the subtraction of a certain constant d from the separations. This constant was found to vary with the size of the capillary tube on which the sample was mounted. In general, the value of d was slightly greater than the diameter of the capillary tube.

The results obtained from three separate series of runs of the series of copper-manganese alloys are tabulated in Table II and are represented graphically in Figs. 5–7. From zero to sixty percent manganese, the two elements form a continuous series of solid solutions, in which the face-centered cubic lattice of copper stretches as more manganese is added. Above sixty percent manganese, the lattice becomes face-centered

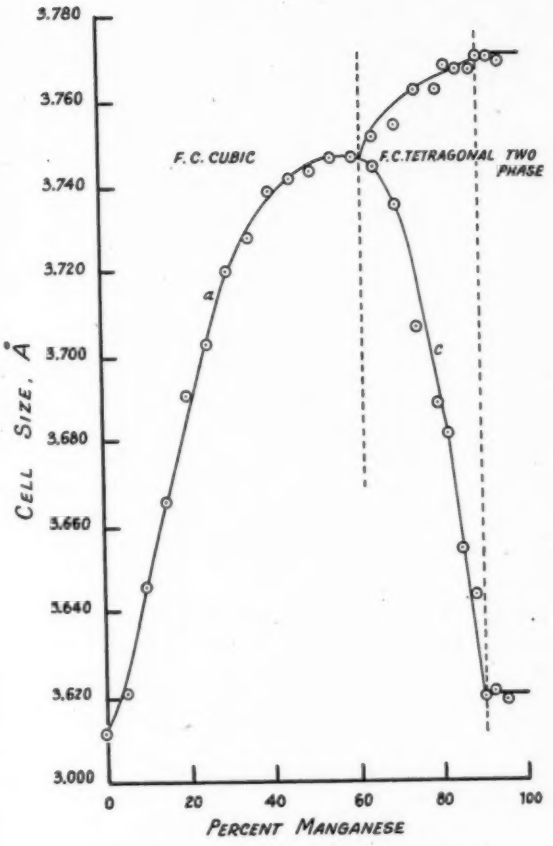

FIG. 6. Lattice parameters *vs.* composition.

tetragonal as indicated on the graphical results. At and above ninety percent manganese, two phases are present, one phase being the solid solution phase corresponding to an alloy with ninety percent manganese, the other phase being that of alpha-manganese. There are no indications of any superlattices being present in the alloys which were investigated.

The powders which were annealed gave parameter values and number and types of phases identical with those tabulated in Table II. This indicates rather definitely that the slowly cooled samples and those that are both slowly cooled and annealed from 7–12 days, of the same composition, are identical in structure; and that both are in equilibrium at room temperature.

CONCLUSIONS

The results presented in this paper certainly do not agree with those that one would expect at low temperatures from consideration of the accepted equilibrium diagram; for the equilibrium diagram indicates that manganese enters into solid solution with copper up to a concentration of approximately twenty percent, and that two phases are present above this concentration. The results agree much closer with those obtained by Persson for copper-manganese alloys in equilibrium at high temperatures, that is, temperatures immediately below the solidus. The face-centered cubic structure of pure copper expands as manganese is added until the structure becomes pseudo-cubic or face-centered tetragonal between sixty and sixty-five percent manganese. It is significant that the composition at which the transformation from the cubic to the tetragonal form occurs is not the same as that found by Persson (compare Figs. 2 and 6). In addition, another significant feature of the present results is the appearance of two phases at ninety percent manganese, this result being particularly interesting because the solid solution phase indicated in the equilibrium diagram and the solid solution phase detected in these alloys do not correspond. One would expect, according to the accepted diagram, this phase to be a face-

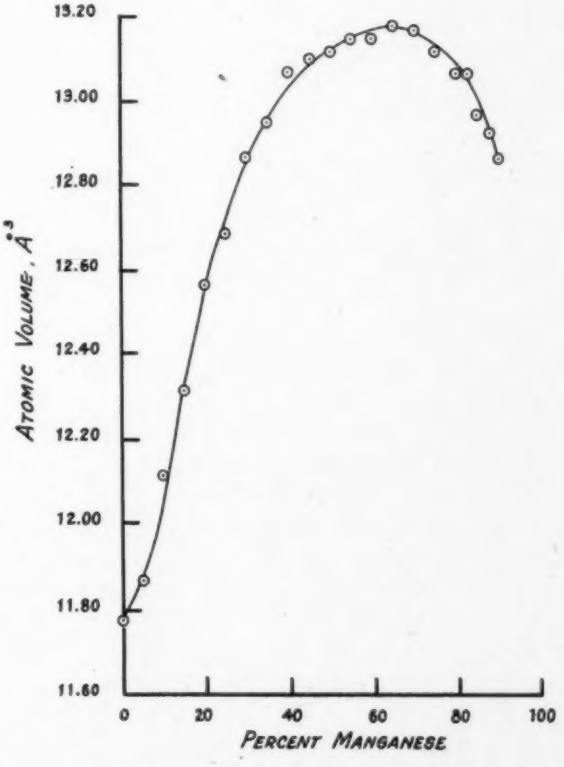

FIG. 7. Atomic volume *vs.* composition.

TABLE II. Tabulated results of x-ray analysis of copper-manganese alloys.

Sample	Phase	Cell size, a Series A Fe $K\alpha$	Series B Fe $K\alpha$	Series C Cr $K\alpha, \beta$	Dimensions of unit cell, average values a	c	c/a	Atomic volume, V
Copper	F.C.C.*	3.611A	3.612A	3.612A	3.612A			11.78A^3
5Mn–95Cu			3.623	3.619	3.621			11.87
10Mn–90Cu			3.645	3.647	3.646			12.12
15Mn–85Cu			3.665	3.667	3.666			12.32
20Mn–80Cu		3.690	3.691	3.691	3.691			12.57
25Mn–75Cu			3.700	3.705	3.703			12.69
30Mn–70Cu			3.716	3.724	3.720			12.87
35Mn–65Cu			3.727	3.729	3.728			12.95
40Mn–60Cu		3.742	3.734	3.742	3.739			13.07
45Mn–55Cu		3.743	3.741	3.743	3.742			13.10
50Mn–50Cu		3.746	3.743	3.742	3.744			13.12
55Mn–45Cu		3.744	3.753	3.743	3.747			13.15
60Mn–40Cu		3.745	3.752	3.744	3.747			13.15
65Mn–35Cu	F.C.T.*	3.757	3.751	3.748	3.752	3.745A	0.998	13.18
70Mn–30Cu		3.759	3.756	3.751	3.755	3.736	.995	13.17
75Mn–25Cu		3.766	3.762	3.760	3.763	3.707	.985	13.12
80Mn–20Cu		3.762	3.763	3.764	3.763	3.689	.980	13.07
82Mn–18Cu		—	3.769	—	3.769	3.682	.977	13.07
85Mn–15Cu		3.771	3.766	3.766	3.768	3.655	.970	12.97
88Mn–12Cu		—	3.769	3.766	3.768	3.644	.967	12.93
90Mn–10Cu		3.772	3.769	3.771	3.771	3.620	.960	12.85
92Mn– 8Cu	F.C.T.	3.775	3.766	3.775	3.771	3.621	.960	
	α-Mn	—						
93Mn– 7Cu	F.C.T.	—	3.771	—	3.771	3.620	.960	
	α-Mn	—	8.902	—	8.902			
95Mn– 5Cu	F.C.T.	3.769	3.774	3.768	3.770	3.619	.960	
	α-Mn	8.898	8.899	8.901	8.899			
96Mn– 4Cu	F.C.T.	—	3.769	—	3.769	3.618	.960	
	α-Mn	—	8.902	—	8.902			
98Mn– 2Cu	α-Mn	8.913	8.907	8.903	8.908			
α-Manganese		8.905	8.895	8.904	8.901			

* F.C.C.—face-centered cubic; F.C.T.—face-centered tetragonal.
The following samples were annealed at the temperature and for the period indicated below, and gave the following parameter results:
66Mn–34Cu, annealed for 7 days at 600°C: a =3.752A, c/a =0.998, face-centered tetragonal.
79Mn–21Cu, annealed for 12 days at 460°C: a =3.764A, c/a =0.981, face-centered tetragonal.
89Mn–11Cu, annealed for 12 days at 460°C: a =3.767A, c/a =0.962, face-centered tetragonal.

centered cubic phase with a cell size corresponding to an alloy of composition 20Mn–80Cu, but instead this phase is found to be a face-centered tetragonal structure corresponding to a composition of 90Mn–10Cu.

If the curves in Figs. 5 and 6 are extrapolated to one hundred percent manganese, the values obtained for the axial ratio c/a and cell size a agree with the accepted values for pure gamma-manganese, *viz.*, 0.934 and 3.774, respectively.

The composition at which the cubic to tetragonal transition takes place is checked by results obtained from analysis of photomicrographs of the alloys. Below sixty percent manganese, the pictures show twinned single-phase structures, typical of face-centered cubic lattices; above sixty percent manganese, up to ninety percent manganese, the pictures show simple grain structures consisting of but one phase, these structures being identified with the face-centered tetragonal lattice. Above ninety percent manganese, two phases appear in the photomicrographs.

Arguments that the slowly cooled specimens examined do not represent equilibrium states at room temperatures seem to be refuted by the identical results obtained from slowly cooled samples annealed at a relatively low temperature of 460°C (refer to Fig. 4) for a considerable period of time (7 to 12 days).

These results alone are insufficient for making definite changes in the accepted equilibrium diagram of the copper-manganese alloy system, but combined with additional experimental evidence, as obtained by the Metallurgical Division of the Bureau of Mines, they should indicate what changes are to be made.

Grateful acknowledgment is made to Mr. R. S. Dean and Dr. C. Travis Anderson of the U. S. Bureau of Mines for furnishing the samples for this investigation.

The Directional Characteristic of a Half-Wave Doublet Goniometer

ROBERT J. DWYER
Trinity College, Hartford, Connecticut
(Received March 24, 1944)

The directional characteristic of a goniometer using two half-wave doublet antennas mounted at right angles is derived. It is shown that, unlike the double loop goniometer, the directional characteristic is not identical with that of a single half-wave doublet that can be rotated, although the variation from such a case is very small.

IN a recent paper Forbes[1] describes a directional antenna system very similar to the Bellini-Tosi goniometer,[2] much used for radio direction finding. A diagram of the system described by Forbes is given in Fig. 1. When the rotatable coil L_3 is parallel to coils L_1, a maximum of energy is picked up from doublet *1* and a minimum from doublet *2*. As L_3 is rotated the relative amount of energy picked up from the two doublets is varied and a directional effect is obtained. In the Bellini-Tosi goniometer loop antennas are used instead of doublets, and it can be shown[3] that for such a system the directional effect is the same as that obtained when a single loop antenna is rotated. The purpose of this investigation is to determine the directional characteristic of the system described by Forbes.

Referring to Fig. 1, let the axis of the coils L_1 lie along the x axis, and that of the coils L_2 along the y axis. Then if θ is the angle the normal to the axis of the rotating coil L_3 makes with the x axis, we have

$$\begin{aligned} M_{31} &= M \sin\theta, \\ M_{32} &= M \cos\theta, \end{aligned} \tag{1}$$

where M_{31} is the mutual inductance between coil *3* and coils *1*, M_{32} between coil *3* and coils *2*, and M the maximum value of each.

Now let a wave approach the antenna system horizontally making an angle α with the line of direction of doublet *1*. The voltage induced in a half-wave doublet may be shown[4] to be proportional to $[\cos \pi/2 \cos\alpha)]/\sin\alpha$. Then the voltages applied to coils *1* and *2* are

$$\begin{aligned} E_1 &= a\frac{\cos\left(\frac{\pi}{2}\cos\alpha\right)}{\sin\alpha}, \\ E_2 &= a\frac{\cos\left[\frac{\pi}{2}\cos(90-\alpha)\right]}{\sin(90-\alpha)}, \end{aligned} \tag{2}$$

where a is a constant of proportionality.

By Eqs. (1), the voltages induced in L_3 are then

$$\begin{aligned} E_{31} &= bE_1 \sin\theta, \\ E_{32} &= bE_2 \cos\theta, \end{aligned} \tag{3}$$

where b is also a proportionality constant.

The total voltage in the rotatable pick-up coil L_3 is then

$$E_3 = E_{31} + E_{32},$$

or

$$E_3 = ab\frac{\cos\left(\frac{\pi}{2}\cos\alpha\right)}{\sin\alpha}\sin\theta + ab\frac{\cos\left[\frac{\pi}{2}\cos(90-\alpha)\right]}{\sin(90-\alpha)}\cos\theta. \tag{4}$$

For a particular value of α, the value of θ giving a maximum of E_3 may be obtained by equating to zero the partial derivative of E_3 with respect to θ.

Thus,

$$\frac{\partial E_3}{\partial\theta} = ab\frac{\cos\left(\frac{\pi}{2}\cos\alpha\right)}{\sin\alpha}\cos\theta - ab\frac{\cos\left[\frac{\pi}{2}\cos(90-\alpha)\right]}{\sin(90-\alpha)}\sin\theta$$

[1] H. C. Forbes, U. S. Patent No. 2,320,124.
[2] Bellini and Tosi, Electrician **62**, 531 (1909).
[3] A. Hund, *Phenomena in High Frequency Systems* (McGraw-Hill Book Company, Inc., New York, 1936), p. 492.
[4] W. R. Smythe, *Static and Dynamic Electricity* (McGraw-Hill Book Company, Inc., New York, 1939), p. 468.

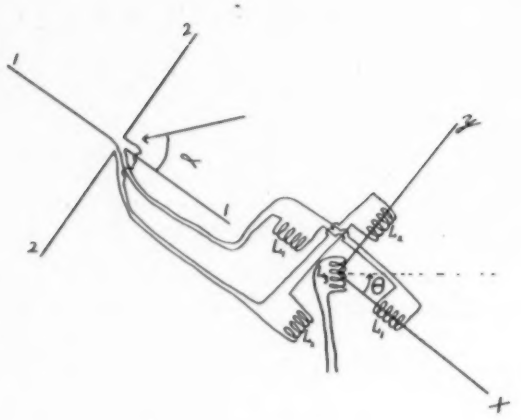

FIG. 1.

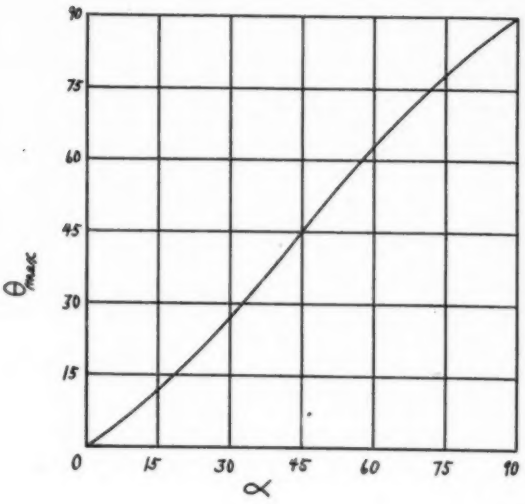

FIG. 2.

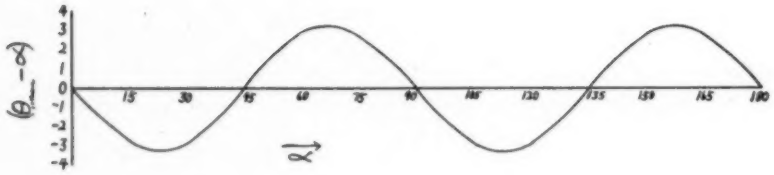

FIG. 3.

and, setting the right-hand side equal to zero, we have

$$\frac{\cos\left[\frac{\pi}{2}\cos(90-\alpha)\right]}{\sin(90-\alpha)}\tan\theta_{\max}=\frac{\cos\left(\frac{\pi}{2}\cos\alpha\right)}{\sin\alpha},$$

$$\tan\theta_{\max}=\frac{\dfrac{\cos\left(\frac{\pi}{2}\cos\alpha\right)}{\sin\alpha}}{\dfrac{\cos\left[\frac{\pi}{2}\cos(90-\alpha)\right]}{\sin(90-\alpha)}}=\frac{\dfrac{\cos\left(\frac{\pi}{2}\cos\alpha\right)}{\sin\alpha}}{\dfrac{\cos\left(\frac{\pi}{2}\sin\alpha\right)}{\cos\alpha}},$$

$$\tan\theta_{\max}=\frac{\cos\left(\frac{\pi}{2}\cos\alpha\right)}{\cos\left(\frac{\pi}{2}\sin\alpha\right)}\cot\alpha. \qquad (5)$$

The value of θ giving a zero value of E_3 for a particular α is obtained by equating E_3 to zero and solving for θ. Thus, from Eq. (4), we obtain

$$ab\frac{\cos\left(\frac{\pi}{2}\cos\alpha\right)}{\sin\alpha}\sin\theta_{\min}+ab\frac{\cos\left(\frac{\pi}{2}\sin\alpha\right)}{\cos\alpha}\cos\theta_{\min}=0,$$

and

$$\tan\theta_{\min}=-\frac{\cos\left(\frac{\pi}{2}\sin\alpha\right)}{\cos\left(\frac{\pi}{2}\cos\alpha\right)}\tan\alpha. \qquad (6)$$

Combining (5) and (6),

$$\tan\theta_{\max}=\frac{1}{\tan\theta_{\min}}, \qquad (7)$$

showing that for all values of α the minimum and maximum values of θ are 90° apart.

Figure 2 is a graph of $\theta_{\max}$ *vs.* α as obtained from Eq. (5). For values of α that are multiples of 45°, $\theta_{\max}$ is equal to α, but between these values there is a slight deviation. This deviation is shown on an enlarged scale in Fig. 3, and the curve is very nearly sinusoidal. Values for $\theta_{\min}$ may be obtained from Fig. 2 by adding 90° to $\theta_{\max}$.

Here and There

Cover Photograph

During studies on the polymerization of styrene in suspensions made by W. P. Hohenstein and H. Mark at the Polytechnic Institute of Brooklyn, polymers were formed in rather regular spheres as indicated in the photograph on the cover. Careful control of the hydrodynamic conditions during polymerization permits the acquisition of plastics of high purity, which is of importance for the use as an electrical insulating material.

Honors and Awards

Selection of William David Coolidge, Vice President and Director of Research for the General Electric Company, and Peter Kapitza, Director of the Institute for Physical Problems, Academy of Sciences, Union of Soviet Socialist Republics, as winners of the Franklin Medals in 1944 has been announced by Dr. Henry Butler Allen, Secretary and Director of The Franklin Institute, Philadelphia.

Since the founding of the Franklin Medal in 1914, it has been awarded by the Institute to such scientists as Thomas A. Edison, Guglielmo Marconi, Charles Fabry, Pieter Zeeman, James H. Jeans, Orville Wright, Albert Einstein, and Charles F. Kettering. The face of the medal carries a medallion of Benjamin Franklin done from the Thomas Sully portrait owned by The Franklin Institute.

Dr. Coolidge, winner of many scientific awards, among them the Howard N. Potts and the Louis Edward Levy Medals of The Franklin Institute, has been selected to receive the coveted Franklin Medal "in recognition of his scientific discoveries, which have profoundly affected the welfare of humanity, especially in the field of the manufacture of ductile tungsten and in the field of improved apparatus for the production and control of x-rays."

Dr. Kapitza's great work has been the invention of a method of producing extraordinarily high magnetic fields, many times greater than were previously thought possible, and the development of ingenious methods for making magnetic measurements of various kinds upon small pieces of matter exposed for a small fraction of a second to such fields. He also designed and constructed an exceptionally efficient machine for making liquid air and liquid hydrogen which is much smaller in size than those used previously.

The medals were presented to Coolidge and Kapitza at the annual Medal Day ceremonies held at The Franklin Institute in Philadelphia, April 19.

Secretary of State Hull, in behalf of the government, today presented the first civilian Medals of Merit for "exceptionally meritorious conduct" to John C. Garand for his invention of the Garand rifle, and to Dr. Albert White Taylor, chief physicist at the Naval Research Laboratory, for his development of radar.

Mr. Garand, head engineer of the U. S. Army's ordnance department, developed the semi-automatic rifle in 16 years of work at the Springfield, Massachusetts Armory.

The citation for the radar work said that Dr. Taylor's "foresight, technical skill, and steadfast perseverance contributed in large measure to the timely introduction of a scientific device which has yielded the United States Navy a definite advantage over her enemies during the present war."

Ten George Westinghouse scholarships, each valued at $1850, were awarded on April 14 to top-ranking seniors in high schools from coast to coast. The winners will attend the College of Engineering of Carnegie Institute of Technology.

The selections were made from among 684 candidates in the seventh annual scholarship competition sponsored by the Westinghouse Electric and Manufacturing Company. Recipients of the awards were chosen on the basis of mental ability, aptitude for engineering, and qualities of leadership and personality. Scholarships for winners who enter the armed services will be held until they return.

Igor Sikorsky, inventor of the helicopter adopted by the Army Air Forces, was presented on February 13 by Fawcett Publications, Inc., with the 1943 aviation trophy and the sum of $1000.

New Appointments

R. M. Foster, of the Bell Telephone Laboratories, has been appointed Professor of Mathematics and Head of the Department at the Polytechnic Institute of Brooklyn.

Dr. Niels Bohr, Professor of Theoretical Physics at the University of Copenhagen, has been elected a member of the Athenaeum Club, London, under a rule which permits the "annual election by the committee of a certain number of persons of distinguished eminence in science, literature, or the arts or for their public services."

Four honorary members, one each from the four principal Allied Nations, have been elected by the British Institute of Metals. They are, for the United States, Dr. Irving Langmuir of the General Electric Company; for Great Britain, Sir Lawrence Bragg of the University of Cambridge; for China, Madame Chiang Kai-Shek; and for the U.S.S.R., Professor Peter Kapitza of the Academy of Sciences, Moscow.

G. Stanley Meikle, Research Director of Purdue Research Foundation, and A. A. Potter, Dean of the Schools of Engineering, have announced establishment of a new joint industry-education enterprise at Purdue University for the "intensive training of graduate students in exploring the field of heat transfer for data upon which many of the practical developments of the future depend." Made possible by a $75,000 grant from the Westinghouse Electric & Manufacturing Company, the five-year training and research program will be directed by Dr. George A. Hawkins of the Purdue faculty who has been appointed

Westinghouse Research Professor in Heat Transfer. Dr.s Max Jakob of the Illinois Institute of Technology will operate with Dr. Hawkins in the capacity of non-resident Research Professor.

Dr. R. G. Sturm, formerly of the Aluminum Research Laboratories at New Kensington, Pennsylvania, has been appointed Professor of Engineering Mechanics at Purdue University and Research Professor of Materials in the Engineering Experiment Station of the university effective July 1, 1944. As Professor of Engineering Mechanics, he will give instruction in elementary courses in mechanics but mainly will develop graduate study in that field. Also it is expected that he will develop instruction and research in the field of engineering materials as part of his duties in the Engineering Experiment Station.

At a meeting of the Directors of the Spencer Lens Company, Buffalo, New York, Scientific Instrument Division of the American Optical Company, on Friday afternoon, March 24, the following officers were elected:

HEYWOOD FOX, *President*,
HAROLD D. RHYNEDANCE, *Vice President in Charge of Sales*,
WALTER G. BUCKLEY, *Vice President in Charge of Manufacturing and Chairman of the Board*,
BRYANT GLENNY, *Treasurer and Assistant Secretary*,
E. E. WILLIAMS, *Assistant Treasurer*,
CHARLES W. BARTON, *Secretary*.

Alan Hazeltine, lately Chairman of the Physics Department at Stevens Institute of Technology, has resigned from the Stevens faculty. For the past few years Dr. Hazeltine has been engaged in developing a new type of physics course in which the basic physical laws have been rigorously derived from facts of common observation and in which practical applications have been stressed.

Grant to University of São Paulo

Cecil M. R. Cross, American Consul General at São Paulo, Brazil, has reported that an announcement has been made by the Director of the Faculty of Philosophy of the University of São Paulo that the state government has guaranteed a sum of Cr. $10,000,000.00 (approximately $500,000 U.S.) to be used for the erection of a School of Physics as a part of the projected University City of São Paulo. The money is to become available during the coming fiscal year and will mark the first serious step in bringing into reality the projected University City.

In part, the grant is a recognition of the importance of physics to the industrial life of the city of São Paulo, but is also in part a recognition of the caliber of the work already accomplished in the physics section of the Faculty of Philosophy.

Course in Textiles and Testing Techniques

The accelerated course in textiles and testing techniques held yearly in the main laboratories of the United States Testing Company, Inc., Hoboken, New Jersey, will be repeated this summer. Marking the seventh year these special classes have been in session, this year's study will be geared to the varied uses, applications, and values of textile testing. Originally planned to broaden and bring up to date theoretical textile studies, the course has grown to become a practical training period in textile testing. This particular curriculum has proved highly successful in that it has made possible the study of laboratory techniques and testing equipment otherwise inaccessible to many persons. Again this year, students will have the instruction of the United States Testing Company's staff technicians under the direction of Mr. G. R. Turner, supervisor of the company's textile laboratory.

Report of Symposium on Cosmic Rays

The Brazilian Academy of Science issued recently a report on the Cosmic-Ray Symposium held in 1941 in Rio de Janeiro during the visit of Professor A. H. Compton and several of his co-workers. The handy volume presents the inaugural addresses held at the meeting and numerous scientific papers by Professors A. H. Compton, W. Jesse, G. Wataghin, G. Occhialini, and many others. The papers are written in English. Free copies may be obtained by applying to the Academia Brasileira de Ciencias: Caixa Postal, 229—Rio de Janeiro, Brazil.

Instruments Urgently Needed for War Work

Instruments urgently needed for essential war work are listed below. These have been requested from the Committee on Location of New and Rare Instruments. Anyone having any of these instruments and willing to sell, rent, lend, or give them for necessary work will perform a service by informing D. H. Killeffer, Chairman, 60 East 42 Street, New York 17, New York.

Weston ammeter No. 622 (0–100 ma)
Weston ammeter No. 280 (0–50)
Surface tension balance
Precision cathetometer 32″ range, 0.003″ error
Babinet compensator (Soleil)
High speed impulse counter (Cenco No. 73506 or No. 73511)
Amsler No. 4 integrator
Gas interferometer (Zeiss or Hilger) (several)
G. E. or Esterline Angus recording milliammeter spring drive 0–5 ma 6″–12″/min. speed
Beckman industrial model M or Coleman model 3A *p*H meter
Weston microammeter—
  No. 643, 100 scale div., res. 385 ohms
  No. 741, 100 scale div., res. 1110 ohms
Potentiometer—L & N 8660
Potentiometers (type K or other) (several) (moderately high or quite high sensitivity)
Campbell Shackelton shielded a.c. ratio box (equivalent to L & N a.c. ratio box 1553)
Abbe refractometer (several)
Spectrotelephotometer (Cenco-Sherd)
Quartz spectrograph
Strobotacs (Gen. Radio 631-B)
Stroboscopic equipment
Western Electric electrometer tube D-96475
Tinius-Olson stiffness testing machine. Cat. No. 932
G. E. x-ray diffraction unit
Recording oscillograph (minimum sensitivity) (Several channels capable of recording one hour at one inch per second. Suitable for aircraft operation.)

500,000 liters per minute at one millionth of atmospheric pressure

A mammoth new vacuum pump of rugged, all-metal construction

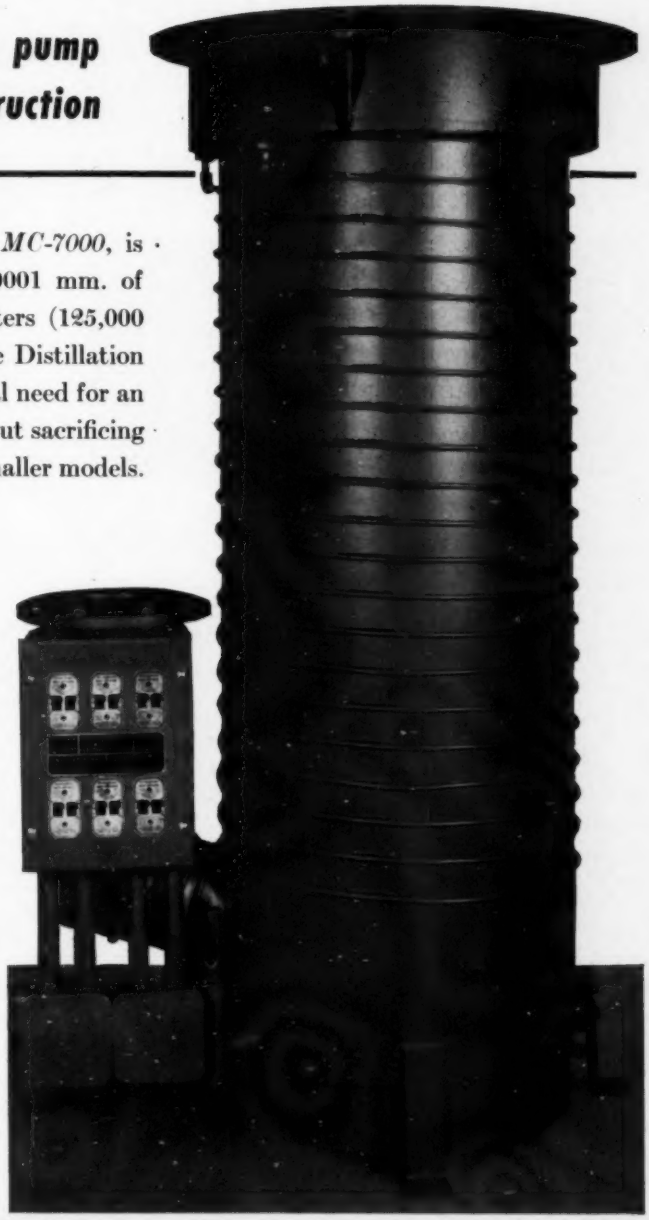

THIS new vertical vacuum pump, *Type MC-7000*, is capable of maintaining a pressure of 0.0001 mm. of mercury while pumping one-half million liters (125,000 gallons) per minute. It was designed by the Distillation Products research staff to meet the industrial need for an extremely fast vacuum diffusion pump without sacrificing the low ultimate vacuum obtainable with smaller models. Note the following characteristics:

SPEED	9000 l/s. at 10^{-4}
ULTIMATE VACUUM	5×10^{-6}
FOREPRESSURE required	30 μ
FOREPRESSURE with MB-200 Booster Pump	300 μ
HEATER INPUT	3100 watts
PUMPING FLUID	Octoil
HEIGHT	62 in.

The *MC-7000* pump is constructed so that an efficient water-cooled baffle can be incorporated without changing the outside dimensions.

Write for details about this pump, as well as for information on 20 other types of DPI diffusion pumps, low-vapor-pressure fluids, greases, vacuum gauges, control circuits, and other items for high-vacuum technology.

DP INC. HIGH-VACUUM HEADQUARTERS

DISTILLATION PRODUCTS, INC.

Jointly owned by EASTMAN KODAK COMPANY and GENERAL MILLS, INC.

ROCHESTER 13, N. Y.

Recent Applications of Physics

Prepared by CLARK GOODMAN, Associate Editor

Material to be included in this section should be submitted to Dr. Clark Goodman, Massachusetts Institute of Technology, Cambridge 39, Massachusetts.

Subsurface Surveys A number of important achievements have resulted from an accurate knowledge of the course taken by oil-field drill holes and the ability to guide the direction of drilling. The Pure Oil Company recently completed several dozen wells drilled from a single platform constructed over bayou land in the Creole Field in Louisiana. For structural reasons it is sometimes desirable to drill into a predetermined

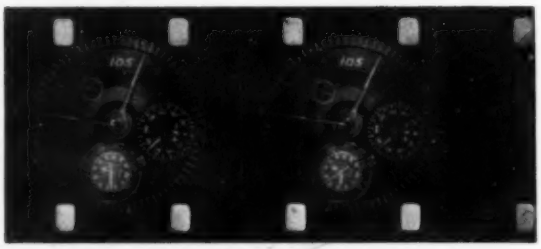

lateral location. Probably the most dramatic use of directional drilling is in extinguishing oil-well fires by tapping the burning well below the surface. A gyroscopic instrument manufactured by the Sperry-Sun Well Surveying Company of Philadelphia gives a permanent photographic record of the inclination and direction of the hole at any depth. Records are made by a movie camera, which photographs the direction of the gyroscopic indicator, the degree of inclination, the time in seconds, and the temperature. A sample record is shown in the accompanying figure. From such records a 3-dimensional projection of the well can be obtained. The instrument is contained in a protective casing about 34 feet long and 5½″ outside diameter, hence will pass through cased holes of 6″ inside diameter or larger.

Lithium Controlled Atmospheres For years physicists have used metallic lithium for laboratory purposes. However, there have been few commercial uses for this lightest and most active of metals. It is well known that lithium has a strong affinity for oxygen, water vapor, carbon monoxide, and carbon dioxide. Recently it has been found that this property makes the metal uniquely suited to the elimination of these undesirable constituents in metallurgical processes. The Lithium Company, Newark, New Jersey, has developed heat-treating furnaces in which a chemically inert atmosphere is provided by a controlled amount of lithium vapor introduced into the incoming gas stream. No addition or loss of carbon from steel occurs in such an atmosphere. Because of the absence of oxygen, the heat-treated metal products do not scale or undergo other changes in surface analysis. By a slight modification, a carbon-rich neutralized atmosphere can be obtained that allows a rapid, bright gas-carburizing of steels. In both processes the correct proportion of lithium is readily maintained by observing the brilliant scarlet flame resulting from the 6707.86Å line.

Electronic Dew-Point Indicator The conventional method of detecting the presence of unwanted water vapor in heat-treating atmospheres is to pass the gases over a surface chilled to between −40 and −70°C and observe the temperature of condensation. At these low temperatures even skilled operators differ in their estimates of the dew point. Furthermore, the process is not continuous. The operator must take periodic samples for test.

Westinghouse has developed an experimental electronic device which furnishes a continuous report and also measures the equally undesirable oxygen content of the furnace gases. A tiny stream of the gas mixture is drawn across an electron beam. As long as the gas is free of impurities, the electron current remains constant. However, the presence of even minute concentrations of oxygen or water vapor causes a sharp decrease in the beam current because these molecules are more readily ionized than the furnace gases.

Pendulous Tester Even among the most active of wartime physicists, few have experienced the questionable pleasure of occupying a ship's crow's nest during a heavy storm. Yet Westinghouse physicists were faced with this unpromising necessity in order to test controls for searchlights, radio apparatus, and signalling devices under such operating conditions. They solved the problem, without experiencing the otherwise inevitable seasickness, simply by building an oscillating mast on land. The tower, shown in the accompanying photograph, when counterweighted below the pivot at its base, constitutes a 50-foot inverted pendulum with an angular amplitude up to 45 degrees and a period of as little as six seconds. A 35-hp variable-speed motor, operating through standard oil-well reduction gear and crank, supplies the power to make the mast roll.

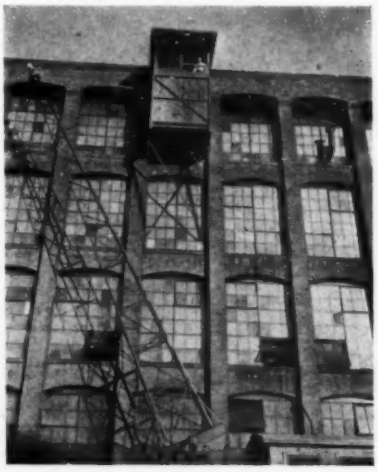

Kodak Plates for
ELECTRON MICROSCOPY

The Kodak plate best suited to electron microscopy, and the one most generally used for this purpose, is the *Kodak Medium Lantern Slide Plate.* It has high contrast and fine granularity.

For higher contrast and finer granularity, the *Eastman Spectroscopic Plate, Type IV-O,* has proved quite suitable. For extremely fine granularity and very high resolving power, the *Eastman Spectroscopic Plate, Type 548-O,* is recommended.

You are invited to write for further information on any problem that may arise in connection with the photographic phases of electron microscopy.

EASTMAN KODAK COMPANY

Research Laboratories **Rochester 4, N. Y.**

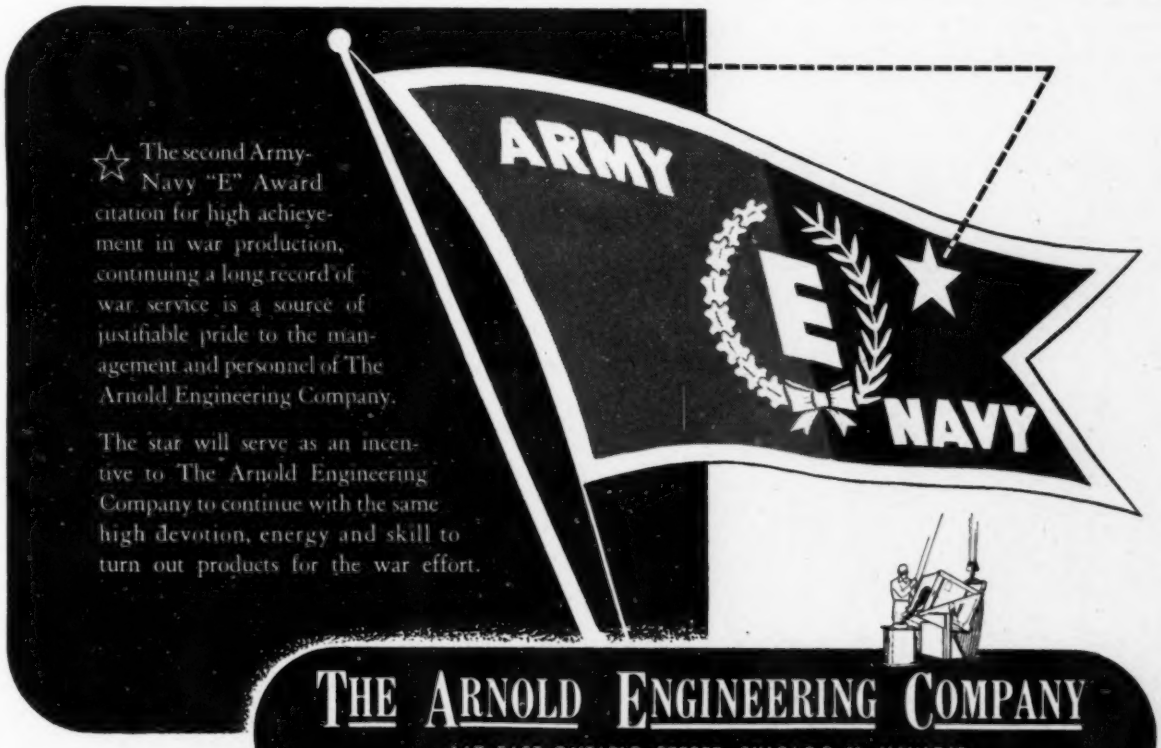

☆ The second Army-Navy "E" Award citation for high achievement in war production, continuing a long record of war service is a source of justifiable pride to the management and personnel of The Arnold Engineering Company.

The star will serve as an incentive to The Arnold Engineering Company to continue with the same high devotion, energy and skill to turn out products for the war effort.

THE ARNOLD ENGINEERING COMPANY

147 EAST ONTARIO STREET, CHICAGO 11, ILLINOIS

Specialists in the Manufacture of ALNICO PERMANENT MAGNETS

Commercial Synthetic Sapphires Aluminum oxide (Al_2O_3) occurs in nature as the mineral corundum. The more familiar gem varieties are ruby, sapphire, topaz, and amethyst. Prior to the war, synthetic corundum was imported from Europe. With the removal of this source, a serious need arose, since this material is unequalled for bearings in watches, balances, electrical meters, and other precision mechanisms. Within the last few years techniques have been developed, largely by the Linde Air Products Company, which make this country independent of foreign sources. The alumina is fed into any oxy-hydrogen flame, and the fused material is deposited on a fireclay pedestal in the form of a carrot-shaped mass known as a "boule." By the addition of pigments, a variety of colors can be produced. The average boule weighs about 200 carats. However, some have been formed as large as 400 carats (80 grams).

Recently crystals of rod corundum have been produced in the range of diameters suitable for jewel bearings (50 to 100 mils). The rod is annealed in the process, and lengths up to 30 inches have been made. To make cylinders for bearings, it is merely necessary to grind centerless the rod, then cut off disks of the desired thickness. Rod corundum substantially reduces fabricating time and costs, because so little grinding is necessary to attain the proper size.

Simulated Stratosphere In global war it is imperative that all equipment, especially electrical apparatus, be tested under combat conditions. An airplane generator may be operating under hot, humid conditions in a South Pacific jungle and within a matter of minutes be called upon for similar service at subzero temperatures and low pressure in the stratosphere. Actual flight testing is not only expensive and time-consuming, but difficult to control. For this reason test chambers that simulate a wide variety of climatic conditions are in use. Typical of these is the Westinghouse unit which can be cooled to −67°F and evacuated to 1/20 atmospheric pressure, representing an altitude of about 70,000 feet. A mixture of crushed dry ice and varsol (similar to kerosene) is used as a refrigerant. One of the difficulties encountered is that the air cannot be recirculated; otherwise metal dust and gases from the insulation would accumulate and falsify the observations. Brush wear, creepage distances required for different voltages, and ventilation needs are among the problems being studied in the Westinghouse chamber illustrated in the accompanying photograph.

Industrial Infra-Red Spectroscopy The recent appearance of a book[1] devoted to industrial applications of infra-red spectroscopy clearly indicates that this branch of applied physics has come of age. The underlying basis of applied infra-red spectroscopy is the fact that practically all organic substances possess selective absorption at certain frequencies in the infra-red portion of the electromagnetic spectrum. A spectrometer, generally a prism type, is used to determine the percent transmission or absorption of the sample at a series of narrow frequency intervals throughout a chosen part of the spectrum. A plot of these transmission or absorption values *versus* frequency or wave-length constitutes an infra-red spectrum, which is characteristic of the sample being studied and which may be used to describe the sample in much the same manner as boiling point, refractive index, melting point, or any other physical property. Since the samples required are small and are not used up or changed in any way, this method of analysis is particularly useful where limited amounts of material are available. In order to identify an unknown, its absorption spectrum is compared with reference curves for known compounds. The 363 representative spectra of organic compounds taken in the rocksalt region that have just been published[1] should serve as a valuable infra-red reference library for this purpose. Other qualitative applications are the recognition of specific chemical bonds, linkages, or groups, the determination of the spatial configuration of the atoms within certain molecules, and the qualitative analysis of a mixture of several components.

The quantitative applications are of even greater usefulness. A mixture of materials can be analyzed quickly and accurately so long as the components present in the mixture are known. From a study of the spectra of known compounds, it is usually possible to find a frequency at which only one component possesses strong absorption. By setting the spectrometer at this particular frequency and comparing the absorption of an unknown with that of known prepared standards, the amount of the particular component in the unknown can be determined. Usually another characteristic frequency can be found for each of the other components. This rapid method, modified suitably to meet existing conditions, has been applied, with an analytical uncertainty of 1 percent or less, to mixtures ranging from simple ones of two hydrocarbons to complex mixtures containing up to six terpenes. This procedure has also been used for measuring rates of reaction or polymerization as a function of temperature, pressure, or the type of catalyst.

[1] R. B. Barnes, R. C. Gore, U. Liddel, and V. Z. Williams, *Infrared Spectroscopy, Industrial Applications and Bibliography* (Reinhold Publishing Corporation, New York, 1944).